NTNU
Norwegian University of
Science and Technology

Reactive Power Compensation using a Matrix Converter

Nathalie Marie-Anna Holtsmark

Master of Science in Energy and Environment
Submission date: June 2010
Supervisor: Marta Molinas, ELKRAFT

Norwegian University of Science and Technology
Department of Electric Power Engineering

Problem Description

A matrix converter combined with an electrical machine for reactive power compensation will be analytically investigated to determine the physical limits of the solution for fulfilling reactive power requirements from a network under normal operating conditions. The possibility to use the suggested topology also for active power or for a load will be investigated. Constraints for reactive power compensation in capacitive and inductive mode will be qualitatively compared to a synchronous condenser and conventional STATCOM solution. A network model will be build and the proposed reactive power compensator will be tested with a control system provided with a command for reactive power requirement from the network.

Assignment given: 26. January 2010
Supervisor: Marta Molinas, ELKRAFT

NTNU
Norwegian University of
Science and Technology

REACTIVE POWER COMPENSATION USING A MATRIX CONVERTER

Nathalie Holtsmark

Master of Science in Energy and Environment
Department of Electrical Power Engineering
Supervisor: Prof. Marta Molinas

June 22, 2010

Abstract

This Master's thesis investigates a new application for the matrix converter: Shunt reactive power compensation. The suggested Matrix Converter-based Reactive power Compensation (MCRC) device is composed of a matrix converter, which input is connected to the grid and an electric machine at the output of the converter. The reactive power flowing in or out of the grid can be regulated with the matrix converter by controlling the magnitude and/or phase angle of the current at the input of the converter. The matrix converter has no bulky DC link capacitor like traditional AC-DC-AC converters. The thought electric machine is a Permanent Magnet (PM) synchronous machine which is compact as well, yielding an overall compact device.

The main focus of the thesis is to evaluate the reactive power range that the MCRC device can offer. The reactive power range depends mainly on the modulation of the matrix converter. Two different modulation techniques are studied: the indirect virtual space vector modulation and the three-vector-scheme. The indirect space vector modulation can provide or draw reactive power at the input of the matrix converter as long as there is an active power flow through the converter that is different from zero. For pure reactive power compensation the indirect space vector modulation cannot be used and the three-vector-scheme must be used instead. Both modulation techniques are presented in details as well as their reactive power compensation range.

To verify the reactive power capabilities of the device, three different simulation models are built in MATLAB Simulink. The first simulation model represents the MCRC device with the matrix converter modulated with the indirect space vector modulation. The second model represents also the MCRC device with the matrix converter modulated with the three-vector-scheme. In both model the PM machine is represented by a simple equivalent circuit. Simulations done with both models show a good accordance between the theoretical analysis of the device and the experimental results. The last simulation model features a simplified version of the MCRC system connected to a grid where a symmetrical fault occurs. The MCRC proves to be efficient in re-establishing the voltage to its pre-fault value.

Preface

This is my Master's thesis in Electrical Power Engineering which is the final achievement of my Master studies in Energy and Environment at the Norwegian University of Science and Technology (NTNU) in Trondheim.

I would first like to thank my advisor, Professor Marta Molinas, for providing me with an interesting project idea and for her help and suggestions during the semester. I would also like to thank Frank Schafmeister for answering my questions and helping me understand the three-vector-scheme modulation.

My office mates have made the long days at school seem like fun. My boyfriend has given me a lot of love and support throughout the semester. Finally, I thank my parents and my grandmother Alice.

Nathalie Holtsmark
Trondheim, Norway
June 22nd 2010

Contents

1 Introduction **1**
1.1 The need for reactive power compensation 1
1.2 The MCRC device in the perspective of well-established compensators . . . 2
1.3 The Master's Thesis 6

Theoretical Analysis of the Matrix Converter-based Reactive Compensation System **11**

2 The PM synchronous machine **11**
2.1 No-load operation of the PM synchronous machine 11
2.2 Loaded operation of the PM synchronous machine 13

3 The matrix converter **15**
3.1 Topology and general operation features of the matrix converter 15
3.1.1 Topology of the matrix converter 15
3.1.2 Modulation index limitation 16
3.2 Conventional indirect space vector modulation 19
3.2.1 Space vector modulation of the VSI 20
3.2.2 Space vector modulation of the CSR 28
3.2.3 Combination of the VSI and CSR signals 34
3.3 Reactive and active power ranges with conventional space vector modulation 34
3.3.1 $\Phi_i \neq \pm 90\,^\circ$ and $\Phi_o \neq \pm 90\,^\circ$ 34
3.3.2 $\Phi_i = \pm 90\,^\circ$ and $\Phi_o = \pm 90\,^\circ$ 41
3.4 Improved reactive power transfer with the three-vector modulation scheme 45
3.4.1 The output voltage forming pulse half period 46
3.4.2 The input reactive current formation pulse 50
3.4.3 Merging of the voltage and reactive current formation pulses 57
3.4.4 Reactive power compensation range 60

Simulation model and simulation results of the Matrix Converter-

based Reactive Compensation System **65**

4 Reactive compensation with conventional modulation **67**

5 Improved reactive compensation with the three-vector-scheme modulation **77**

6 Conclusion and further work **83**
6.1 Conclusion 83
6.2 Further work 85

Bibliography **86**

Appendix **88**

A Modulation sequence in three-vector-scheme modulation **A-0**

B Simulation model of matrix converter with conventional space vector modulation **B-0**

C Simulation model of matrix converter with the three-vector-scheme modulation **C-0**

D Simulation model of the MCRC system connected to a grid for voltage support **D-0**

E Conference paper **E-0**

Chapter 1

Introduction

1.1 The need for reactive power compensation

The electricity grid is under a lot of strain: The load and the electricity generation are increasing year after year. Nevertheless the expansion of the grid is limited because of economical and environmental reasons. It is therefore becoming very important to utilize the power transfer capabilities of the grid to its maximum. For a simple lossless line like the one presented in figure 1.1, the power transfer is as in equation (1.1).

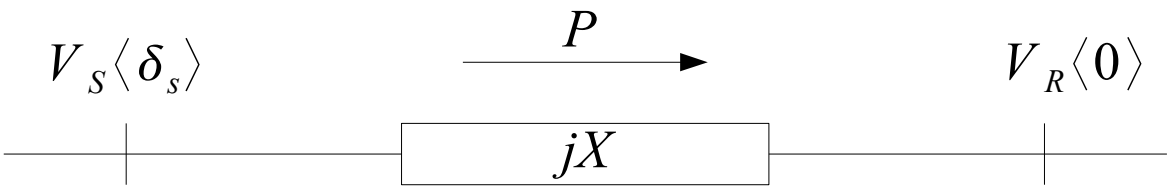

Figure 1.1: *A simple power transmission line.*

$$P_S = P_R = \frac{V_S V_R}{X} \sin \delta_s \tag{1.1}$$

V_S is the voltage at the generation bus and is assumed to be constant. We see from equation (1.1) that there are three parameters that can be controlled to increase the power transfer; V_R, the voltage at the load, X, the reactance of the line and δ_s, the power angle. In addition to the transmission lines reaching their loading maximum, there are many disturbances:

The continuous variation of the load, random occurence of faults on the power lines and the introduction of new renewable energies, like wind or solar power, which have varying and unpredictable generation. These variations all make it very important to be able to dynamically control V_R, X and δ.

The reactive power at the receiving end of the line can be calculated as in equation (1.2) and plotted as a function of the recieving end voltage V_R as in figure 1.2.

$$Q_R = \frac{V_S V_R \cos\delta - V_R^2}{X} \tag{1.2}$$

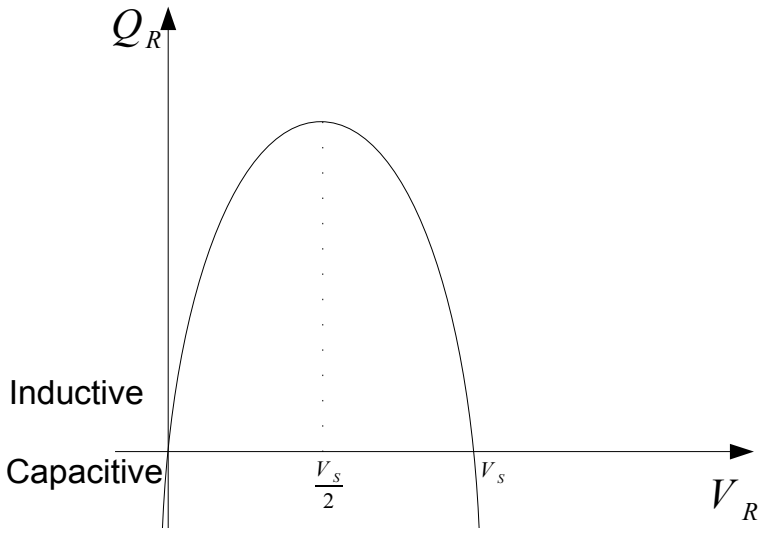

Figure 1.2: *The receiving end reactive power Q_R as a function of the receiving end voltage V_R for a constant sending end voltage V_S.*

The voltages in a power system must be kept close to a nominal voltage and thus it can be assumed that $V_R \geq \frac{V_S}{2}$ at all times and the curve on the right handside of the peak is the relevant operation region [13]. In this operation region an increase in reactive power (increase in inductive reactive power) will lead to a decrease in V_R while a decrease (increase in capacitive reactive power) will lead to an increase in V_R. This illustrates the strong connection between voltage and reactive power and at the same time indicates a way of controlling the receiving end voltage V_R: by injecting or drawing reactive power.

1.2 The MCRC device in the perspective of well-established compensators

In this thesis we investigate a Matrix Converter-based Reactive power Compensation (MCRC) device. The purpose of the device, as the name indicates, is to provide to or

absorb reactive power from the grid on the input side, in a controlled manner. The system is depicted in figure 1.3 and is composed of a matrix converter, a Permanent Magnet (PM) synchronous machine at the output of the matrix converter and an input filter on the grid side. The matrix converter controls the reactive power at its input by controlling the input current. The matrix converter also controls the output voltage.

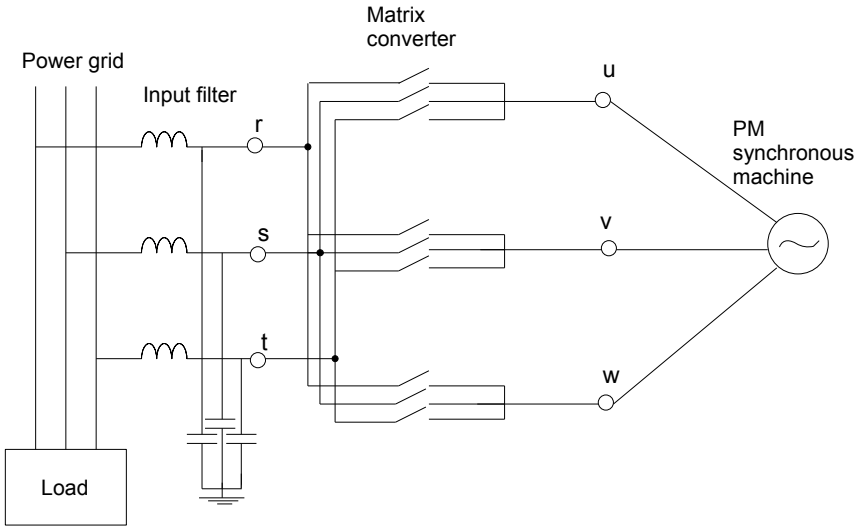

Figure 1.3: *The MCRC system composed of a matrix converter connected to a PM machine and the grid through an input filter.*

It is interesting to briefly compare qualitatively the suggested device with other well-established reactive power compensators right away to determine if it presents some advantages and if so, what those are. The device can compensate for reactive power, but it can also act as an energy buffer since it comprises a PM machine. In this preliminary comparison however only the pure reactive compensation is considered. It is assumed that no mechanic load is put on the shaft of the rotor so that no active power flows through the matrix converter. The compensation devices object of this comparison are the synchronous condenser and the STATCOM.

The synchronous condenser, depicted in figure 1.4 is a synchronous machine that "floats" on the bus to which it is connected; the rotor is nearly in phase with the rotating flux in the stator as almost no load is put on the rotor shaft [8] (only small friction losses will draw a small amount of active power).

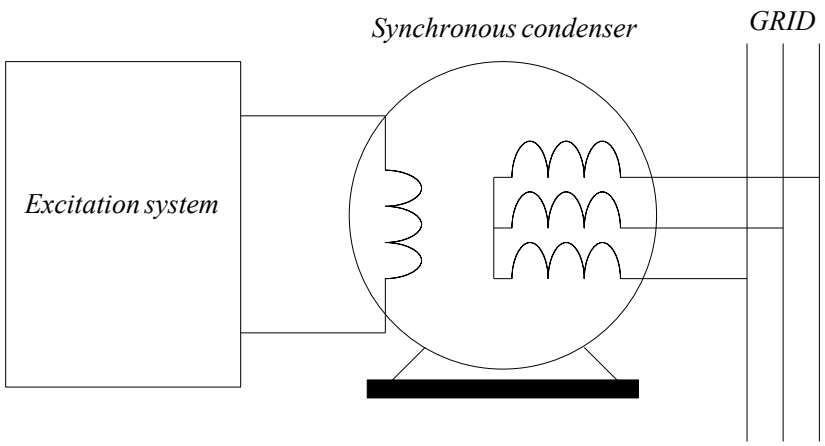

Figure 1.4: *A general representation of the synchronous condenser composed of three-phase armature windings and an excitation winding controlled by an excitation system, the synchronous condenser is connected in shunt to a grid.*

The PM synchronous machine in the MCRC system is really functioning on the same principle as the synchronous condenser. The main difference between the two compensating devices is the manner the reactive power is controlled. In a conventional synchronous machine, used as a synchronous condenser, the reactive power absorbed or produced can be controlled by adjusting the field excitation [8]. It is thus operational and constructional features of the machine that will limit the reactive power transfer: the stator current must not exceed the thermal limit of the armature winding, the field current must not overheat the field winding and the stator magnetic circuit end region must not be overheated either [13]. In a PM machine however the field excitation voltage is created by permanent magnets which cannot be changed and reactive power must be controlled otherwise. This is the role of the matrix converter interface. This means that in the MCRC device it is the matrix converter which dictates the reactive power range of the device. The second difference is the size of the device. The traditional synchronous condenser is very large in size [9]. On the other side the MCRC system benefits from the compactness of the PM synchronous machine and of the matrix converter to presumably form an overall small device.

The second object of comparison is the STATCOM. The STATCOM is a voltage source converter with an energy storage unit that is usually a capacitor [24] and is represented in figure 1.5. It is connected in shunt to the grid through a coupling transformer. In the simplified model of the STATCOM in figure 1.5 the transformer is represented by its leakage inductance. The output voltage of the VSC is kept in phase with the grid voltage. Hence the current that flows through the reactance will be in almost perfect quadrature with the grid voltage. By changing the magnitude of the VSC output voltage, the magnitude of the current and its direction can be controlled. When the magnitude of the VSC output voltage is larger than the grid voltage, the current is leading the voltage by 90° and the STATCOM is emulating a capacitor. On the other hand when the voltage magnitude of the output VSC is lower than the grid voltage, the current will be lagging the voltage by 90° the STATCOM emulates an inductance. In a VSC the maximum modulation index is

$\frac{\hat{V}_{LL,converter}}{e_{dc}} = 1$. In order to have reactive current flowing into the grid, the amplitude of the converter output and hence the DC link voltage, needs to be larger than the grid voltage amplitude. The STATCOM and the MCRC device are both composed of an energy storage unit (respectively a capacitor and a PM machine) and a converter interface. However the control of the reactive power is done differently in both devices. As was just explained the voltage over the capacitor needs to be at least as large as the grid voltage for full inductive and capacitive current control. In the MCRC system the output voltage must actually be lower than the grid voltage because of intrinsic limitation of the matrix converter, see section 3.1. However the size of the output voltage and excitation voltage does affect the reactive power range directly, see section 3.3. The reactive power is controlled through the input current. The matrix converter can control the magnitude or the phase angle of the input current depending on the modulation. The limited size of the emf voltage will keep the volume of the electric machine small. This feature further participates into making the matrix converter solution compact. Another advantage of the MCRC system is that it contains no large storage element like capacitors and inductors, unlike the STATCOM. This is beneficial in several way: first the capacitor a component subjected to significant wear-out [3] and also most capacitors have temperature dependent characteristics (cpacitance, leakage current, impedance...) [5] which limits the application field of the device.

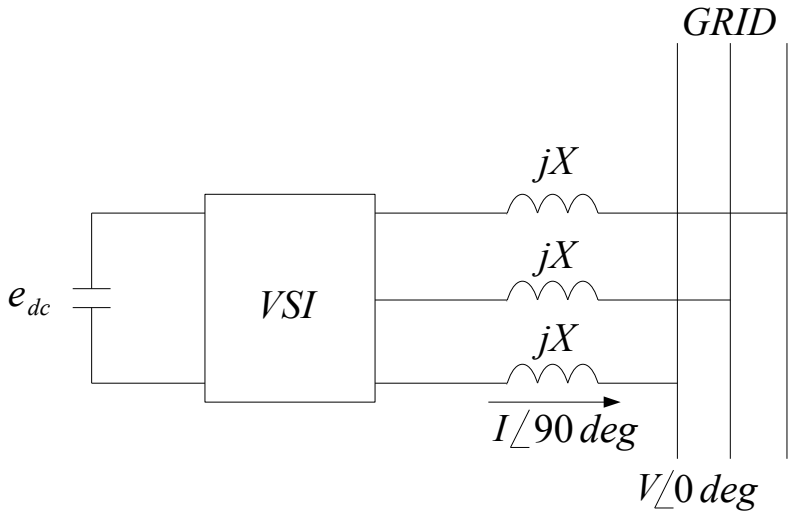

Figure 1.5: *A general representation of a STATCOM connected to a grid in shunt.*

This brief and rather superficial comparison of the MCRC device with the synchronous condenser and the STATCOM, indicates that there are clear advantages, although not quantified, to this new suggested MCRC device: compact, no large storage element(capacitor or reactor). With this preliminary aknowledgement we can proceed with the analysis of the device.

1.3 The Master's Thesis

The Master's thesis is divided into two main parts: The first part is dedicated to a theoretical analysis of the MCRC system while the second part is its experimental counterpart presenting all the simulation results.

The analysis of the MCRC device starts out with the PM machine in chapter 2. Two different operation modes of the PM machine will be investigated: loaded or at no-load. It is important to clearly distinguish these two cases: when loaded the PM machine will be absorbing or producing active power and can act as an energy buffer in addition to providing or absorbing reactive power. An energy buffer function is a nice extra feature, but requires that there is a physical energy buffer in the system: some inertia on the rotor shaft (a flywheel for instance) which is not investigated in this thesis. When the PM machine is not loaded, no active power is flowing through the matrix converter and the MCRC system is a purely reactive power compensation device. No inertia is then needed on the rotor shaft.

The matrix converter, which is the object of chapter 3, provides both the control of the reactive power transfer to the grid side and the control of the PM machine. The main focus of the Master's thesis is the analysis of the reactive power compensation ability of the matrix converter. The control of the PM machine is only mentioned very briefly in section 3.3. In the preliminary project to this thesis, [7], the matrix converter was also suggested for reactive power compensation. The matrix converter was controlled with the conventional indirect space vector modulation and there were indications that this modulation led to limitations in the amount of reactive power transferable to the input. The conventional indirect space vector modulation was presented in [7]. It will be presented here again in section 3.2, following a brief general presentation of the matrix converter in section 3.1. The reader that has already read [7] or that is familiar to the indirect space vector modulation could skip section 3.2 without losing much information. The range of transferable reactive power at the input when the matrix converter is modulated with the conventional indirect space vector technique will be investigated in section 3.3 for the two following cases: loaded PM machine and machine running at no load. It will be shown that, in the no load situation, no reactive power can be transferred at the input of the matrix converter. The reason for this serious limitations, will be explained in details. This means that the matrix converter cannot be used for pure reactive compensation when modulated with indirect space vector modulation and can only be used for the case of loaded PM machine and active power transfer through the matrix converter.

Although the conventional modulation technique does not work for the purpose of transmitting only reactive power, it doesn't mean the matrix converter should be discarted altogether for pure reacive power compensation in the MCRC system. The input reactive power depends among other factors, on the modulation technique [6]. In fact the conventional indirect space vector modulation can be modified so as to enable reactive power transfer on the input side of the matrix converter for no active power transfer through the

converter. The modulation technique, called the three-vector-scheme, has been developed by Kolar and Schafmeister in [21] and [20]. It is quite complex but will be explained in details in section 3.4. The reactive compensation range of the Three-Vector-Scheme will be also presented.

Part II of the thesis is dedicated to simulation results. Chapter 4 presents all the results from simulations with the MCRC system with the matrix converter modulated with the conventional indirect space vector modulation. Chapter 5 presents the results from the simulations performed with the matrix converter modulated with the three-vector-scheme. The simulations results are chosen such as to illustrate some of the theory that was developed in part I. The last results are performed with a simulation model that features a simplified version of the MCRC device connected to a grid which is subject to a three-phase symmetrical fault. The purpose of the simulation is to show that the MCRC device can effectively compensate for reactive power and perform voltage support.

Theoretical Analysis of the Matrix Converter-based Reactive Compensation System

Chapter 2

The PM synchronous machine

2.1 No-load operation of the PM synchronous machine

The theoretical analysis of the MCRC system starts out with the PM machine in the no-load operation mode. In this first analysis of the PM machine the ohmic losses in the armature windings and friction losses on the rotor of the PM synchronous machine are ignored. The PM machine will be studied with the help of a simple equivalent circuit. The single-phase equivalent circuit is contained within the stippled-line rectangle in the single-phase circuit of the MCRC system depicted in figure 2.1. Let's go in detail through the

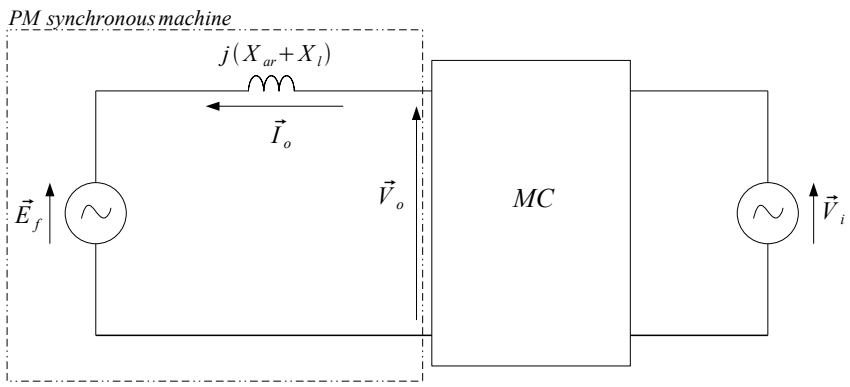

Figure 2.1: *The per-phase simplified representation of the MCRC system.*

different elements of the model of the PM synchronous machine in figure 2.1. The terminal voltage of the PM machine corresponds to the output voltage of the matrix converter and is denoted as $\vec{V_o} = V_o\angle 0$ in figure 2.1. The terminal voltage is set as the reference here with phase angle equal to 0. As the permanent magnets and the rotating flux they generate,

sweep across the stator conductors, a counter-emf or excitation voltage is created in the armature windings [8]. The excitation voltage depends only on the permanent magnet properties and will therefore be represented by a voltage source in our model, $\vec{E}_f = E_f\angle\delta$ in figure 2.1. The angle δ is called the rotor angle and is the phase angle of the excitation voltage with respect to the reference voltage at the terminal of the synchronous machine $\vec{V}_o$. δ also corresponds to the displacement between the stator flux and the rotor. Here since there is no load on the rotor and the friction losses are neglected, δ is zero.

The three-phase current flowing in the stator, which corresponds to the output current of the matrix converter and is hence named $\vec{I}_o$, also generates a rotating field flux called armature-reaction flux. This will induce a voltage in the stator windings. The armature-reaction flux and induced voltage depend on the armature current's magnitude and phase angle. The armature-reaction voltage is therefore represented in our model in figure 2.1 by a fictitious armature-reaction reactance X_{ar}. In addition the model includes an armature leakage reactance X_l which accounts for the flux leakage in the armature windings. The armature current can be calculated as in equation (2.1) with positive current defined in the direction shown in figure 2.1. This current direction, into the machine, corresponds to the motor operation of the PM machine although it is really at the the limit generator/motor when running at no-load.

$$\vec{I}_o = \frac{\vec{V}_o - \vec{E}_f}{j\left(X_{ar} + X_l\right)} = \frac{V_o - E_f}{jX_s} \tag{2.1}$$

In equation (2.1), $X_s = X_{ar} + X_l$, is the synchronous reactance. From equation (2.1) we see that the current is purely reactive and that its direction will depend on the relative magnitude of the excitation voltage $\vec{E}_f$ and the terminal voltage $\vec{V}_o$. In figure 2.2 the phasor diagram for $\vec{E}_f$, $\vec{V}_o$ and $\vec{I}_o$ are represented. When E_f is larger than V_o, $\vec{I}_o$ is leading

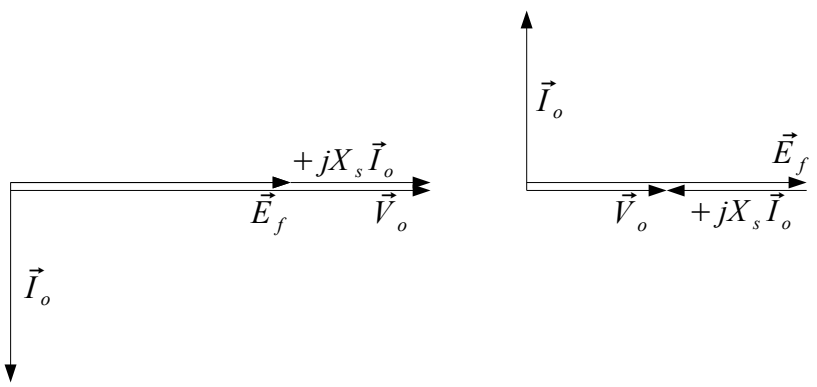

Figure 2.2: *Phasor diagram of $\vec{V}_o$, $\vec{E}_f$ and $\vec{I}_o$ for $V_o \geq E_f$ (to the left) and $V_o \leq E_f$ (to the right).*

the voltage $\vec{V}_o$, the synchronous machine acts as a capacitor. When E_f is smaller than V_o, $\vec{I}_o$ is lagging the voltage $\vec{V}_o$ and the synchronous machine acts as an inductor. This analysis shows that no matter the sign of the output angle displacement, leading or lagging, the

angle between the voltage and current will be 90° in this no load operation mode of the PM machine. From an active power balance consideration, there should be a 90° displacement angle at the input also, as the active power into the converter should match the output active power and also be equal to zero ($P_i = P_o$ in a lossless matrix converter). Furthermore the purpose of the MCRC system is to provide reactive power and hence it is optimum to have a 90° phase shift between the input voltage and current for maximum reactive power transfer. To summarize, the MCRC system imposes on the matrix converter a 90° phase shift between voltage and current at the input and the output, leading or lagging. The question is now; how does the matrix converter behave under the no-load operation of the PM machine that imposes a 90° phase shift between voltage and current at the input and output of it?

2.2 Loaded operation of the PM synchronous machine

The loaded operation mode of the PM machine will now be investigated. In this case active power flows into the machine. We will simply assume in this section that their is a corresponding load on the rotor shaft. Until now the armature resistance was neglected in this analysis. We will now calculate the active and reactive power provided to the synchronous machine including the resistance in the analysis as this will prove useful when analyzing the simulation results in part II. The PM machine will be considered to be in motor mode as previously, the current thus flowing in the direction indicated in figure 2.3. Thus the rotor angle is negative, $\vec{E}_f = E_f\angle -\delta$, with $\delta \geq 0$. The terminal voltage is still the reference angle.

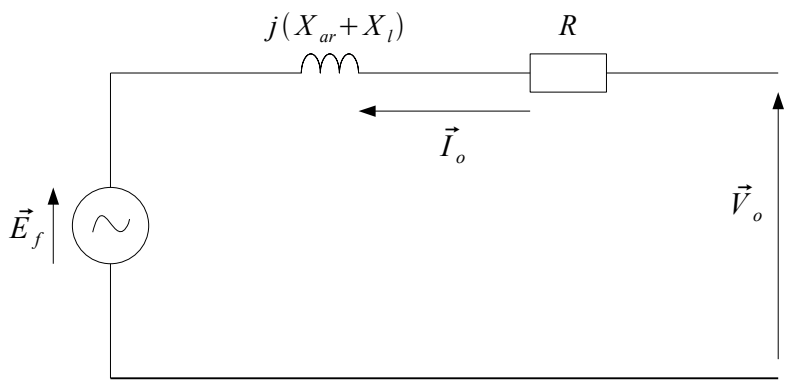

Figure 2.3: Per-phase equivalent circuit of the PM machine.

The apparent power at the terminal of the machine can be calculated as in equation (2.2)

[13].

$$\vec{S}_o = P_o + jQ_o = \vec{V}_o \vec{I}_o^* \tag{2.2}$$

The output armature current $\vec{I}_o$ can be calculated as in equation (2.3):

$$\vec{I}_o = \frac{\vec{V}_o - \vec{E}_f}{R + jX_s} = \frac{V_o - E_f \cos\delta + jE_f \sin\delta}{R + jX_s} \tag{2.3}$$

$$\vec{I}_o = \frac{(V_o - E_f \cos\delta + jE_f \sin\delta)(R - jX_s)}{R^2 + X_s^2} \tag{2.4}$$

$$\vec{I}_o = \frac{V_o R - E_f R \cos\delta + E_f X_s \sin\delta}{R^2 + X_s^2} + j\frac{E_f R \sin\delta - V_o X_s + E_f X_s \cos\delta}{R^2 + X_s^2} \tag{2.5}$$

Thus the active and reactive power can be found by multiplying the complexe conjugate of $\vec{I}_o$ with V_o:

$$P_o = \frac{V_o^2 R + V_o E_f X_s \sin\delta - V_o E_f R \cos\delta}{R^2 + X_s^2} \tag{2.6}$$

$$Q_o = \frac{V_o^2 X_s - V_o E_f R \sin\delta - V_o E_f X_s \cos\delta}{R^2 + X_s^2} \tag{2.7}$$

Now if the resistance can be neglected, $R = 0$, the active and reactive power expression are simplified as follows:

$$P_o = \frac{V_o E_f X_s \sin\delta}{X_s} \tag{2.8}$$

$$Q_o = \frac{V_o^2 - V_o E_f \cos\delta}{X_s} \tag{2.9}$$

From equation (2.5) the expression for the output current I_o and the output displacement angle Φ_o can be found.

$$I_o = \sqrt{\left(\frac{V_o R - E_f R \cos\delta + E_f X_s \sin\delta}{R^2 + X_s^2}\right)^2 + \left(\frac{E_f R \sin\delta - V_o X_s + E_f X_s \cos\delta}{R^2 + X_s^2}\right)^2} \tag{2.10}$$

$$\Phi_o = -\tan^{-1}\left(\frac{E_f R \sin\delta - V_o X_s + E_f X_s \cos\delta}{V_o R - E_f R \cos\delta + E_f X_s \sin\delta}\right) \tag{2.11}$$

The active power, $P_o = P_i$, flowing through the matrix converter and the output reactive power Q_o are dictated by the PM machine through its parameter $\vec{E}_f$, X_s and R and the matrix converter through the terminal voltage $\vec{V}_o$ according to equations (2.6) and (2.7). In the no-load case no active power is flowing through the converter and at the ouput of the matrix converter there is only reactive current. However, in both loaded and no-load situations, the input reactive power Q_i, which is the most important quantity to determine in the MCRC device, cannot be determined by looking at the PM machine alone. The matrix converter needs to be analyzed for this purpose.

Chapter 3

The matrix converter

The last chapter ended with an important remark: The input reactive power of the MCRC system cannot be calculated without analyzing the matrix converter both in the loaded and no-load situations. The modulation technique of the matrix converter will in fact decide along with the output power factor, the magnitude and polarity of the input reactive power [6]. In this chapter a theoretical analysis of the matrix converter will be carried out to assess the reactive compensation range of the MCRC device and also to try to answer the question formulated at the end of section 2; How will the matrix converter behave when there is a 90 ° phase shift between voltage and current at the input and the output, that is when there is no active power transfer? To start the analysis a brief presentation of some important features of the matrix converter is given in section 3.1. The modulation influences the reactive power range at the input of the matrix converter. It is therefore important to study the modulation technique carefully to understand what limitation it will impose on the input reactive power transfer. After the modulation technique is studied in section 3.2, the reactive power formation at the input of the matrix converter is investigated with and without active power flow through the converter in section 3.3. It turns out that the matrix converter cannot transfer reactive power at the input if their is no active power flow through it. A modulation technique called three-vector-scheme is presented in the last section to enable reactive power compensation in the no-load situation.

3.1 Topology and general operation features of the matrix converter

3.1.1 Topology of the matrix converter

The matrix converter is an AC-AC converter made up of semiconductor-based switches. The matrix converter itself contains no energy storage components such as capacitors or

reactors, although a filter at the input is needed in combination with the converter [23]. The size of the needed filter can be reduced by increasing the switching frequency. There are two main topologies for the matrix converter: Direct matrix converter, figure 3.1 and indirect matrix converter, figure 3.2. The matrix converter that is the object of attention in this thesis and that will be build in a MATLAB Simulink model will be configurated with the direct topology. It is composed of nine switches that form a three by three array connecting the input to the output directly.

It is also relevant to take a closer look at the indirect topology as the space vector modulation of the converter will be that of a indirect matrix converter. This is called virtual indirect control as the space vector modulation outputs 12 gating signals as if it was providing the twelve switches of an indirect matrix converter. The 12 signals will be combined into 9 signals to provide for the real matrix converter with a logic circuit. This modulation technique was chosen for its simplicity compared to other techniques [2, 11]. As can be seen in figure 3.2, the indirect matrix converter consists of a Current Source Rectifier (CSR) part, a DC link, e_{dc}, and a Voltage Source Inverter (VSI) part.

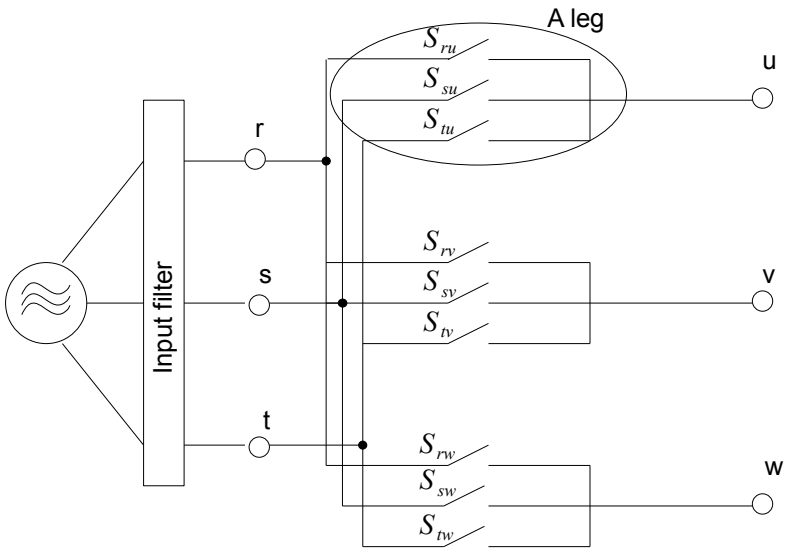

Figure 3.1: *The direct matrix converter topology.*

3.1.2 Modulation index limitation

The voltage transfer ratio of a nine switch direct AC-AC matrix converter has a limit that can not be exceeded without increasing the complexity of the modulation and/or decreasing the quality of the waveforms [23]. Venturini and Alesina proved meticulously in [2], that no matter what modulation technique is used, $V_o = \frac{\sqrt{3}}{2} V_i$ is an absolute limit for the voltage ratio. Let's look at the main features of the proof.

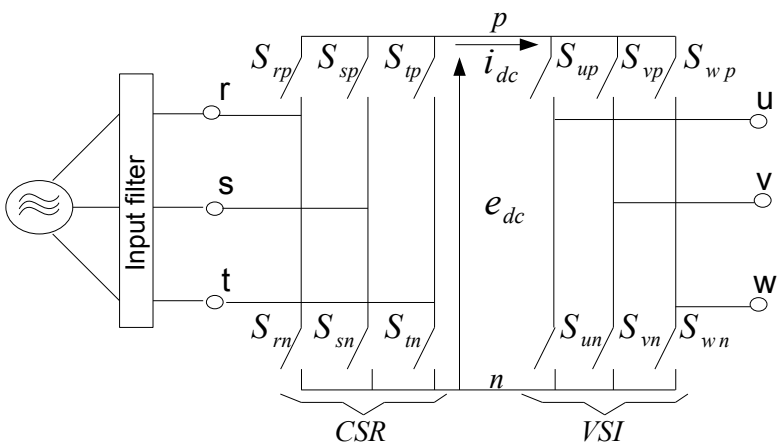

Figure 3.2: *The indirect matrix converter topology.*

Since the matrix converter directly connects the output voltage to the input voltage, via the bidirectional switches, the target output voltage can never exceed the continuous input voltage envelope which is made of the upper and lower bound of the input three-phase voltage. The input phase voltage is defined as in equation (3.1).

$$\begin{bmatrix} v_r(t) \\ v_s(t) \\ v_t(t) \end{bmatrix} = \begin{bmatrix} \hat{V}_i \cos(\omega_i t) \\ \hat{V}_i \cos(\omega_i t - \frac{2\pi}{3}) \\ \hat{V}_i \cos(\omega_i t + \frac{2\pi}{3}) \end{bmatrix} \tag{3.1}$$

A three-phase AC voltage is represented in figure 3.3. The envelope of this voltage signal is shown with a bold red line for the upper bound and a bold green line for the lower bound. If the three phase signal in figure 3.3 represents the input voltage, then the target output voltage waveform must fit into the input voltage envelope. Let's define a voltage transfer ratio or modulation index q as:

$$q = \frac{\hat{V}_o}{\hat{V}_i} = \frac{V_o}{V_i} \tag{3.2}$$

The already-mentioned limitation that the output peak-to-peak voltage can never exceed the difference between two input phase voltages can be translated into equation (3.3) if we define IVLB(t) and IVUB(t) as the input voltage lower and upper bound, and OVLB(t) and OVUB(t) as the output voltage lower and upper bound. The output bounds must be contained within the input bounds.

$$IVLB(t) \leq OVLB(t) \leq OVUB(t) \leq IVUB(t) \tag{3.3}$$

The maximum possible voltage ratio is obtained when the maximum output voltage range coincide with the minimum input voltage:

$$\min_{0 \leq \omega_{in} t \leq 2\pi} (IVUB(t) - IVLB(t)) = \max_{0 \leq \omega_o t \leq 2\pi} (OVUB(t) - OVLB(t)) \tag{3.4}$$

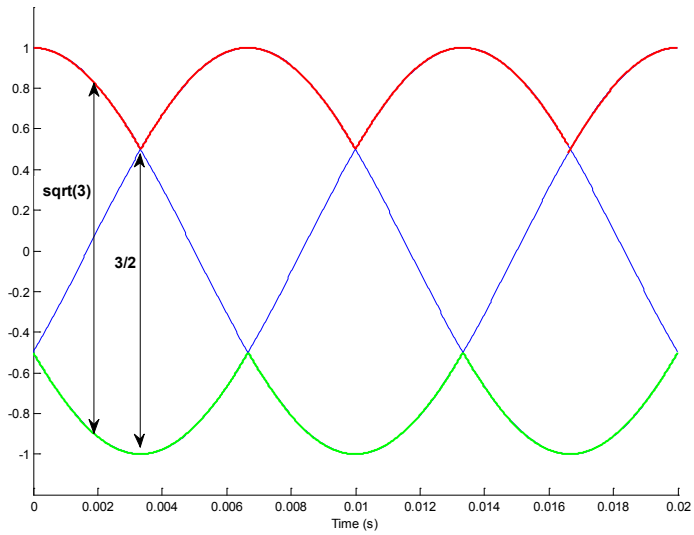

Figure 3.3: *Three-phase AC voltage with amplitude of 1 with $f = 50Hz$ and its envelope in a red bold line (upper bound) and green bold line (lower bound).*

For a sinusoidal three-phase voltage system, the maximum range of voltage (from lower peak to upper peak) is $\sqrt{3}$ of the phase voltage amplitude and the minimum range is 3/2 of the phase voltage amplitude, both indicated in figure 3.3. Hence, in the case of sinusoidal three-phase input and output voltages, relation (3.4) becomes:

$$3/2\hat{V}_i = \sqrt{3}\hat{V}_o \tag{3.5}$$

which corresponds to the maximum voltage (amplitude or rms-value alike) transfer ratio:

$$q_{max} = \frac{\hat{V}_o}{\hat{V}_i} = \frac{V_o}{V_i} = \frac{\sqrt{3}}{2} \cong 0.866 \tag{3.6}$$

A maximum transfer ratio of $q_{max} = 0.866$ is valid in the case of unity power factor at the input. When q_{max} is exceeded, overmodulation mode is entered and the input current and output voltage will contain more harmonics [17]. Furthermore if there is a displacement angle of Φ_{in} between the input voltage and the input current, the voltage transfer ratio is further reduced to:

$$q_{max,\Phi} = q_{max}\cos(\Phi_i) = \frac{\sqrt{3}}{2}\cos\Phi_i \tag{3.7}$$

See [4] for a thorough explanation. We will also come back to this in section 3.2.1.

3.2 Conventional indirect space vector modulation

There are several ways to modulate a converter: Carrier-based PWM and space vector modulation being the most common. The modulation is done on a single-phase basis in carrier-based PWM modulation. Because of this, the maximum input to output voltage ratio is 0.5 if no measures, like third harmonic injection in the reference voltage, are taken to increase the ratio. The maximum output voltage contained in the band delimited by the red line for carrier-based PWM is shown in figure 3.4. The output voltage cannot exceed the red lines because then there is a risk that no input voltage is available to build the output voltage.

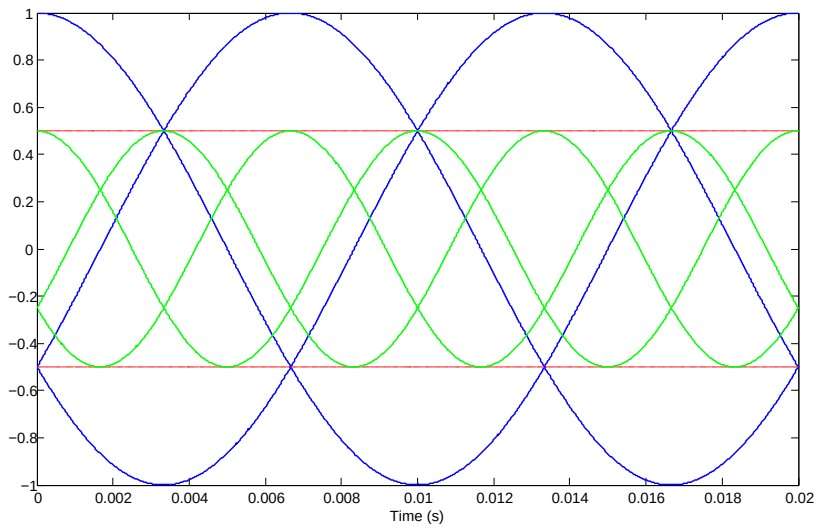

Figure 3.4: *The input voltage (in blue) and the maximum output voltage (in green) for carrier-based PWM.*

Space vector modulation technique is inspired by motor drive control and contrary to carrier-based modulation, it considers all three phases as one. Hence the maximum transfer ratio of 0.866 can be obtained without third harmonic injection or other measures that would add complexity. As was already mentioned, for modulating the matrix converter's output voltage and input current, virtual indirect control is used. We consider the matrix converter as being build up of two virtual parts: a CSR and a VSI. The modulating signals that would provide for the switches of each converter part are built with two independant space vector modulation blocks and then with a logic circuit the signals for the matrix converter are formed. We will first start by explaining the space vector modulation of the VSI part and then continue with the CSR part of the matrix converter. First a common angle measurement reference should be instaured for clarity. The reference when measuring angles is defined from now to be the input voltage which was defined in equation (3.1).

3.2.1 Space vector modulation of the VSI

A VSI is represented in figure 3.5.

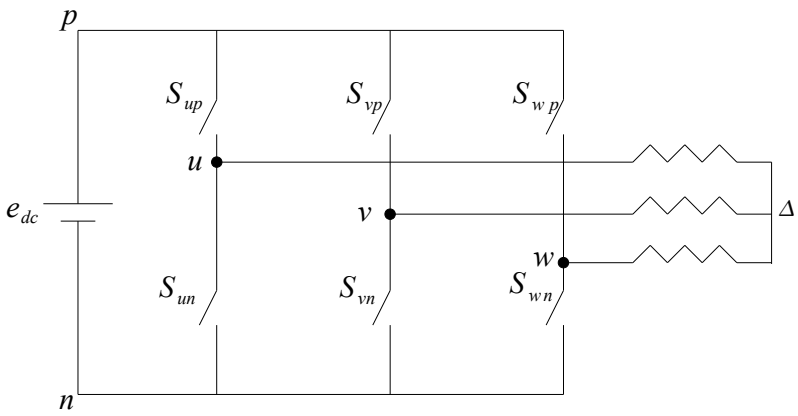

Figure 3.5: *The voltage source inverter part of the matrix converter.*

e_{dc} is the virtual DC link voltage which is assumed constant. The converter is made up of three poles, each connected to one of the three output phase, u, v or w. We define Δ as the isolated neutral on the load side, n the negative side of the DC link and p as the positive side of the DC link. The switches are named like in previous nomenclature. We assume that the three-phase resistive load is balanced so that we get the following equalities for the output phase voltages and output currents:

$$v_{u\Delta}(t) + v_{v\Delta}(t) + v_{w\Delta}(t) = 0 \tag{3.8}$$

$$i_u(t) + i_v(t) + i_w(t) = 0 \tag{3.9}$$

We define a space vector $\vec{v}_{o,sp}$ in terms of the output phase voltages such that:

$$\vec{v}_{o,sp}(t) = v_{u\Delta}(t) + v_{v\Delta}(t)e^{(j\frac{2\pi}{3})} + v_{w\Delta}(t)e^{(j\frac{4\pi}{3})} \tag{3.10}$$

The output phase voltages being:

$$v_{u\Delta}(t) = \hat{V}_o \cos(\omega_o t - \xi) \tag{3.11}$$

$$v_{v\Delta}(t) = \hat{V}_o \cos(\omega_o t - \frac{2\pi}{3} - \xi) \tag{3.12}$$

$$v_{w\Delta}(t) = \hat{V}_o \cos(\omega_o t + \frac{2\pi}{3} - \xi) \tag{3.13}$$

The angle ξ is measured with respect to the input voltage as previously defined. the angle ξ can be set to zero right away, assuming that that the output voltage should be in phase with the input voltage. Let's insert equations (3.11), (3.12) and (3.13) into the equation (3.10) of the output phase voltage space vector.

$$\vec{v}_{o,sp}(t) = \hat{V}_o \cos(\omega_o t) + \hat{V}_o \cos(\omega_o t - \frac{2\pi}{3})e^{(j\frac{2\pi}{3})} + \hat{V}_o \cos(\omega_o t + \frac{2\pi}{3})e^{(j\frac{4\pi}{3})} \tag{3.14}$$

After some manipulation we obtain equation (3.15).

$$\vec{v}_{o,sp}(t) = \frac{3}{2}\hat{V}_o e^{j\omega_o t} \tag{3.15}$$

We see from equation (3.15) that the space vector has constant length $\frac{3}{2}\hat{V}_o$ and rotates at angular speed ω_o. An interesting feature of the output phase voltage space vector is that it is equal to the inverter pole voltage space vector which will prove very useful as we can use these two space vectors interchangeably.

$$\vec{v}_{sp,pole}(t) = v_{un}(t) + v_{vn}(t)e^{(j\frac{2\pi}{3})} + v_{wn}(t)e^{(j\frac{4\pi}{3})} \tag{3.16}$$

$$\vec{v}_{sp,pole}(t) = v_{u\Delta}(t) + v_{\Delta n}(t) + (v_{v\Delta}(t) + v_{\Delta n}(t))e^{(j\frac{2\pi}{3})} + (v_{w\Delta}(t) + v_{\Delta n}(t))e^{(j\frac{4\pi}{3})} \tag{3.17}$$

$$\vec{v}_{sp,pole}(t) = v_{u\Delta}(t) + v_{v\Delta}(t)e^{(j\frac{2\pi}{3})} + v_{w\Delta}(t)e^{(j\frac{4\pi}{3})} + v_{\Delta n}(t)\underbrace{(1 + e^{(j\frac{2\pi}{3})} + e^{(j\frac{4\pi}{3})})}_{=0} = \vec{v}_{o,sp}(t) \tag{3.18}$$

The inverter pole voltages $v_{un}(t)$, $v_{vn}(t)$ and $v_{wn}(t)$, between a phase and the negative side of the DC link, are either equal to 0 when the lower switch is ON or e_{dc} when it is OFF. In each of the three poles of the converter, the two switches are complementary, in order not to short-circuit the input or disconnect an output phase. This gives us $2^3 = 8$ switching states, all depicted in figure 3.6.

Two of these switching states (when all the upper switches are open [nnn] or closed [ppp]) will yield space vectors equal to zero, called zero vectors because the output phases are short-circuited. The 6 other space vectors corresponding to the six remaining switching states are all different from zero and are called active vectors. They are fixed directions vectors and in the complex plane, they are distributed as shown in figure 3.7.

Let's take an active vector, $\vec{u}_{pnn}$ and see how it is build. The switching state corresponding to $\vec{u}_{pnn}$ is as indicated in figure 3.7, [pnn], which indicates that for phase u the upper switch S_{up} is ON, for phase v the lower switch S_{vn} is ON and for phase w the lower switch S_{wn} is ON. Hence the pole voltages are as follow:

$$v_{un}(t) = e_{dc} \tag{3.19}$$

$$v_{vn}(t) = 0 \tag{3.20}$$

$$v_{wn}(t) = 0 \tag{3.21}$$

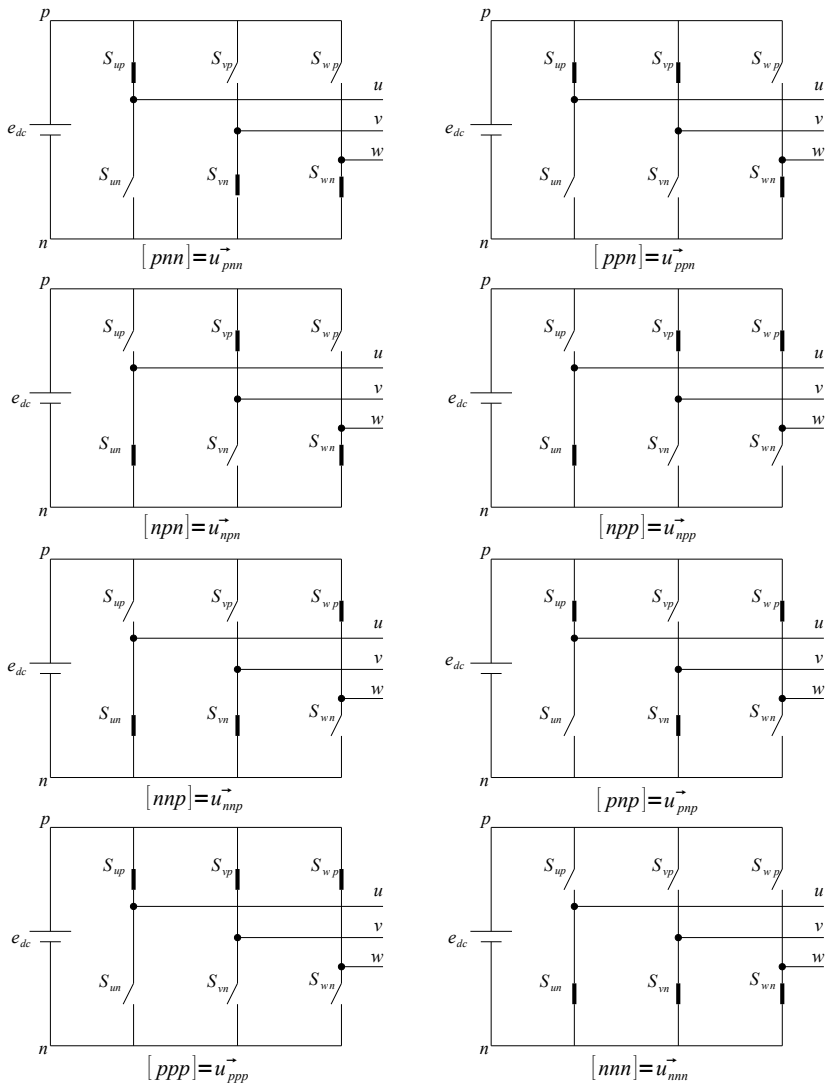

Figure 3.6: *The eight switching states of the virtual VSI part of the matrix converter made of the six active vectors and the two zero vectors (bottom two).*

We can insert equation (3.19), (3.20) and (3.21) into equation (3.17) to obtain:

$$\vec{v}_{sp,pole} = \vec{v}_{o,sp} = e_{dc} + 0e^{(j\frac{2\pi}{3})} + 0e^{(j\frac{4\pi}{3})} = e_{dc} \tag{3.22}$$

Here the property previously shown, that the space vector of the pole voltages is equal to the space vector of the output phase voltage is used. The other active vectors can be computed in a similar manner. The active vectors delimit 6 so-called sectors also indicated in figure 3.7. An updated reference space vector $\vec{v}_{o,sp}$ is calculated every time intervall T_s, which is the switching period. As the reference space vector $\vec{v}_{o,sp}(t)$ sweeps along the sectors at an angular speed of ω_o, every T_s when it is recalculated, it is considered having

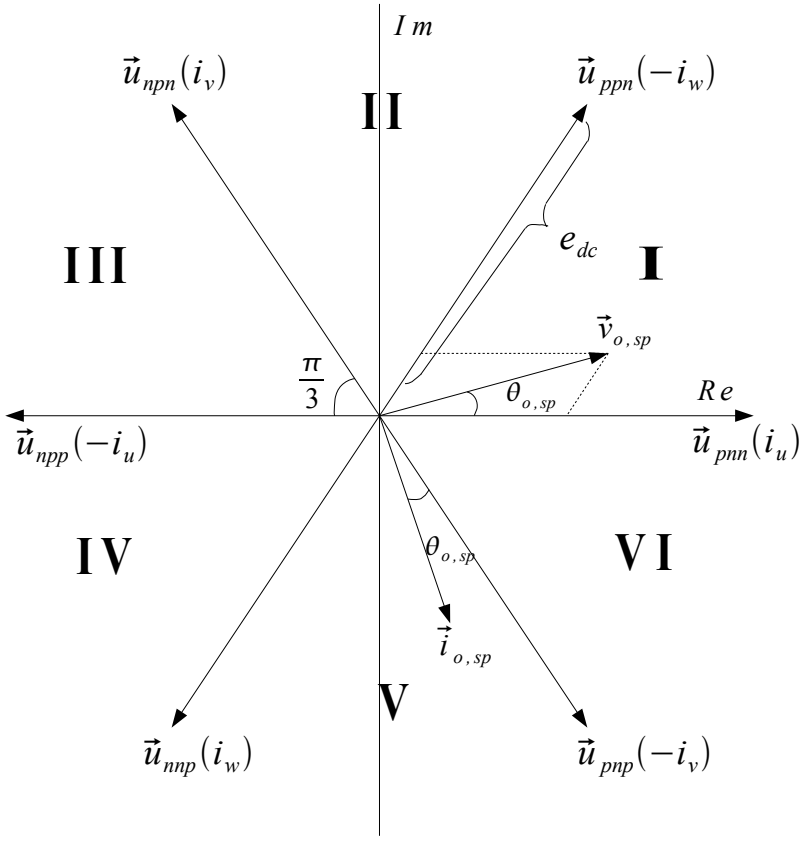

Figure 3.7: *The voltage active space vectors represented in the complex plane.*

constant direction (constant angle) throughout the switching period T_s and we define the angle $\theta_{o,sp}$ as the angle that $\vec{v}_{o,sp}$ forms with the real axis at the instant the space vector is calculated. The angle is indicated in figure 3.7.

$$\vec{v}_{o,sp} = \frac{3}{2}\hat{V}_o e^{j\theta_{o,sp}} \tag{3.23}$$

The space vector $\vec{v}_{o,sp}$ is build with the adjacent vectors of the sector where it lies, $\vec{u}_x$, $\vec{u}_y$ and one of the zero vectors $\vec{u}_z$ if the reference space vector $\vec{v}_{o,sp}$ does not have the maximum possible length. Later in this section will be seen what this maximum possible length is. The desired space vector, $\vec{v}_{o,sp}$, is synthesized by applying $\vec{u}_x$, $\vec{u}_y$ and $\vec{u}_z$ for respective time intervalls T_x, T_y and T_z. Let's calculate the gate-timing intervalls for sector I, see figure 3.8.

$$\int_0^{T_s} \vec{v}_{o,sp}(t)dt = \int_0^{T_{pnn}} \vec{u}_{pnn}dt + \int_{T_{pnn}}^{T_{pnn}+T_{ppn}} \vec{u}_{ppn}dt \tag{3.24}$$

$$\int_0^{T_s} \frac{3}{2}\hat{V}_o e^{j\theta_{o,sp}}dt = \int_0^{T_{pnn}} \vec{u}_{pnn}dt + \int_{T_{pnn}}^{T_{pnn}+T_{ppn}} \vec{u}_{ppn}dt \tag{3.25}$$

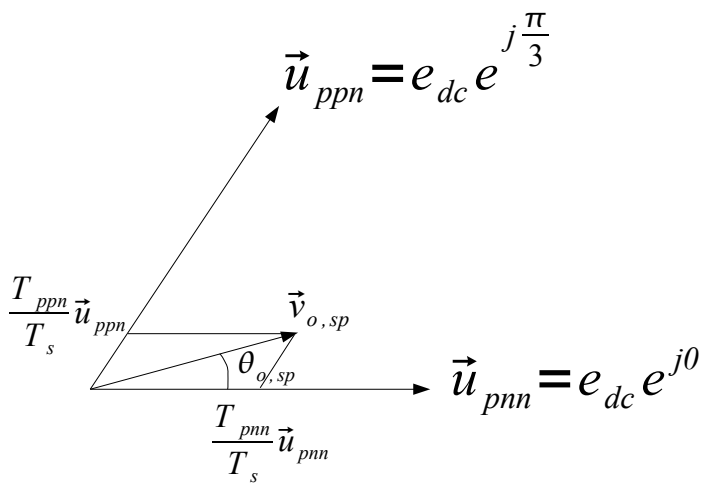

Figure 3.8: *Switch gating times calculation for sector I.*

$$T_s \frac{3}{2}\hat{V}_o \begin{bmatrix} \cos\theta_{o,sp} \\ \sin\theta_{o,sp} \end{bmatrix} = T_{pnn} e_{dc} \begin{bmatrix} 1 \\ 0 \end{bmatrix} + T_{ppn} e_{dc} \begin{bmatrix} \cos\frac{\pi}{3} \\ \sin\frac{\pi}{3} \end{bmatrix} \tag{3.26}$$

We get the following relations (3.27) and (3.28), by solving the two equations in (3.26) and introducing the voltage ratio index that was defined for the matrix converter, $q = \frac{\hat{V}_o}{\hat{V}_i}$ with $0 \leq q \leq q_{max,\Phi}$.

$$T_{pnn} = T_s \frac{3}{2} \frac{\hat{V}_o \sin(\frac{\pi}{3} - \theta_{o,sp})}{e_{dc} \sin\frac{\pi}{3}} = T_s \frac{3}{2} \frac{q\hat{V}_i \sin(\frac{\pi}{3} - \theta_{o,sp})}{e_{dc} \sin\frac{\pi}{3}} \tag{3.27}$$

$$T_{ppn} = T_s \frac{3}{2} \frac{\hat{V}_o \sin\theta_{o,sp}}{e_{dc} \sin\frac{\pi}{3}} = T_s \frac{3}{2} \frac{q\hat{V}_i \sin\theta_{o,sp}}{e_{dc} \sin\frac{\pi}{3}} \tag{3.28}$$

Finally if the length of the desired space vector $\vec{v}_{o,sp}$ does not have the maximum possible length, q is not set to be $q_{max,\Phi}$, there will remain some unused time in the switching periode T_s. A zero vector must be applied since they are the only vectors that will not modify the output voltage.

$$T_z = T_s - T_{pnn} - T_{ppn} \tag{3.29}$$

Now let's extend these gating times to the other sectors. Sector I spreads from 0 to 60°, sector II from 60° to 120°, sector III from 120° to 180°, etc. If the reference space vector $\vec{v}_{o,sp}$ is located in sector II it is the angle between $\vec{u}_{ppn}$ and $\vec{v}_{o,sp}$ that is useful for calculating T_{ppn}, T_{npn} and T_z and not $\theta_{o,sp}$, which is the angle between the real axis and $\vec{v}_{o,sp}$. Hence 60°, the angle of sector I, has to be substracted from $\theta_{o,sp}$ in order to use the same equations (3.27), (3.28) and (3.29). The same can be done for the other sectors and a generalized expression of the gate-timing interval T_x(for applying $\vec{u}_x$ lower bound of the sector), T_y(for applying the upper bound $\vec{u}_y$ of the sector) and T_z can be found for all the sectors.

$$T_x = T_s \frac{3}{2} \frac{q\hat{V}_i \sin(\frac{\pi}{3} - (\theta_{o,sp} + ROTATION))}{e_{dc} \sin\frac{\pi}{3}} \tag{3.30}$$

$$T_y = T_s \frac{3}{2} \frac{q\hat{V}_i \sin(\theta_{o,sp} + ROTATION)}{e_{dc} \sin \frac{\pi}{3}} \tag{3.31}$$

$$T_z = T_s - T_x - T_y \tag{3.32}$$

The angle $\theta_{o,sp}$ is always comprised between $-180\,^\circ$ and $180\,^\circ$ in the build MATLAB Simulink model, so for sector I,II and III, the needed rotation is $ROTATION = -60\,^\circ \cdot (sector - 1)$ and for sector IV, V and VI the rotation is $ROTATION = +60\,^\circ \cdot (7 - sector)$.

To apply this VSI modulation for the matrix converter, the DC link voltage e_{dc}, that appears in equation (3.30) and (3.31), still needs to be computed in order to calculate the switch gating times. To do that, we will use the fact that in the indirect matrix converter the DC link voltage e_{dc} is the middle stage of the converter and that the input power is equal to the DC link power. Remember however that for the direct matrix converter the DC link is only virtual.

$$P_i = \frac{3}{2} \hat{V}_i \hat{I}_i \cos \Phi_i = P_{dc} = e_{dc} i_{dc} \tag{3.33}$$

$$e_{dc} = \frac{3}{2} \frac{\hat{V}_i \hat{I}_i \cos \Phi_i}{i_{dc}} \tag{3.34}$$

The current ratio of the CSR part, $\frac{\hat{I}_i}{i_{dc}}$, will be fixed to 1. This is actually the maximum possible current ratio for the CSR as we will see in section 3.2.2. By fixing the current ratio, the independant control of the input current amplitude is lost and will depend on the voltage transfer ratio, see section 3.2.2. There is independent control of three variables in the matrix converter: the output voltage magnitude $\hat{V}_o$ and phase angle ξ and the input displacement angle Φ_i.

$$e_{dc} = \frac{3}{2} \hat{V}_i \cos \Phi_i \tag{3.35}$$

In a space vector controlled VSI, the maximum output phase voltage obtainable without entering overmodulation mode and hence adding a lot of harmonics to the output voltage, is $\hat{V}_{o,max} = \frac{e_{dc}}{\sqrt{3}}$ [17]. This limit can be understood by geometrical considerations. In the complex plane the space vector cannot exceed the circle μ that has radius equal to the length of the bissectrice of the triangle formed by the active vectors, that is $\hat{V}_{o,sp,max} = e_{dc} \cos \frac{\pi}{6} = \frac{\sqrt{3}}{2} e_{dc}$, see figure 3.9. Hence when the space vector of the output voltage has length equal to $\frac{\sqrt{3}}{2}$, the limit between the linear modulation region and overmodulation region is reached. The reason can be shown with the example illustrated in figure 3.9: when the space vector has length like the bissectrice of the sector, just like is depicted in figure 3.9, the two active vectors will be applied for half of the switching period, and the zero vectors will not be applied at all. This linear modulation/overmodulation limit corresponds to equation (3.36) and (3.37).

$$T_s = T_1 + T_2 \tag{3.36}$$

$$T_z = 0 \tag{3.37}$$

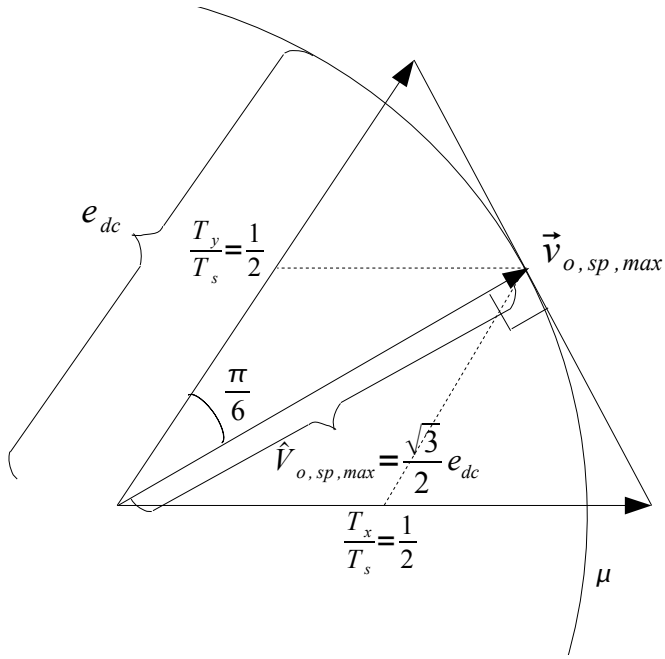

Figure 3.9: *Maximum length of the reference space vector.*

The space vector amplitude can be converted back to the output phase voltage amplitude with equation (3.38) to find the well-known VSI modulation index limit.

$$\hat{V}_{o,sp} = \frac{3}{2}\hat{V}_o \tag{3.38}$$

$$\frac{3}{2}\hat{V}_{o,max} = \frac{\sqrt{3}}{2}e_{dc} \tag{3.39}$$

$$\hat{V}_{o,max} = \frac{1}{\sqrt{3}}e_{dc} \tag{3.40}$$

If the reference space vector is further increased above the modulation limit, the sum of gate-timing intervals for the active vectors will be more than one. The zero vector gate-timing interval will be negative. It is obviously not possible to apply a switching state for a negative time interval, but this translate into the switching cycle being abruptly ended. Because of this, when reaching overmodulation mode, the output voltage can no longer vary proportionally with the reference space vector voltage as it did in the linear modulation range. The output voltage can no longer be controlled with the modulation index q. To verify the maximum modulation index from equation (3.7), we insert the equation (3.35) for the DC link voltage into equation (3.40).

$$\hat{V}_{o,max} = \frac{1}{\sqrt{3}}\frac{3}{2}\hat{V}_i \cos\Phi_i \tag{3.41}$$

$$\frac{\hat{V}_{o,max}}{\hat{V}_i} = \frac{\sqrt{3}}{2}\cos\Phi_i = q_{max}\cos\Phi_i = q_{max,\Phi} \tag{3.42}$$

Just like the VSI, the matrix converter modulation is separated into a linear modulation range and an overmodulation range. Since the modulation index of the CSI is fixed to its maximum, it will not affect the modulation index of the matrix converter. The limit is $q_{max} = \frac{\sqrt{3}}{2}$ for unity power factor.

Now that everything needed to calculate the gate-timing intervals has been provided we need to look at the sequence in which the vectors or switching states are going to be applied within a switching period T_s. We have already seen that the section in which the reference space vector lies will decide the active vectors to be applied. There are switching patterns in which it is not the adjacent active vectors that are applied but these sequences produce higher THD (Total Harmonic Distortion) and/or switching losses, so they have not been considered here [18]. There are many different possible switching patterns and they can differ on the following characteristics [18]:

- the choice of which zero vector to apply during the switching period, $\vec{u}_7$, $\vec{u}_8$ or both;
- the choice of whether to split the switch gating time intervalls or not;
- the choice of the sequence in which to apply the two active vectors and the chosen zero vector(s).

All these choices are important as they affect the THD in the output current and voltage as well as the switching losses [18]. It was decided to use a symmetric sequence for the modulation of VSI. Each active switching state is applied twice for half the switch-gating time interval calculated, and both zero vectors are applied during a switching period, see figure 3.10. This yields a total of 6 commutations which is more than for other patterns where the switching states are not applied twice, however this symmetric pattern seems to create lower THD [18]. There is hence a trade-off between switching losses and THD.

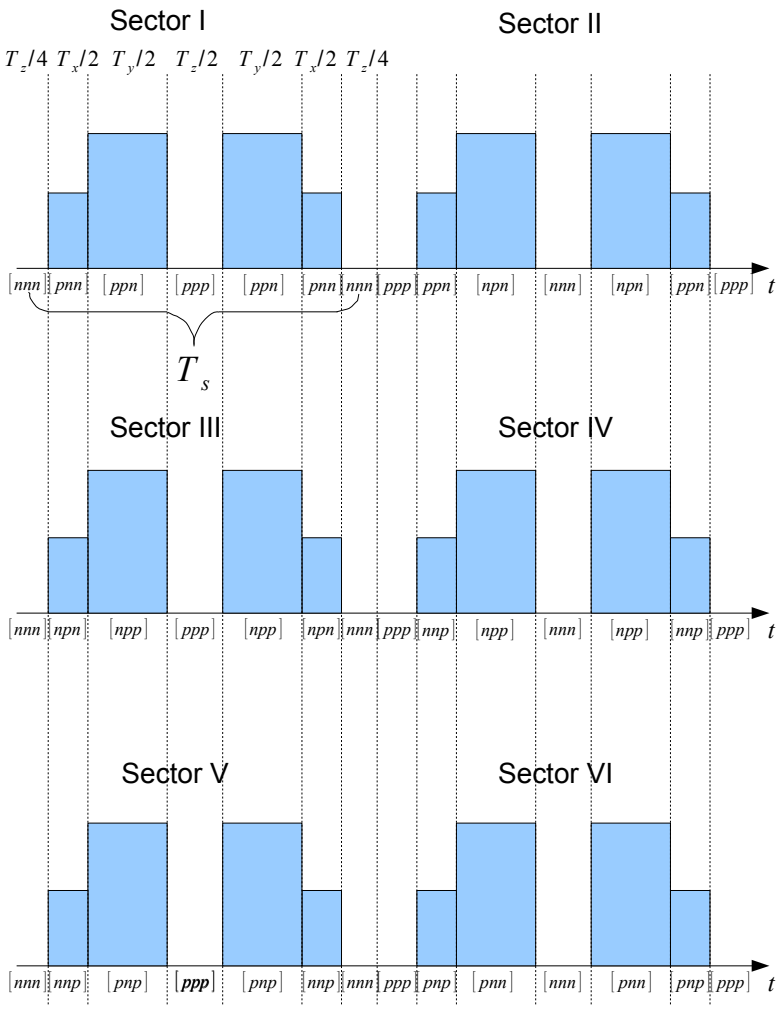

Figure 3.10: *The sequence of the switching states in the virtual VSI part.*

3.2.2 Space vector modulation of the CSR

The space vector modulation of the virtual CSR part of the matrix converter, see figure 3.11, is very similar to the modulation of the VSI part. Hence the description of the modulation will be succinct.

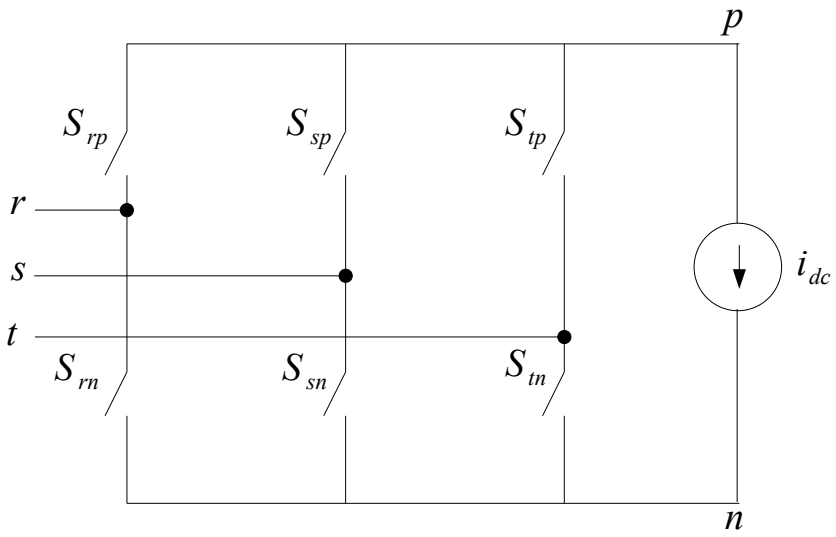

Figure 3.11: *The current source rectifier part of the matrix converter.*

The main difference in the two modulations is that the input phase currents,

$$i_r(t) = \hat{I}_i \sin(\omega_i t - \Phi_i) \tag{3.43}$$

$$i_s(t) = \hat{I}_i \sin(\omega_i t - \frac{2\pi}{3} - \Phi_i) \tag{3.44}$$

$$i_t(t) = \hat{I}_i \sin(\omega_i t + \frac{2\pi}{3} - \Phi_i) \tag{3.45}$$

are the parameters we want to control. The phase angle Φ_i is measured with respect to the input voltage and is thus the input phase displacement. We will control them with a single space vector reference, as was done for the VSI part, which is defined in equation (3.46).

$$\vec{i}_{i,sp}(t) = i_r(t) + i_s(t)e^{(j\frac{2\pi}{3})} + i_t(t)e^{(j\frac{4\pi}{3})} \tag{3.46}$$

After inserting (3.43), (3.44) and (3.45) into (3.46) and after some manipulations we get the equation (3.47) that gives the reference space vector to be fed into the CSR modulation block.

$$\vec{i}_{i,sp}(t) = \frac{3}{2}\hat{I}_i e^{j\underbrace{(\omega_i t - \Phi_i)}_{\theta_{i,sp}(t)}} \tag{3.47}$$

The CSR has $3^2 = 9$ switching states as only one of the upper switches (S_{rp}, S_{sp} or S_{tp}) and only one of the lower switches should be ON at any time (S_{rn}, S_{sn} or S_{tn}). At least one because the current always must have a path to flow in and no more than one to avoid short-circuiting the input voltages. The switching states are all presented in figure 3.12.

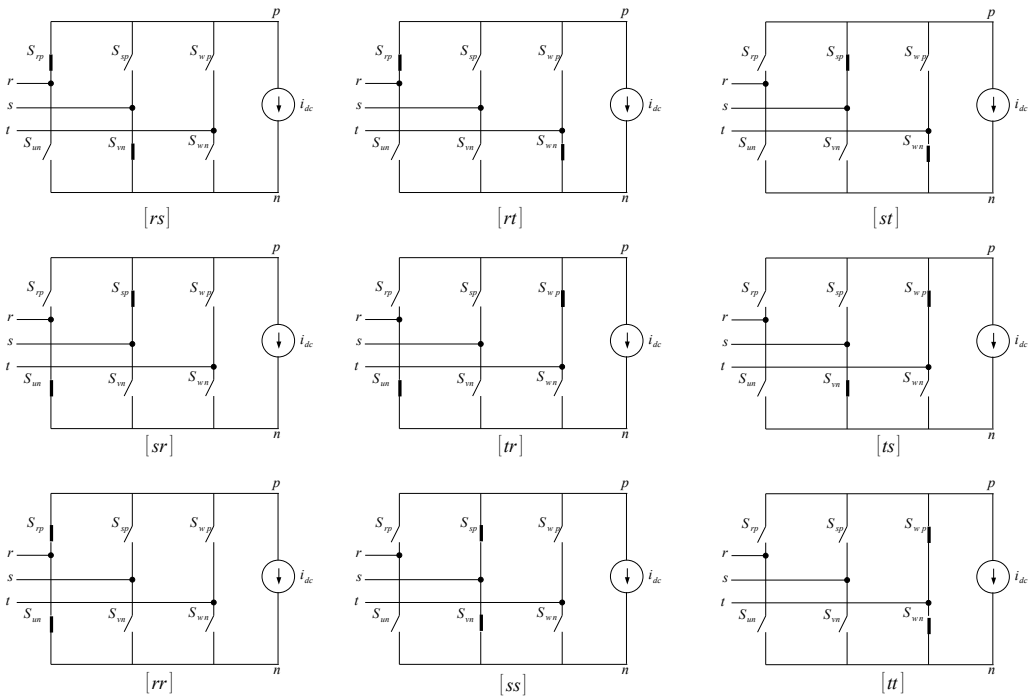

Figure 3.12: *The nine switching states of the vitual CSR part of the matrix converter.*

Among the nine switching states there are 6 that correspond to active vectors, distributed in the complex plane as in figure 3.13 and 3 that correspond to zero vectors. The zero vectors correspond to switching states where the two switches that are connected to the same input phase are ON at the same time. Let's look at $[rr]$ for instance. S_{rp} and S_{rn} are ON at the same time and hence:

$$i_r(t) = i_{dc} = -i_{dc} \tag{3.48}$$

To satisfy equation (3.48), $i_r(t)$ must be equal to zero. We also have:

$$i_s(t) = 0 \tag{3.49}$$

$$i_t(t) = 0 \tag{3.50}$$

Hence the space vector corresponding to the switching state $[rr]$ is 0, see equation (3.51).

$$\vec{i}_{i,sp}(t) = 0 + 0e^{(j\frac{2\pi}{3})} + 0e^{(j\frac{4\pi}{3})} = 0 \tag{3.51}$$

Let's also look at an active vector and see how it is built, for instance $[rs]$. The switching state $[rs]$ corresponds to the active vector $\vec{i}_{rs}$. S_{rp} and S_{sn} are ON and the closed path that is formed is conducting the input phase current $i_r(t) = -i_t(t)$ that is also corresponding to the virtual DC link current, i_{dc}. We can then write:

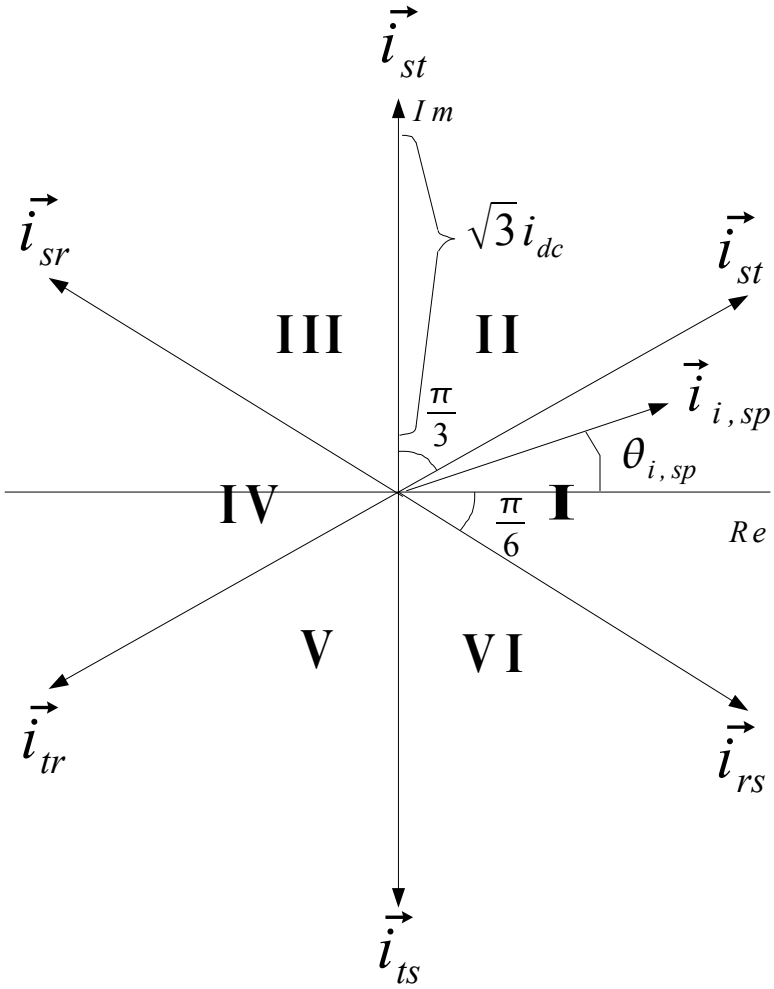

Figure 3.13: *The current active vectors in the complex plane.*

$$i_r(t) = i_{dc} = -i_s(t) \tag{3.52}$$

$$i_t(t) = 0 \tag{3.53}$$

The space vector corresponding to this switching state $[rs]$ is:

$$\vec{i}_{rs} = i_{dc} - i_{dc}e^{j\frac{2\pi}{3}} + 0e^{j\frac{-2\pi}{3}} = i_{dc}(1 - e^{j\frac{2\pi}{3}}) = \sqrt{3}i_{dc}e^{-j\frac{\pi}{6}} \tag{3.54}$$

The other active vectors are calculated in a similar manner.

The formulas (3.27), (3.28) and (3.29), developed earlier in section 3.2.1 to calculate the switch-gating time intervals for the VSI switching states, can be used for the CSR. However as can be seen in figure 3.13 the space vector angle $\theta_{i,sp}$ is measured from the real axis which does not correspond to the lower active vector of sector I like it does for the VSI

active vector, see figure 3.7 in section 3.2.1. Therefore 30° need to be added to $\theta_{i,sp}$ in order to use equation (3.27), (3.28) and (3.29).

$$T_x = T_s \frac{3}{2} \frac{\hat{I}_i \sin(\frac{\pi}{3} - (\theta_{i,sp} + \frac{\pi}{6})}{\sqrt{3} i_{dc} \sin \frac{\pi}{3}} \tag{3.55}$$

$$T_y = T_s \frac{3}{2} \frac{\hat{I}_i \sin(\theta_{i,sp} + \frac{\pi}{6})}{\sqrt{3} i_{dc} \sin \frac{\pi}{3}} \tag{3.56}$$

$$T_z = T_s - T_x - T_y \tag{3.57}$$

The ratio $\frac{\hat{I}_i}{i_{dc}} = 1$ is fixed as was previously mentioned. Only $\theta_{i,sp} = \omega_i t - \Phi_i$ and consequently Φ_i are controlled. The ratio $\frac{\hat{I}_i}{i_{dc}} = 1$ is the maximum achievable current ratio in a CSR. The length of the bissectrice of the triangle formed by two adjacent active vectors is the maximum length of the space vector, just like for the VSI modulation. For the CSR modulation it is $\hat{I}_{i,sp,max} = \sqrt{3} i_{dc} \cos \frac{\pi}{6} = \frac{3}{2} i_{dc}$. The space vector amplitude can be converted back to the input phase current amplitude with equation (3.58).

$$\hat{I}_{i,sp,max} = \frac{3}{2} \hat{I}_{i,max} \tag{3.58}$$

$$\frac{3}{2} \hat{I}_{i,max} = \frac{3}{2} i_{dc} \tag{3.59}$$

$$\hat{I}_{i,max} = i_{dc} \tag{3.60}$$

The different vectors are also applied in a symmetric sequence shown in figure 3.14 during a switching period T_s. Just one zero vector is applied during a switching period unlike two for the VSI modulation. In addition it can be mentioned that since the ratio $\frac{\hat{I}_i}{i_{dc}}$ is set to the maximum possible value there will be no zero vector applied during the switching period.

It was mentioned earlier that the independent control of the input current amplitude was not possibe since the CSR current ratio $\frac{\hat{I}_i}{i_{dc}} = 1$ is fixed and that the input current amplitude will thus depend on the voltage transfer ratio. Let's now see how. The voltage modulation index was previously defined as:

$$q = \frac{\hat{V}_o}{\hat{V}_i} \tag{3.61}$$

with $q_{max} = \frac{\sqrt{3}}{2}$ being the absolute maximum for the modulation index. The maximum modulation index is reduced to $q_{max,\Phi} = q_{max} \cos \Phi_i$ when the input displacement angle is different from zero. Let's now introduce a new modulation index M that represents the liberty of control that remains after the modulation index has been corrected for the input displacement angle. M can vary freely between 0 and $\frac{\sqrt{3}}{2}$ no matter what the input power factor, $\cos \Phi_i$, is.

$$\hat{V}_o = M \cos \Phi_i \hat{V}_i \tag{3.62}$$

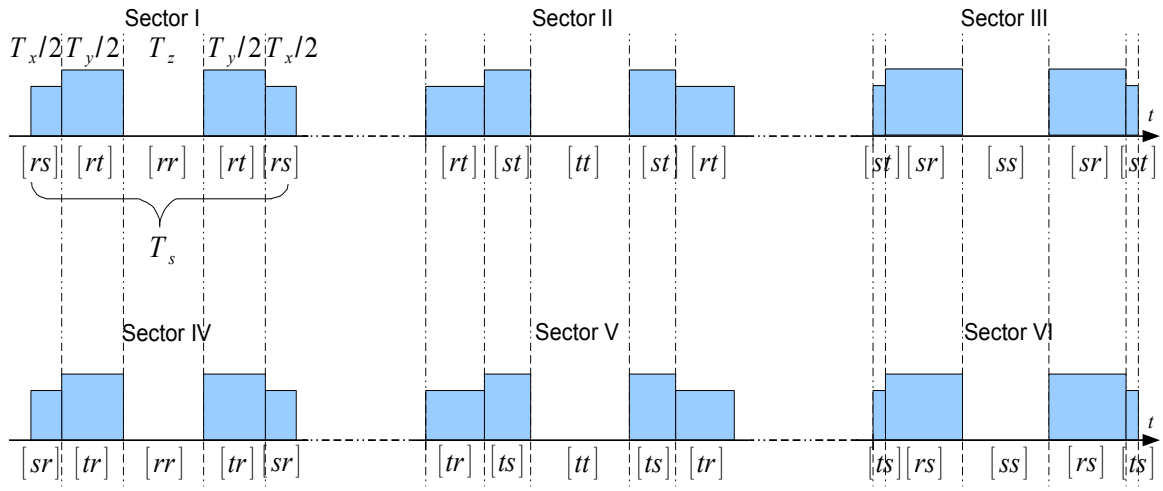

Figure 3.14: *The sequence of the switching states in the virtual CSR.*

$$\frac{\hat{V}_o}{\hat{V}_i} = q = M \cos \Phi_i \tag{3.63}$$

Let's see how M influences the current modulation by finding out how the VSI modulation influences the DC link current. The power balance equation gives the following.

$$P_{dc} = e_{dc} i_{dc} = P_o = \frac{3}{2} \hat{V}_o \hat{I}_o \cos \Phi_o \tag{3.64}$$

Equation (3.35) from section 3.2.1 can be inserted in equation (3.64) to find an expression for i_{dc}.

$$i_{dc} = \frac{\frac{3}{2} \hat{V}_o \hat{I}_o \cos \Phi_o}{\frac{3}{2} \hat{V}_i \cos \Phi_i} \tag{3.65}$$

Equation (3.63) can be inserted in equation (3.65)

$$\hat{I}_i = i_{dc} = \frac{M \cos \Phi_i \hat{I}_o \cos \Phi_o}{\cos \Phi_i} \tag{3.66}$$

$$\hat{I}_i = M \hat{I}_o \cos \Phi_o \tag{3.67}$$

Equation (3.67) mirrors equation (3.63) and indicates how the current magnitude ratio is dependent on the modulation index of the voltage modulation M and the output power factor $\cos \Phi_o$. To summarize, the operating range of the matrix converter is the following, with M varying freely between 0 and $\frac{\sqrt{3}}{2}$, but as a common set point or operating point for the current and voltage modulations, set by the voltage modulation index q:

$$\hat{V}_o = M \hat{V}_i \cos \Phi_i \tag{3.68}$$

$$\hat{I}_i = M \hat{I}_o \cos \Phi_o \tag{3.69}$$

This analysis will prove very useful in section 3.3 when the active and reactive power transfer capabilities of the matrix converter will be analyzed.

3.2.3 Combination of the VSI and CSR signals

Now that both modulations of the virtual VSI and CSR have been studied, we must combine the 12 switch-gating signals into 9 switch-gating signals that will provide the 9 switches of the matrix converter [11]. The logic circuit, used for the conversion, is shown in the simulation model of the MCRC device in figure B.2 in appendix B. The signals indicated in figure B.2 are named like the switches they correspond to, see figure 3.1 and figure 3.2 in section 3.1. For a more thourough explanation of the conversion logic circuit see [7].

3.3 Reactive and active power ranges with conventional space vector modulation

After having given a necessary presentation of the matrix converter and the indirect space vector modulation, we can get to the core of the matter. In this section the reactive compensation range of the matrix converter will be studied for the two following situations:

1. The matrix converter allows active power flow through it ($\Phi_i \neq \pm 90\,^\circ$ and $\Phi_o \neq \pm 90\,^\circ$) and the PM machine acts as an energy buffer;
2. The matrix converter does not allow any active power flow through it ($\Phi_i = \pm 90\,^\circ$ and $\Phi_o = \pm 90\,^\circ$), the PM machine runs at no load and the matrix converter provides pure reactive compensation.

3.3.1 $\Phi_i \neq \pm 90\,^\circ$ and $\Phi_o \neq \pm 90\,^\circ$

The reactive and active power transfers in an indirect matrix converter [10] are depicted in figure 3.15. Although the matrix converter is direct rather than indirect as in figure 3.15, it is a useful to visualize the matrix converter in this manner as it modulated like it is indirect. The virtual DC link clearly tranfers only active power according to equation (3.70).

$$P_{in} = P_{out} = P_{dc} = e_{dc} i_{dc} \tag{3.70}$$

The output reactive power depends on the load. For the MCRC system it will depend on the operation of the PM machine. The reactive power is created independantly at the input of the matrix converter and stems from a reactive power exchange between the phases via the switches of the converter [6] as is illustrated in figure 3.15. The magnitude range and polarity of the reactive power depends on the modulation technique used and the load power factor [6] as has been previously mentioned. When modulating the matrix converter with conventional indirect space vector modulation the reactive power and active power transfer are closely related. Let's calculate the relation between active and reactive power.

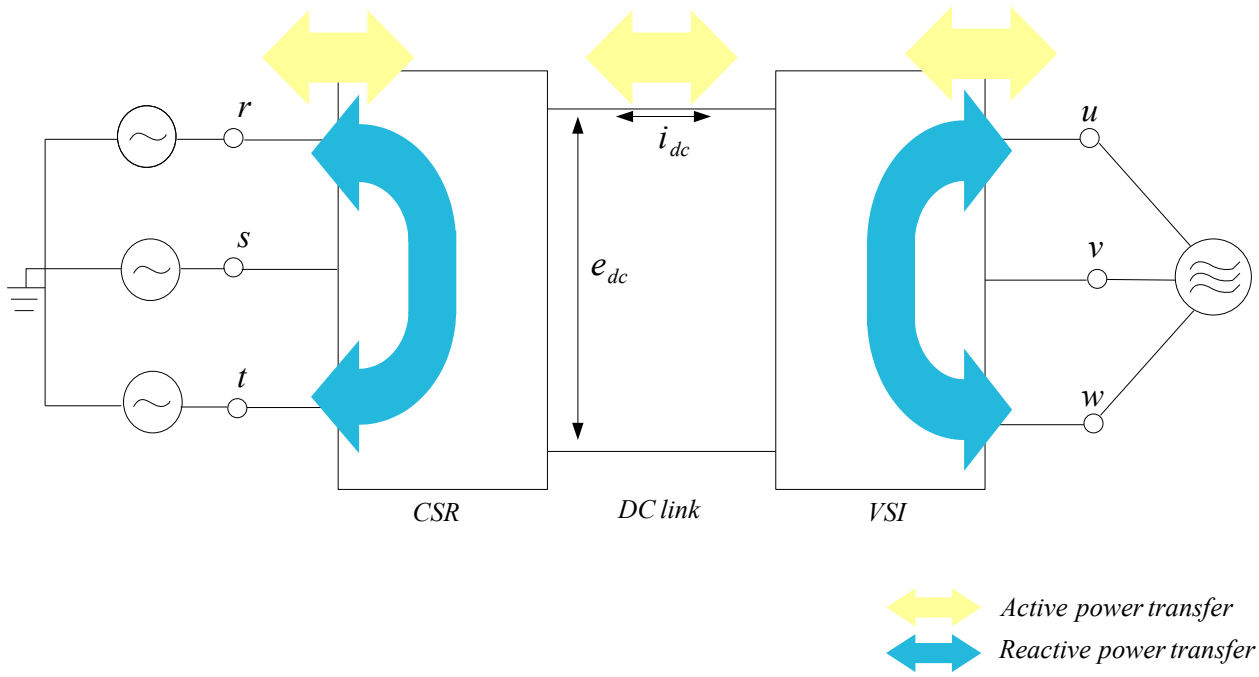

Figure 3.15: *The transfer of active and reactive power in an indirect matrix.*

The active power at the input of the matrix converter can be calculated as in equation (3.71).

$$P_i = \frac{3}{2}\hat{V}_i\hat{I}_i\cos\Phi_i \tag{3.71}$$

The reactive power at the input of the matrix converter can be calculated as in equation (3.72).

$$Q_i = \frac{3}{2}\hat{V}_i\hat{I}_i\sin\Phi_i = \frac{3}{2}\hat{V}_i\hat{I}_i\cos\Phi_i\frac{\sin\Phi_i}{\cos\Phi_i} \tag{3.72}$$

$$Q_i = P_i\tan\Phi_i \tag{3.73}$$

Equation (3.73) shows how the active and reactive powers are directly related to eachother through the tangent of the input displacement angle Φ_i.

Let's now investigate the reactive power compensation range as a function of the matrix converter parameters. We can insert equation (3.69), $\hat{I}_i = M\hat{I}_o\cos\Phi_o$ with $0 \leq M \leq \frac{\sqrt{3}}{2}$, into equation (3.71).

$$P_i = \frac{3}{2}M\hat{V}_i\hat{I}_o\cos\Phi_o\cos\Phi_i \tag{3.74}$$

Equation (3.69) and (3.74) can be inserted in equation (3.73)

$$Q_i = \frac{3}{2}M\hat{V}_i\hat{I}_o\cos\Phi_o\cos\Phi_i\tan\Phi_i \tag{3.75}$$

q and $\cos\Phi_i$ are related through the equation $q = \frac{\hat{V}_o}{\hat{V}_i} = M\cos\Phi_i$. So it is possible to write $\Phi_i = \cos^{-1}\frac{q}{M}$ and insert it in the expression of the active power (3.74) and the reactive power (3.75).

$$P_i = \frac{3}{2}M\hat{V}_i\hat{I}_o\cos\Phi_o\frac{q}{M} = \frac{3}{2}q\hat{V}_i\hat{I}_o\cos\Phi_o \tag{3.76}$$

$$Q_i = \frac{3}{2}M\hat{V}_i\hat{I}_o\cos\Phi_o\frac{q}{M}\tan\cos^{-1}\frac{q}{M} \tag{3.77}$$

Equation (3.77) can be simplified by using the trigonometric relation (3.78).

$$\tan\theta = \pm\sqrt{\sec^2\theta - 1} = \pm\sqrt{\frac{1}{\cos^2\theta} - 1} \tag{3.78}$$

The sign of the $\tan\theta$ depends on θ: If $\theta \geq 0$ then $\tan\theta \geq 0$ and if $\theta \leq 0$ then $\tan\theta \leq 0$ for $\theta \in [-\pi; \pi]$.

$$Q_i = \pm\frac{3}{2}M\hat{V}_i\hat{I}_o\cos\Phi_o\frac{q}{M}\sqrt{\frac{1}{\cos^2\cos^{-1}\frac{q}{M}} - 1} \tag{3.79}$$

$$Q_i = \pm\frac{3}{2}M\hat{V}_i\hat{I}_o\cos\Phi_o\frac{q}{M}\sqrt{\frac{1}{(\frac{q}{M})^2} - 1} \tag{3.80}$$

$$Q_i = \pm\frac{3}{2}M\hat{V}_i\hat{I}_o\cos\Phi_o\sqrt{1 - (\frac{q}{M})^2} \tag{3.81}$$

The input reactive power can be both negative and positive, according to the sign of Φ_i. This indicates that reactive power can be either provided or drawn by the matrix converter no matter the direction of the active power flow. Only the positive reactive power will be written from now. From equation (3.81), it is clear that for larger M the input reactive power is also larger. If the modulation index M is set to its maximum value of $\frac{\sqrt{3}}{2}$, we have $\cos\Phi_i = \frac{q}{\frac{\sqrt{3}}{2}}$ which is the maximum possible input displacement angle. This also an indication that the reactive power will be maximum.

$$Q_i = \frac{3\sqrt{3}}{4}\hat{V}_i\hat{I}_o\cos\Phi_o\sqrt{1 - (\frac{q}{\frac{\sqrt{3}}{2}})^2} \tag{3.82}$$

The corresponding active power which was found in equation (3.76) is:

$$P_i = \frac{3}{2}q\hat{V}_i\hat{I}_o\cos\Phi_o \tag{3.83}$$

In figure 3.16 and 3.17 are plotted the input active and reactive power ranges as functions of the modulation index q and the output power factor $\cos\Phi_o$ according to equation (3.82) and (3.83). The parameters $\hat{I}_o$ and $\hat{V}_i$ are set to constant values. It is clear from figure 3.16 and 3.17 that the input active and reactive powers are maximum for maximum output power factor, $\cos\Phi_o = 1$ ($\Phi_o = 0\,°$). However the active power is maximum for the normalized

modulation index $q_n = 1$ while the reactive power is maximum for $q_n = 0$. Oppositely the active power is zero for $q_n = 0$ while the reactive power is zero for $q_n = 1$. For zero output power factor $\cos\Phi_o = 0$ both active and reactive powers are zero.

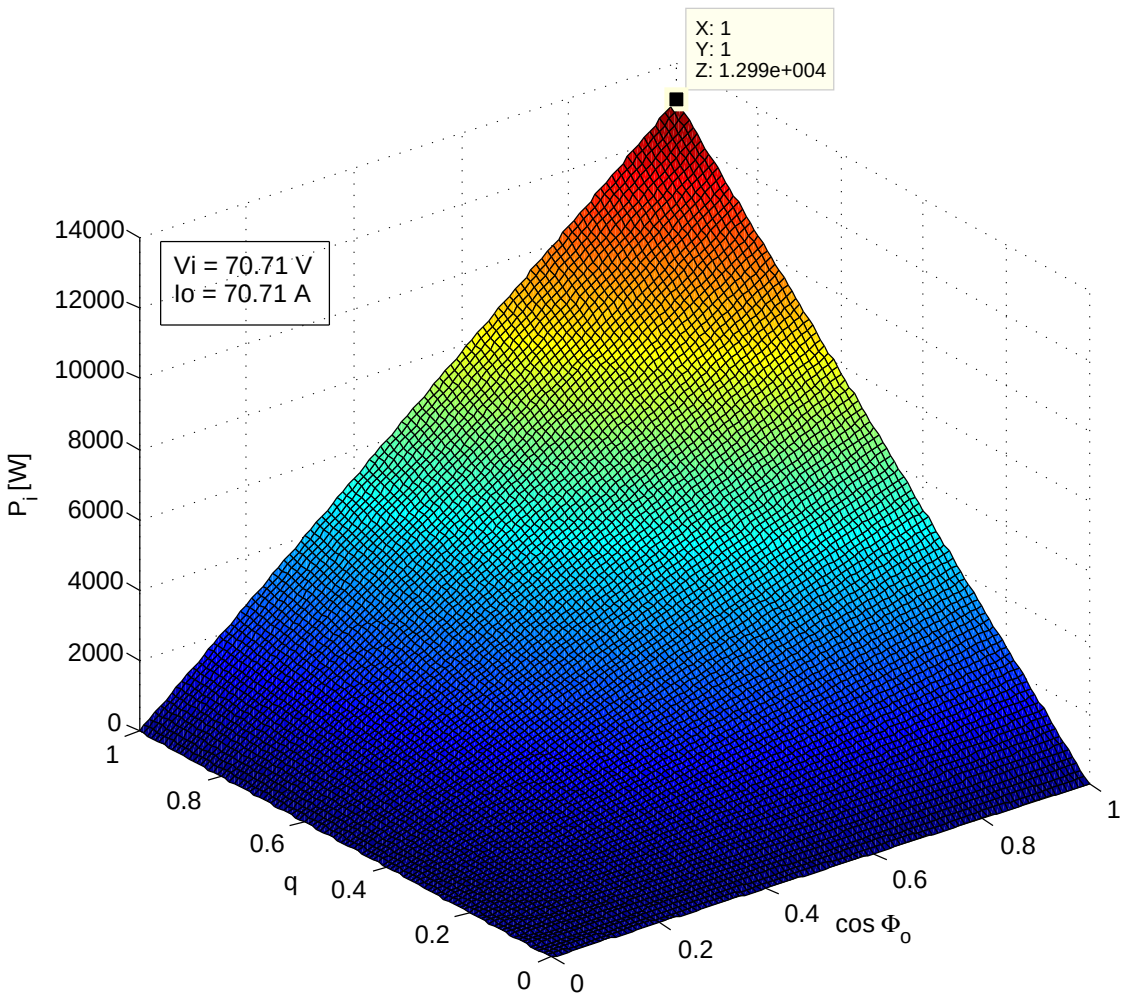

Figure 3.16: *The active power (in [W]) through the matrix converter as a function of the normalized modulation index* $q_n = \frac{q}{q_{max}} = \frac{2}{\sqrt{3}}\frac{\hat{V}_o}{\hat{V}_i}$, $q \in [0;1]$, *and the output power factor* $\cos\Phi_o$ *for constant output current magnitude* $\hat{I}_o = 100\,A$ *and constant input voltage* $\hat{V}_i = 100\,V$ *(The parameter values are indicated as RMS values in the graph).*

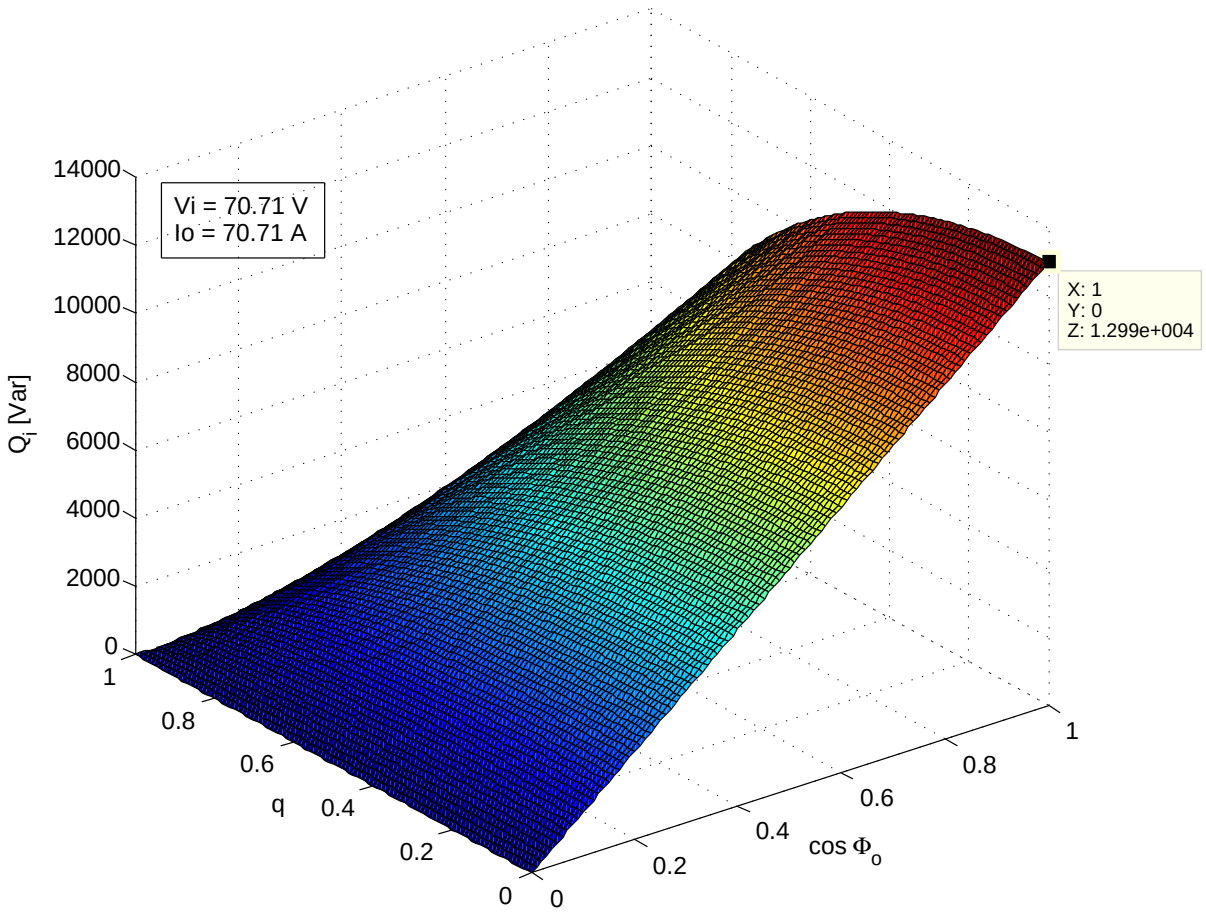

Figure 3.17: *The maximum reactive power (in [VAR]) at the input of the matrix converter as a function of the normalized modulation index* $q_n = \frac{q}{q_{max}} = \frac{2}{\sqrt{3}}\frac{\hat{V}_o}{\hat{V}_i}$, $q \in [0;1]$, *and the output power factor* $\cos\Phi_o$ *for constant output current magnitude* $\hat{I}_o = 100\,A$ *and constant input voltage* $\hat{V}_i = 100\,V$ *(The parameter values are indicated as RMS values in the graph).*

While an increasing output power factor gives increasing input active and reactive power, the modulation index has opposite effect on active and reactive power. An increasing modulation index yields increasing input active power but yields decreasing input reactive power. Because of this effect of the modulation index there is always a trade-off between active and reactive input power. This is due to the fact that the modulation index and the input power factor limit eachother according to the relation $q_{max} = \frac{\sqrt{3}}{2} = M\cos\Phi_i$. M increases the active power while $\cos\Phi_i$ increases the input reactive power at the input of the converter. However the product of these two parameters must remain constant equal to $\frac{\sqrt{3}}{2}$. To understand better this trade-off between active and reactive power, one of them should be expressed as a function of the other. This can be done by first taking the square of equations (3.82) and (3.83).

$$P_i^2 = \left(\frac{3}{2}q\hat{V}_i\hat{I}_o\cos\Phi_o\right)^2 \tag{3.84}$$

$$Q_i^2 = \left(\frac{3\sqrt{3}}{4}\hat{V}_i\hat{I}_o\cos\Phi_o\right)^2\left(1-\left(\frac{q}{\frac{\sqrt{3}}{2}}\right)^2\right) \tag{3.85}$$

$$Q_i^2 = \left(\frac{3\sqrt{3}}{4}\hat{V}_i\hat{I}_o\cos\Phi_o\right)^2 - \left(\frac{3\sqrt{3}}{4}\hat{V}_i\hat{I}_o\cos\Phi_o\right)^2\left(\frac{q}{\frac{\sqrt{3}}{2}}\right)^2 \tag{3.86}$$

$$Q_i^2 = \left(\frac{3\sqrt{3}}{4}\hat{V}_i\hat{I}_o\cos\Phi_o\right)^2 - \left(\underbrace{\frac{3\sqrt{3}}{4}\frac{2}{\sqrt{3}}\hat{V}_i\hat{I}_o\cos\Phi_o q}_{P_i}\right)^2 \tag{3.87}$$

In equation (3.86) the expression for the active power can be recognized and thus we can write expression (3.88) which is the equation of a circle centered at the origin and with radius $\frac{3\sqrt{3}}{4}\hat{V}_i\hat{I}_o\cos\Phi_o$ in the $P_i - Q_i$ plane as is depicted in figure 3.18:

$$Q_i^2 + P_i^2 = \left(\frac{3\sqrt{3}}{4}\hat{V}_i\hat{I}_o\cos\Phi_o\right)^2 = S_i^2 \tag{3.88}$$

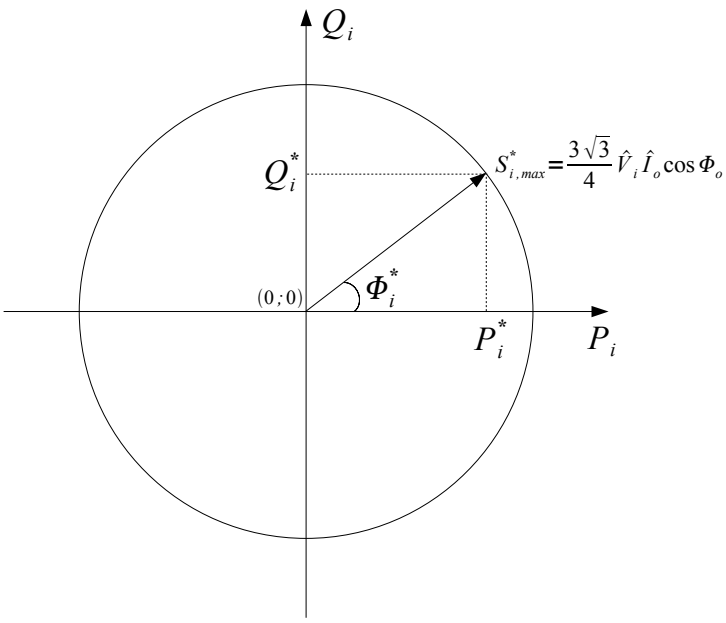

Figure 3.18: *The circle defining the maximum range of active and reactive power at the input of the matrix converter with radius equal to the available apparent power at the input of the matrix converter.*

The radius of the limit circle corresponds to the maximum apparent power available at the input of the matrix converter. S_i depends on the output power factor $\cos\Phi_o$, the input voltage V_i and the output current I_o. If V_i and I_o are set as constant parameters then S_i

depends only on $\cos\Phi_o$ and is maximum for unity power factor and zero for zero power factor. The reason for this is that when the output power factor is zero no current is transmitted to the input of the matrix converter (this phenomenon will be explained in the next section) and thus the apparent power is zero. Also, the circle representation shows clearly how the matrix converter can be operated in the four quadrants of the $P_i - Q_i$ plane. For instance for a given positive active power flow on the right hand side of the $P_i - Q_i$ plane, as in figure 3.18 the reactive power can be positive or negative depending on the sign of Φ_i.

In the case of the MCRC system there should be a speed control of the PM machine to keep the speed at a constant value. A d-q analysis can be used to build a controller for the PM synchronous machine [14]. When applying speed control both magnitude and phase angle of the terminal voltage will be modified in order to keep the speed at the reference value. Thus both q and $\cos\Phi_o$ will vary continously. Exactly how these parameters will vary is difficult to predict and will depend on disturbances and reference signal modifications. The property of the MCRC will also make $\vec{I_o}$ vary according to equation (2.5) in section 2.2 when the magnitude or the phase of the output voltage of the matrix converter are modified. Thus the three dimensional plots in figure 3.16 and 3.17 cannot be used as such for assessing the active and reactive power range of the MCRC system. In the matrix converter q, Φ_o and I_o are independant parameters, but when the PM machine is introduced in the MCRC system they become dependant according to the equations (2.10) and (2.11). Thus the active and reactive power ranges can be plotted in two dimensions, as a function of only q for instance, rather than in a three-dimensional plot by introducing the equations (2.10) and (2.11) for the output current and power factor into the expressions of the input active and reactive powers in the equations (3.82) and (3.83). The active power as a function of the modulation index q, the input voltage $\hat{V}_i$ and the excitation voltage magnitude $\hat{E}_f$ and angle δ is:

$$P_i = \frac{3}{2} q \hat{V}_i \hat{I}_o \cos\Phi_o \tag{3.89}$$

The corresponding maximum achievable input reactive power is:

$$Q_i = \frac{3\sqrt{3}}{4} \hat{V}_i \hat{I}_o \cos\Phi_o \sqrt{1 - \left(\frac{q}{\frac{\sqrt{3}}{2}}\right)^2} \tag{3.90}$$

with;

$$\hat{I}_o = \sqrt{\left(\frac{\hat{V}_o R - \hat{E}_f R\cos\delta + \hat{E}_f X_s \sin\delta}{R^2 + X_s^2}\right)^2 + \left(\frac{\hat{E}_f R\sin\delta - \hat{V}_o X_s + \hat{E}_f X_s \cos\delta}{R^2 + X_s^2}\right)^2} \tag{3.91}$$

and,

$$\cos\Phi_o = \cos\left(\tan^{-1}\left(\frac{\hat{E}_f R\sin\delta - \hat{V}_o X_s + \hat{E}_f X_s \cos\delta}{\hat{V}_o R - \hat{E}_f R\cos\delta + \hat{E}_f X_s \sin\delta}\right)\right) \tag{3.92}$$

These equations (3.89) and (3.90) will be useful in part II to compare the measured active power and maximum reactive power with the theoretical power ranges.

3.3.2 $\Phi_i = \pm 90\,^\circ$ and $\Phi_o = \pm 90\,^\circ$

In the special case of $\Phi_i = \pm 90\,^\circ$ and $\Phi_o = \pm 90\,^\circ$ there is no active power flow through the matrix converter. Let's first look at equation (3.73). The active power P_i is zero, however the term $\tan \Phi_i$ will diverge to infinity because $\Phi_i = \pm 90\,^\circ$. Therefore it is difficult to use equation (3.73) to determine the reactive power transfer in this particular case and one needs to go into the details of the space vector modulation and the internal mechanisms of the matrix converter to understand it.

In order to examine the capability of the matrix converter to transfer reactive power with zero power factor at the input and the output of the converter is to look at the influence of the CSR modulation on the virtual DC link voltage value and oppositely the influence of the VSI modulation on the virtual DC link current value.

The case of $\Phi_i = -90\,^\circ$ and $\Phi_o = 90\,^\circ$ will be considered here. However the conclusions can be generalized to $\Phi_i = \pm 90\,^\circ$ and $\Phi_o = \pm 90\,^\circ$. First we examine the impact of conventional CSR modulation on the virtual DC link voltage for $\Phi_i = -90\,^\circ$. In figure 3.19 are depicted the input voltage and input current space vectors $\vec{v}_{i,sp}$ and $\vec{i}_{i,sp}$ which are separated by a $\Phi_i = -90\,^\circ$ angle. The current space vector lies in sector III and it is therefore the active vectors $\vec{i}_{st}$ and $\vec{i}_{sr}$ that will be applied to build it. The duty ratios for applying $\vec{i}_{st}$ and $\vec{i}_{sr}$ are calculated as follow:

$$d_{st} = \sin(\frac{\pi}{3} - \theta_{i,sp}) \tag{3.93}$$

$$d_{sr} = \sin(\theta_{i,sp}) \tag{3.94}$$

Here the same equations (3.27) and (3.28) for the VSI modulation are used since the angle $\theta_{i,sp}$ is measured from the lower active vector $\vec{i}_{st}$ and not the bissectrice of the sector (see section 3.2.2). The duty ratios are the gating times divided by the switching period $d_x = \frac{T_x}{T_s}$.

Each time an active vector and its corresponding switching combination are applied in the CSR ($\vec{i}_{rs}$, $\vec{i}_{rt}$, $\vec{i}_{st}$...) a different input line voltage will be impressed on the DC link (v_{rs}, v_{rt}, v_{st}...). In fact each of the 6 active vectors corresponds to one of the 6 input line-to-line voltage because a CSR switching combination connects one of the three input phases to the positive side of the DC link and another input phase to the negative side of the DC link. Thus it is the time interval of the application of a switching combination and the value of the line voltages applied at the given instant that will determine the value of the DC link voltage. For the case depicted in figure 3.19 it is respectively the line voltages v_{st} and v_{sr} that are impressed on the virtual DC link during the switching of $\vec{i}_{st}$ and $\vec{i}_{sr}$. The DC link voltage can be calculated according to the following equation (3.95).

$$e_{dc} = d_{st} v_{st} + d_{sr} v_{sr} \tag{3.95}$$

For CSR modulation, the desired input phase current components are being build by applying the appropriate active vectors for the appropriate amount of time calculated according to the reference space vector. The input phase voltage however is fixed and if its

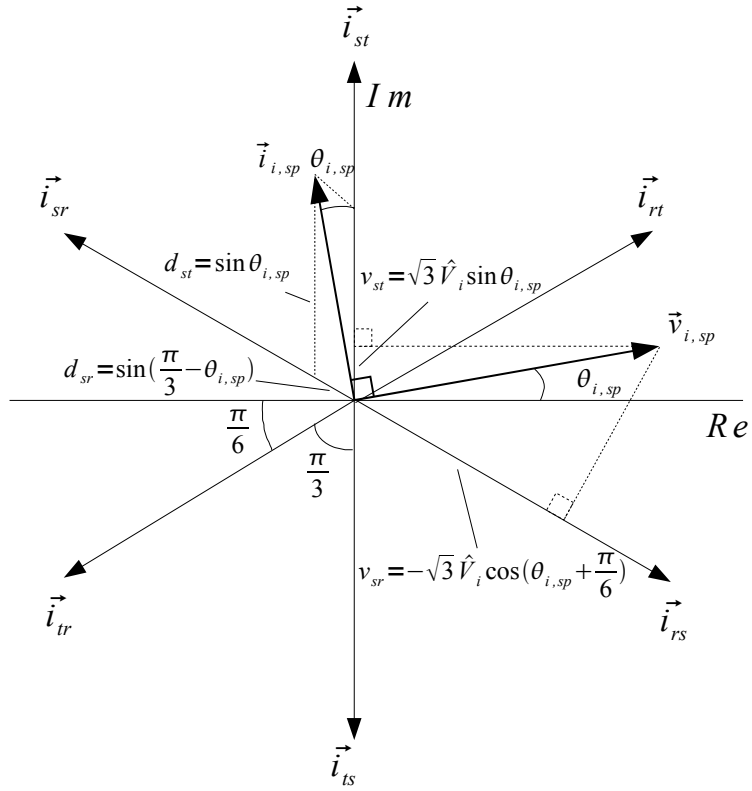

Figure 3.19: *The input voltage and current space vector represented in the complexe plane,* $\Phi_i = -90\,°$.

value should be calculated, the opposite process can be used. At a given time instant the voltage space vectors is constructed by a unique combination of voltage phase components. The value that these components have at that given instant can be found by projecting the space vector onto the active vectors that are being applied and by multiplying the projection by $\frac{2}{3}$ [15]. Let's see how we can apply this for the given situation: We have the current active vectors ($\vec{i}_{rs}$, $\vec{i}_{rt}$, $\vec{i}_{st}$...) in figure 3.19 that represent the line voltages that are applied to the DC link and we have the input voltage space vector $\vec{v}_{i,sp}$ that is build with phase voltages. To obtain the line voltages shouldn't the line voltage space vector be projected onto the active vectors? Let's compute the input line voltage space vector:

$$\vec{v}_{L,i,sp}(t) = v_{rs} + v_{st}e^{\left(j\frac{2\pi}{3}\right)} + v_{tr}e^{\left(j\frac{4\pi}{3}\right)} \tag{3.96}$$

Let's express the line voltages as functions of the phase voltages by inserting ground o:

$$\vec{v}_{L,i,sp}(t) = v_{ro} + v_{os} + (v_{so} + v_{ot})\, e^{\left(j\frac{2\pi}{3}\right)} + (v_{to} + v_{or})\, e^{\left(j\frac{4\pi}{3}\right)} \tag{3.97}$$

$$\vec{v}_{L,i,sp}(t) = \underbrace{v_{ro} + v_{so}e^{\left(j\frac{2\pi}{3}\right)} + v_{to}e^{\left(j\frac{4\pi}{3}\right)}}_{\vec{v}_{i,sp}} + \underbrace{v_{os} + v_{ot}e^{\left(j\frac{2\pi}{3}\right)} + v_{or}e^{\left(j\frac{4\pi}{3}\right)}}_{A} \tag{3.98}$$

Let's compute A:

$$A = -v_{or} - v_{ot} + v_{ot}e^{\left(j\frac{2\pi}{3}\right)} + v_{or}e^{\left(j\frac{4\pi}{3}\right)} \tag{3.99}$$

$$A = v_{or}\left(e^{\left(j\frac{4\pi}{3}\right)} - 1\right) + v_{ot}\left(e^{\left(j\frac{2\pi}{3}\right)} - 1\right) \tag{3.100}$$

We can now insert the relation $v_{or} = e^{\left(j\frac{2\pi}{3}\right)}v_{ot}$ in equation (3.100).

$$A = e^{\left(j\frac{2\pi}{3}\right)}v_{ot}\left(e^{\left(j\frac{4\pi}{3}\right)} - 1\right) + v_{ot}\left(e^{\left(j\frac{2\pi}{3}\right)} - 1\right) \tag{3.101}$$

$$A = v_{ot}\left(1 - e^{\left(j\frac{2\pi}{3}\right)}\right) + v_{ot}\left(e^{\left(j\frac{2\pi}{3}\right)} - 1\right) = 0 \tag{3.102}$$

The term A being zero, it is clear from equation (3.98) that the line voltage space vector and the phase voltage space vector are equal to eachother.

Now that it is proved that $\vec{v}_{i,sp} = \vec{v}_{L,i,sp}$, we can now proceed and compute the magnitude of the line voltages v_{st} and v_{sr} by projecting $\vec{v}_{i,sp}$ onto the active vectors $\vec{i}_{st}$ and $\vec{i}_{sr}$ and by multiplying by the factor $\frac{2}{3}$ [12].

$$v_{st} = \frac{2}{3}\hat{V}_{i,sp}\sin\theta_{i,sp} = \frac{2}{3}\frac{3}{2}\hat{V}_{LL}\sin\theta_{i,sp} = \sqrt{3}\hat{V}_i\sin\theta_{i,sp} \tag{3.103}$$

$$v_{sr} = -\frac{2}{3}\hat{V}_{i,sp}\cos(\theta_{i,sp} + \frac{\pi}{6}) = -\frac{2}{3}\frac{3}{2}\hat{V}_{LL}\cos(\theta_{i,sp} + \frac{\pi}{6}) = -\sqrt{3}\hat{V}_i\cos(\theta_{i,sp} + \frac{\pi}{6}) \tag{3.104}$$

Equation (3.93), (3.94), (3.103) and (3.104) can be inserted in the expression of the DC link voltage in (3.95).

$$e_{dc} = \sin(\frac{\pi}{3} - \theta_{i,sp})\sqrt{3}\hat{V}_i\sin\theta_{i,sp} - \sin\theta_{i,sp}\sqrt{3}\hat{V}_i\cos(\theta_{i,sp} + \frac{\pi}{6}) \tag{3.105}$$

$$e_{dc} = \sqrt{3}\hat{V}_i\sin\theta_{i,sp}[\sin(\frac{\pi}{3} - \theta_{i,sp}) - \cos(\theta_{i,sp} + \frac{\pi}{6})] \tag{3.106}$$

$$e_{dc} = \sqrt{3}\hat{V}_i\sin\theta_{i,sp}[\sin\frac{\pi}{3}\cos\theta_{i,sp} - \cos\frac{\pi}{3}\sin\theta_{i,sp} - \cos\theta_{i,sp}\cos\frac{\pi}{6} + \sin\theta_{i,sp}\sin\frac{\pi}{6}] \tag{3.107}$$

$$e_{dc} = \sqrt{3}\hat{V}_i\sin\theta_{i,sp}\underbrace{[\frac{\sqrt{3}}{2}\cos\theta_{i,sp} - \frac{1}{2}\sin\theta_{i,sp} - \frac{\sqrt{3}}{2}\cos\theta_{i,sp} + \frac{1}{2}\sin\theta_{i,sp}]}_{=0} \tag{3.108}$$

$$e_{dc} = 0 \tag{3.109}$$

This analysis done for the particular example in figure 3.19 can be generalized for the current space vector lying in any sector and the DC link voltage would in all cases be zero like was found for the studied case as long as the current space vector lies 90° ahead of the voltage space vector. The same analysis can also be performed for the current space vector lagging the voltage space vector by 90° and the DC link voltage would be also found to be zero.

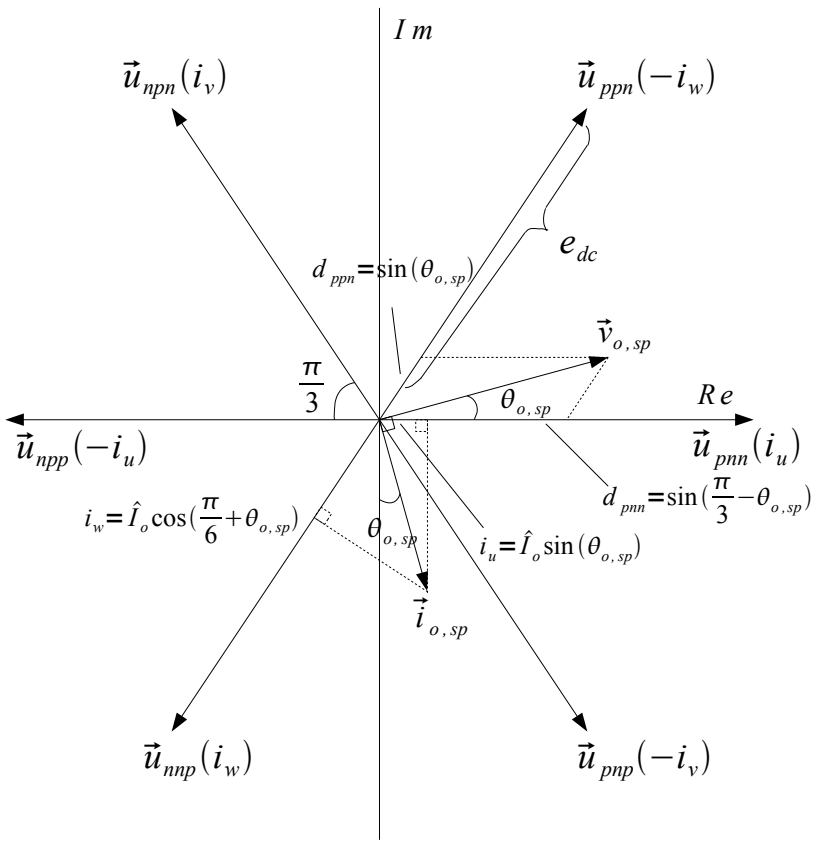

Figure 3.20: *The input voltage and current space vector represented in the complexe plane,* $\Phi_o = -90\,^\circ$.

Now the effect of the VSI modulation on the virtual DC link current can be observed in a similar manner.

$$i_{dc} = d_{pnn} i_u - d_{ppn} i_w \tag{3.110}$$

$$i_{dc} = \sin(\frac{\pi}{3} - \theta_{o,sp})\hat{I}_o \sin\theta_{o,sp} - \sin\theta_{o,sp}\hat{I}_o \cos(\frac{\pi}{6} + \theta_{o,sp}) \tag{3.111}$$

$$i_{dc} = \hat{I}_o \sin\theta_{o,sp}[(\sin\frac{\pi}{3}\cos\theta_{o,sp} - \cos\frac{\pi}{3}\sin\theta_{o,sp}) - (\cos\frac{\pi}{6}\cos\theta_{o,sp} - \sin\frac{\pi}{6}\sin\theta_{o,sp})] \tag{3.112}$$

$$i_{dc} = \hat{I}_o \sin\theta_{o,sp}\underbrace{[(\frac{\sqrt{3}}{2}\cos\theta_{o,sp} - \frac{1}{2}\sin\theta_{o,sp}) - (\frac{\sqrt{3}}{2}\cos\theta_{o,sp} - \frac{1}{2}\sin\theta_{o,sp})]}_{=0} \tag{3.113}$$

This analysis can also be extended to any sector and to $90\,^\circ$ output displacement angle leading or lagging as for the CSR case. The virtual DC link current is zero in the case of zero power factor at the output. This will in turn affect the CSR modulation because the active vector which have length $\sqrt{3}i_{dc}$, see section 3.2.2, will be zero. Thus no input current can be build with these active vectors. Similarly, when the input power factor is zero, the

active vectors in the VSI modulation will be zero and no voltage can be build at the output. We can conclude with this that the matrix converter is not very useful, especially not for reactive power compensation, in this operation mode. However modifications can be made to the modulation in order to extend the operation range of the matrix converter, as will be presented in section 3.4.

3.4 Improved reactive power transfer with the three-vector modulation scheme

In the previous section 3.3 we saw that the reactive power at the input was dependent of the active power transfer and that no input reactive power can be generated in the operating conditions of $\Phi_i = -90\,^\circ$ and $\Phi_o = 90\,^\circ$ when using virtual indirect space vector modulation. In [21] and [20] is described a modulation technique that will enable reactive power formation at the input of the converter with zero power factor at the input and the output of the converter, thus with no active power transfer. The modulation technique is in fact a modified version of the indirect space vector modulation.

To summarize, the issue with the conventional modulation was that, for an output power factor of 0, the VSI modulation affects the average current DC link to be zero and similarly, for an input power factor of zero, the CSR modulation afftects the average voltage DC link to be zero. Since the modulation of the VSI and CSR were done simultaneously throughout a switching period, they affected eachother; The average DC link voltage to be used by the VSI was always zero and the average DC link current to be used by the CSR was always zero. As a consequence the output voltage and input current to be build can only be zero as well. The idea of the new modulation in [21] and [20] is to form the output voltage and input current independently of eachother in two subsequent steps within a switching period so that they do not undermine eachother. Since the output voltage and the input current are formed independently with the new modulation the transfer ratios of current and voltage can be set at different operating points. For the conventional modulation the current transfer ratio was linked to the voltage transfer ratio through the modulation index, $M \in [0; \frac{\sqrt{3}}{2}]$, according to the following equations:

$$\hat{V}_o = M\hat{V}_i \cos\Phi_i \tag{3.114}$$

$$\hat{I}_i = M\hat{I}_o \cos\Phi_o \tag{3.115}$$

In the novel modulation scheme the current and voltage transfer ratios can be set independently within the overmodulation limit. The voltage transfer ratio will be called $q = \frac{\hat{V}_o}{\hat{V}_i}$ as before, while the current transfer ratio will be called $q_i = \frac{I_{i,q}}{I_o}$. The index q in $I_{i,q}$ indicates that it is reactive current.

There are two different versions of the modified modulation technique called two-vector-scheme and three-vector-scheme. The two techniques are advantageous at different voltage

ratio levels q. The two-vector-scheme has higher current ratio for high voltage ratio, while the three-vector-scheme has higher q_i for low q. The three-vector-schemehas the overall highest current transfer ratio. The focus will therefore be on the three-vector-scheme.

All the derivations in this section are based on the work in [21], [20] and [19].

3.4.1 The output voltage forming pulse half period

The first half of the switching period, which is called the voltage forming pulse half period in [21], is dedicated to forming the output voltage as the name indicates. The only modifications that are necessary during this half period are to be done in the CSR modulation so that it doesn't influence the average DC link voltage to be zero like in the conventional modulation. The modulation of the VSI remains the same as it is in the conventional indirect modulation, previously presented in section 3.2.1.

The voltage DC link needs to have an average value different from zero so that an output voltage can be built. In the conventional modulation of the CSR the active vectors utilized are those forming the sector where the current space vector lies. They correspond to the highest positive input phase currents. We saw in section 3.3.2 that using these active vectors led to connecting line voltages to the DC link such that the average DC link voltage was zero. Now that the aim of the modulation is no longer to form an input current and an output voltage at the same time, but rather only an output voltage in this first step, it is the active vectors that will give the highest DC link voltage that will be utilized. The highest DC link voltage is obtained by connecting the highest positive line voltage to the DC link. That means that the active vectors forming the sector where the space vector of the input voltage lies should be applied. For the case of $-\frac{\pi}{6} \leq \theta_{i,sp} \leq \frac{\pi}{6}$ depicted in figure 3.21 the active vectors $\vec{i}_{rs}$ and $\vec{i}_{tr}$ should be applied so that the line voltages u_{rs} and u_{rt} are switched to the DC link.

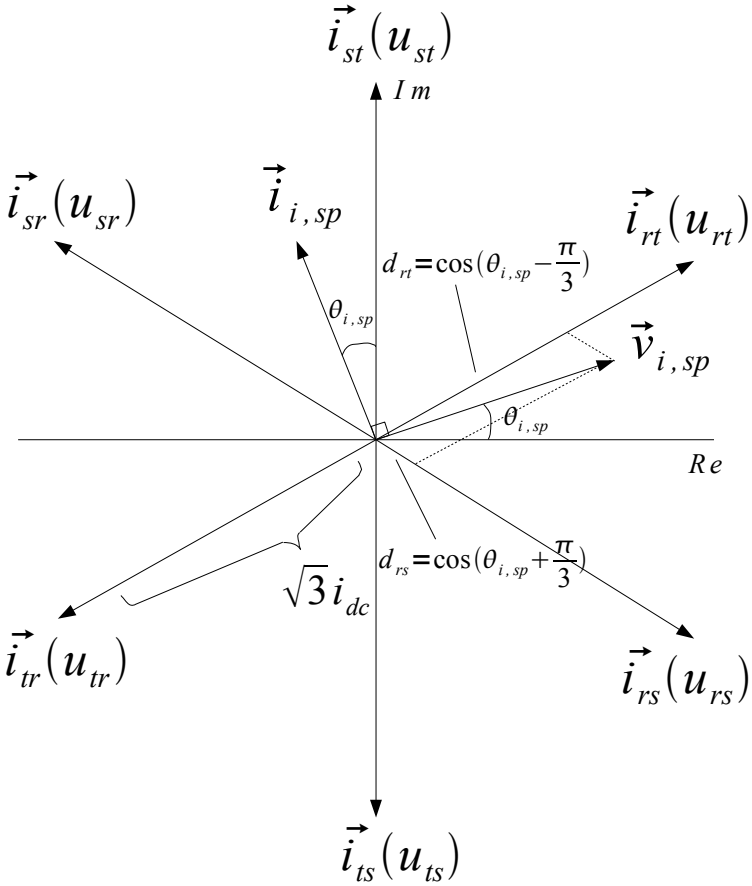

Figure 3.21: *Modulation of the CSR part during the output voltage forming pulse half period for* $-\frac{\pi}{6} \leq \theta_{i,sp} \leq \frac{\pi}{6}$.

The modulation of the CSR part during the first half of the switching period is really just like the space vector of the input current was rotated 90° back so as to be superimposed on the space vector of the input voltage. The equation derived in section 3.2.2 are then used to calculate the gating time intervalls of the active vectors.

$$T_{rs} = T_s \frac{3}{2} \frac{\hat{I}_i \sin(\frac{\pi}{3} - (\theta_{i,sp} + \frac{\pi}{6})}{\sqrt{3} i_{dc} \sin \frac{\pi}{3}} \tag{3.116}$$

$$T_{rt} = T_s \frac{3}{2} \frac{\hat{I}_i \sin(\theta_{i,sp} + \frac{\pi}{6})}{\sqrt{3} i_{dc} \sin \frac{\pi}{3}} \tag{3.117}$$

The ratio $\frac{\hat{I}_i}{i_{dc}}$ is kept to its maximum which is 1 such that no zero vectors will be applied. The expression for the duty cycles, d_{rs} and d_{rt}, can then be simplified to equation (3.118) and (3.119).

$$d_{rs} = \frac{T_{rs}}{T_s} = \sin(\frac{\pi}{3} - (\theta_{i,sp} + \frac{\pi}{6}) = \cos(\theta_{i,sp} + \frac{\pi}{3}) \tag{3.118}$$

$$d_{rt} = \frac{T_{rt}}{T_s} = \sin(\theta_{i,sp} + \frac{\pi}{6}) = \cos(\theta_{i,sp} - \frac{\pi}{3}) \tag{3.119}$$

Computing the DC link voltage will show how this modification of the CSR modulation is effective in bringing the DC link voltage to a value different from zero.

$$e_{dc} = d_{rs}v_{rs} + d_{tr}v_{rt} \tag{3.120}$$

$$e_{dc} = \cos(\theta_{i,sp} + \frac{\pi}{3})\sqrt{3}\hat{V}_i \cos(\theta_{i,sp} + \frac{\pi}{6}) + \cos(\theta_{i,sp} - \frac{\pi}{3})\sqrt{3}\hat{V}_i \cos(\theta_{i,sp} - \frac{\pi}{6}) \tag{3.121}$$

$$\begin{aligned} e_{dc} = \sqrt{3}\hat{V}_i[&(\frac{1}{2}\cos\theta_{i,sp} - \frac{\sqrt{3}}{2}\sin\theta_{i,sp})(\frac{\sqrt{3}}{2}\cos\theta_{i,sp} - \frac{1}{2}\sin\theta_{i,sp}) \\ &+(\frac{1}{2}\cos\theta_{i,sp} + \frac{\sqrt{3}}{2}\sin\theta_{i,sp})(\frac{\sqrt{3}}{2}\cos\theta_{i,sp} + \frac{1}{2}\sin\theta_{i,sp})] \end{aligned} \tag{3.122}$$

$$\begin{aligned} e_{dc} = \sqrt{3}\hat{V}_i[&\underbrace{\frac{1}{4}\cos\theta_{i,sp}\sin\theta_{i,sp} - \frac{1}{4}\cos\theta_{i,sp}\sin\theta_{i,sp}}_{=0} + \\ &2\frac{\sqrt{3}}{4}\underbrace{(\cos^2\theta_{i,sp} + \cos^2\theta_{i,sp})}_{1}] = \sqrt{3}\hat{V}_i\frac{\sqrt{3}}{2} = \frac{3}{2}\hat{V}_i \end{aligned} \tag{3.123}$$

Although the value of the DC link voltage was calculated for the specific case of sector I, $-\frac{\pi}{6} \leq \theta_{i,sp} \leq \frac{\pi}{6}$, the result can be generalized to any other sector. By simply rotating the space vector back to sector I, the same formulas apply. The formulas of the duty ratios of the VSI are the same as for the conventional modulation. The equations of the duty ratios are repeated for the generic case of $0 \leq \theta_{o,sp} \leq \frac{\pi}{3}$ depicted in figure 3.22.

$$d_{pnn} = \frac{3}{2}\frac{q\hat{V}_i \sin(\frac{\pi}{3} - \theta_{o,sp})}{e_{dc}\sin\frac{\pi}{3}} \tag{3.124}$$

$$d_{ppn} = \frac{3}{2}\frac{q\hat{V}_i \sin\theta_{o,sp}}{e_{dc}\sin\frac{\pi}{3}} \tag{3.125}$$

The expression for e_{dc} in equation (3.123) can be inserted into the duty ratio formulas equations (3.124) and (3.125) to obtain the simplified formulas in equations (3.126) and (3.127).

$$d_{pnn} = \frac{2}{\sqrt{3}}q\sin(\frac{\pi}{3} - \theta_{o,sp}) \tag{3.126}$$

$$d_{ppn} = \frac{2}{\sqrt{3}}q\sin\theta_{o,sp} \tag{3.127}$$

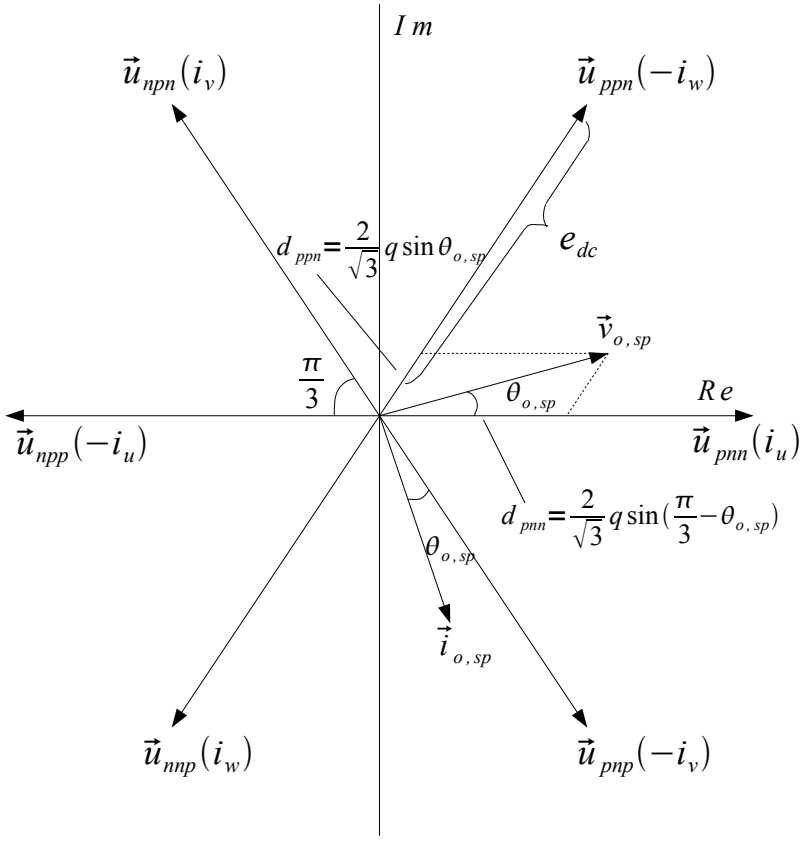

Figure 3.22: *Modulation of the VSI part during the output voltage forming pulse half period for* $0 \leq \theta_{o,sp} \leq \frac{\pi}{3}$.

Finally to complete the description of the first part of the three-vector-scheme the relative duty ratios are computed as in equations (3.128), (3.129), (3.130) and (3.131) and represented in figure 3.23.

$$d_{pnn,rs} = d_{pnn}d_{rs} \tag{3.128}$$

$$d_{pnn,rt} = d_{pnn}d_{rt} \tag{3.129}$$

$$d_{ppn,rs} = d_{ppn}d_{rs} \tag{3.130}$$

$$d_{ppn,rt} = d_{ppn}d_{rt} \tag{3.131}$$

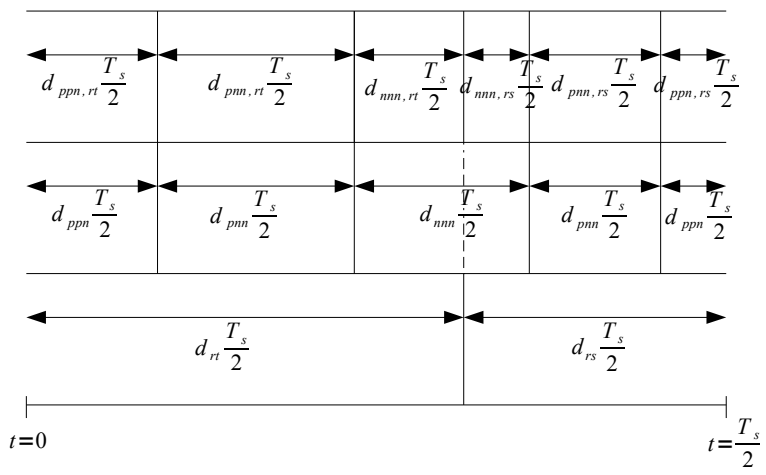

Figure 3.23: *The duty ratios of the VSI (middle) and CSR (lower) part of the matrix converter and the relative duty ratios (upper) for the voltage forming first half of the switching period for the generic case of the output voltage space vector in sector I.*

3.4.2 The input reactive current formation pulse

The second part of the switching period is dedicated to the input reactive current formation and is hence called reactive input current forming pulse half period in [21]. In this time interval the objective is to form an reactive input current and hence the average DC link current must be different from zero. The VSI modulation needs to be modified so that the average DC link current is different from zero although the displacement angle at the output is 90°. To do this the same trick as was used for the CSR modulation is used. It is not the active vectors forming the sector where the output voltage space vector is lying that are applied as before, but the active vector the closest to the space vector of the output current. By doing this not only is the average DC link current not going to be zero but the highest output phase current is going to be flowing through the DC link. For the case of the space vector of the output voltage lying in sector I, $0 \leq \theta_{o,sp} \leq \frac{\pi}{3}$, the space vector of the output current will lie closer to the active vector $\vec{u}_{pnp}$ and the highest phase current is then the corresponding $-i_v$ as is shown in figure 3.24.

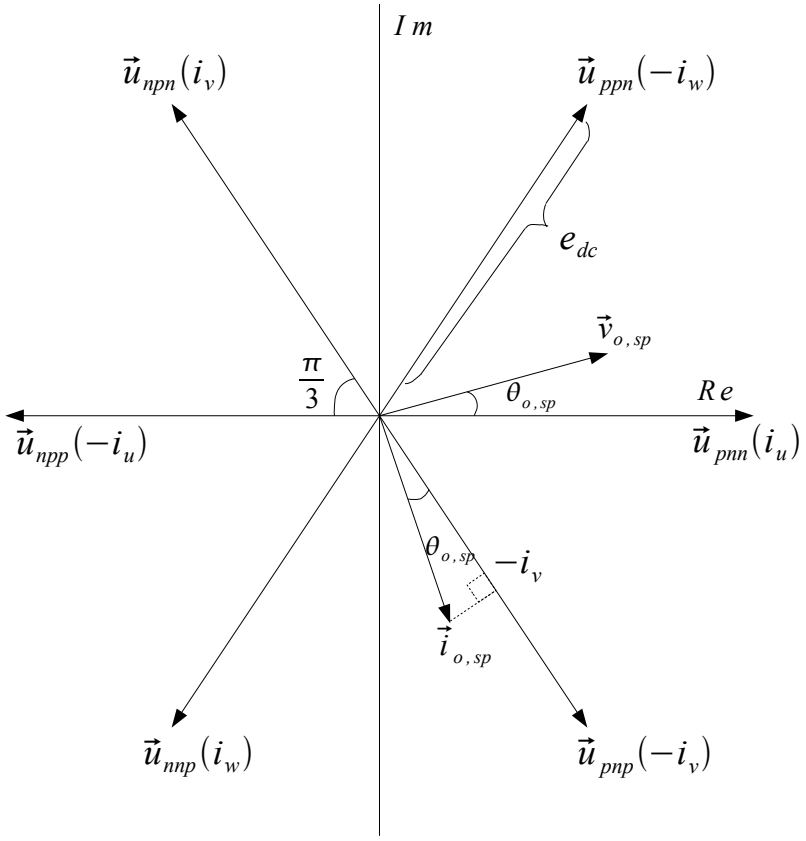

Figure 3.24: *Modulation of the VSI part during the input reactive current forming pulse half period for* $0 \leq \theta_{o,sp} \leq \frac{\pi}{3}$.

In table 3.1 are represented all the sectors where the voltage space vector lies and the corresponding active vector that should be applied so that the highest positive output current flows through the DC link.

Table 3.1: *Sector of output voltage space vector (left column), the corresponding active vectors to apply in the three-vector-scheme (middle column) and the corresponding DC link current (right column).*

sector	active vector	i_{dc}
I	$\vec{u}_{pnp}$	$-i_v$
II	$\vec{u}_{pnn}$	i_u
III	$\vec{u}_{ppn}$	$-i_w$
IV	$\vec{u}_{npn}$	i_v
V	$\vec{u}_{npp}$	$-i_u$
VI	$\vec{u}_{nnp}$	i_w

For the generic case illustrated in figure 3.24, $0 \leq \theta_{o,sp} \leq \frac{\pi}{3}$, the DC link current can be calculated as:

$$i_{dc} = -i_v = \frac{2}{3}\hat{I}_{o,sp}\cos(\frac{2\pi}{3} - \frac{\pi}{2} - (\frac{\pi}{3} - \theta_{o,sp})) = \hat{I}_o\cos(\theta_{o,sp} - \frac{\pi}{6}) \tag{3.132}$$

Now the CSR modulation remains to be explained. In the three-vector-scheme it is the two active vectors closest to the input current space vector (the active vectors forming the sector where the current space vector lies) that should be applied in practice for highest possible input reactive current formation. However it is important that at least one of the two current active vectors applied during the reactive current formation pulse half period is the same as one of the two current active vectors applied during the voltage formation pulse half period. Only three different current active vectors should hence be applied for the CSR modulation during the entire switching period, hence the name three-vector-scheme. The reason for this constraint is that the reactive current and voltage forming pulses half period later needs to be merged and they can only be merged if the same input current active vector is applied. The pulse merging process will be explained in the next section 3.4.3. For the configuration of figure 3.25, the space vector of the input voltage lies in sector I and the space vector of the input current, which is 90° ahead lies in sector III like previously. During the voltage formation pulse half period the active vectors $\vec{i}_{rs}$ and $\vec{i}_{rt}$ were applied. Hence if the active vectors $\vec{i}_{st}$ and $\vec{i}_{sr}$ which form the sector III are applied in the reactive current formation pulse half period, all four current active vectors are different and no pulse merging can be implemented. To overcome this apparent dilemma the active vector $\vec{i}_{rs}$ is going to be used in the reactive current forming pulse half period instead of $\vec{i}_{sr}$. To obtain the desired input current despite using the opposite current active vector, the current of opposite polarity is going to flow in the DC link. Therefore instead of applying the voltage active vector corresponding to the highest positive output current in the VSI modulation, inversion will be made and the opposite voltage active vector will be applied. In figure 3.24, for instance, instead of $\vec{u}_{pnp}$, the opposite vector $\vec{u}_{npn}$ will be applied when $\vec{i}_{rs}$ is applied.

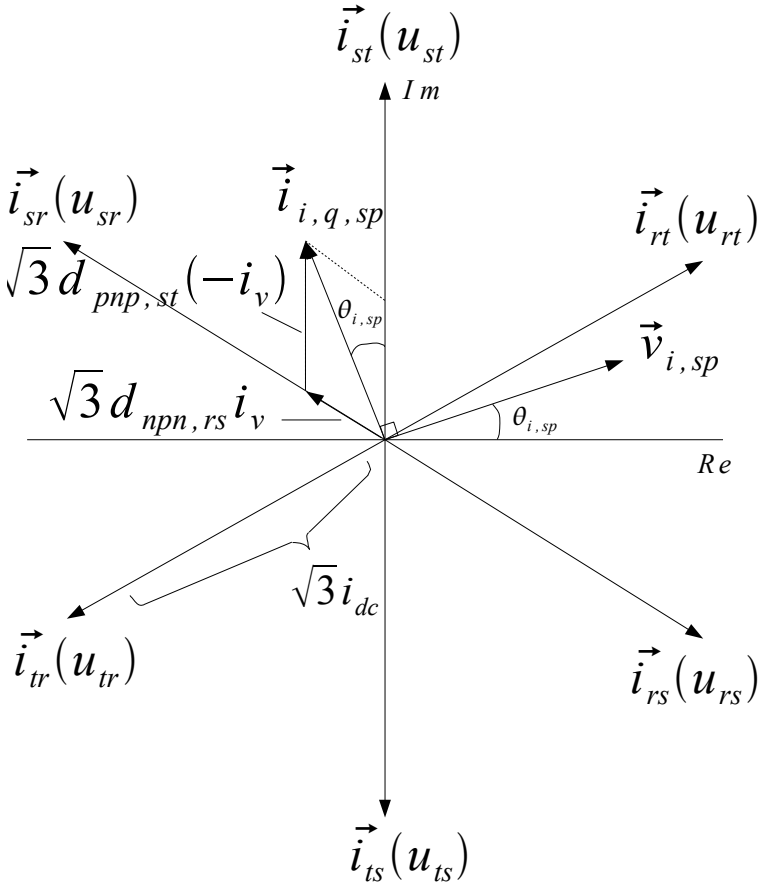

Figure 3.25: *Modulation of the CSR part during the input reactive current forming pulse half period for* $0 \leq \theta_{i,sp} \leq \frac{\pi}{6}$.

Input reactive current can only be formed when current flows in the DC link. For our generic case the input current will be formed when $-i_v$ and then i_v flows through the DC link. During the remainder of the current forming pulse half period only zero voltage vectors are applied, thus it is a current equal to zero that flow in the DC link during the rest of the half period. Because reactive input current is formed only when the voltage active vectors are used, the relative duty ratios $d_{pnp,st}$ and $d_{npn,rs}$, indicated in figure 3.25, are going to be calculated right away. In figure 3.26 the geometrical relations used to calculated the relative duty ratios are indicated.

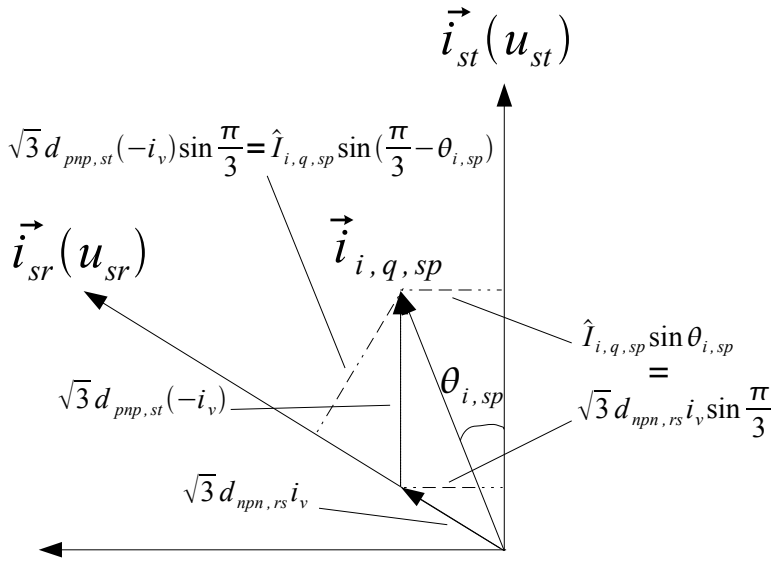

Figure 3.26: *The geometrical relations used to calculated the relative duty ratios $d_{pnp,st}$ and $d_{npn,rs}$ in the second half of the pulse period dedicated to input reactive current formation, here for the input current space vector in sector III and $\theta_{i,sp} \geq 0$ and the output voltage space vector in sector I ($\vec{u}_{pnp}$ and $\vec{u}_{npn}$ used in VSI modulation).*

Let's start by calculating the duty ratio $d_{npn,rs}$. As was seen in section 3.2.2 the active vectors in the modulation of the CSR part of the matrix converter have length $\sqrt{3}i_{dc}$. During the time interval $\vec{u}_{npn}$ is applied, the average DC link current has value $i_{dc} = d_{npn,rs}i_v = -d_{npn,rs}\hat{I}_o\cos(\theta_{o,sp} - \frac{\pi}{6})$. Thus the active vectors has length $\left|-\sqrt{3}d_{npn,rs}\hat{I}_o\cos(\theta_{o,sp} - \frac{\pi}{6})\right|$. The geometric relation indicated in figure 3.26 is:

$$\left|-\sqrt{3}d_{npn,rs}i_v\sin\frac{\pi}{3}\right| = \left|\hat{I}_{i,q,sp}\sin\theta_{i,sp}\right| \tag{3.133}$$

The negative sign on the left hand side in equation (3.133) is due to $\vec{i}_{rs}$ being applied instead of $\vec{i}_{sr}$. The value of i_v can be inserted in equation (3.133).

$$\left|-\sqrt{3}d_{npn,rs}(-\hat{I}_o\cos(\theta_{o,sp} - \frac{\pi}{6}))\sin\frac{\pi}{3}\right| = \left|\hat{I}_{i,q,sp}\sin\theta_{i,sp}\right| \tag{3.134}$$

The two negative signs on the left hand side of equation (3.134) cancel eachother, thus the absolute signs can be removed. On the right hand side $\theta_{i,sp} \geq 0$ and the absolute signs can also be removed here. Finally by rearranging the terms in equation (3.134) the expression of $d_{npn,rs}$ can be obtained:

$$d_{npn,rs} = \frac{\hat{I}_{i,q,sp}\sin\theta_{i,sp}}{\sqrt{3}\hat{I}_o\cos(\theta_{o,sp} - \frac{\pi}{6})\sin\frac{\pi}{3}} = \frac{\frac{3}{2}\hat{I}_{i,q}\sin\theta_{i,sp}}{\sqrt{3}\hat{I}_o\cos(\theta_{o,sp} - \frac{\pi}{6})\frac{\sqrt{3}}{2}} \tag{3.135}$$

$$d_{npn,rs} = \frac{\hat{I}_{i,q} \sin\theta_{i,sp}}{\hat{I}_o \cos(\theta_{o,sp} - \frac{\pi}{6})} \tag{3.136}$$

In a similar manner, by using the geometrical relation in figure 3.26, the duty ratio $d_{pnp,st}$ is calculated.

$$\sqrt{3} d_{pnp,st}(-i_v) \sin\frac{\pi}{3} = \hat{I}_{i,q,sp} \sin(\frac{\pi}{3} - \theta_{i,sp}) \tag{3.137}$$

$$d_{pnp,st} = \frac{\frac{3}{2}\hat{I}_{i,q} \sin(\frac{\pi}{3} - \theta_{i,sp})}{\frac{\sqrt{3}\sqrt{3}}{2}\hat{I}_o \cos(\theta_{o,sp} - \frac{\pi}{6})} \tag{3.138}$$

$$d_{pnp,st} = \frac{\hat{I}_{i,q} \cos(\theta_{i,sp} + \frac{\pi}{6})}{\hat{I}_o \cos(\theta_{o,sp} - \frac{\pi}{6})} \tag{3.139}$$

Let's calculate the DC link voltage to see how the modified CSR modulation influences it.

$$\begin{aligned} e_{dc} &= -d_{npn,rs} u_{rs} + d_{pnp,st} u_{st} \\ &= -\frac{\hat{I}_{i,q} \sin\theta_{i,sp}}{\hat{I}_o \cos(\theta_{o,sp} - \frac{\pi}{6})} \sqrt{3}\hat{V}_i \cos(\theta_{i,sp} + \frac{\pi}{6}) \\ &\quad + \frac{\hat{I}_{i,q} \cos(\theta_{i,sp} + \frac{\pi}{6})}{\hat{I}_o \cos(\theta_{o,sp} - \frac{\pi}{6})} \sqrt{3}\hat{V}_i \sin\theta_{i,sp} = 0 \end{aligned} \tag{3.140}$$

The negative sign is due to the VSI active vector inversion. The modified CSR modulation makes the DC link voltage be zero and thus, does not influence voltage formation at the output (no output voltage formation) which is the purpose of the modulation since there should only be input reactive current formation in this intervall. In addition this property of the modified modulation ensures the average power through the matrix converter to be zero during the input reactive current pulse half period.

$$p = \underbrace{e_{dc}}_{=0} i_{dc} = 0 \tag{3.141}$$

During the first output voltage pulse half period the average active power should also be zero. This is the case since the conventional modulation is used for the VSI part. Recall that this modulation makes the average DC link current go down to zero for an output power factor of zero and thus the average power will also be zero.

The relative duty ratios for the voltage forming pulse half period are represented in figure 3.27.

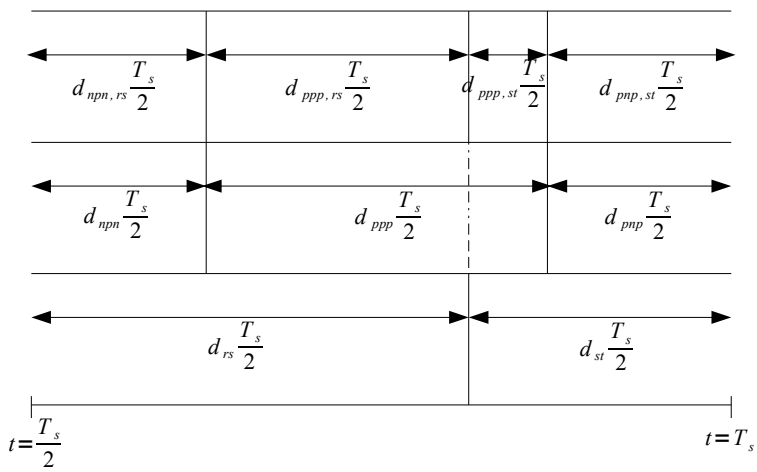

Figure 3.27: *The duty ratios of the VSI (middle) and CSR (lower) part of the matrix converter and the relative duty ratios (upper) during the input reactive current forming half of the switching period for the generic case of the input voltage space vector in sector I such that $\theta_{i,sp} \geq 0$ and the input current space vector in sector III.*

At this point it is important to make a comment about the sector location of the current and voltage space vectors in the CSR modulation. In the generic case used to explain the CSR modulation, the input voltage space vector was in sector I, such that $0 \leq \theta_{i,sp} \leq \frac{\pi}{6}$. Since the input current space vector is 90 ° ahead of the voltage space vector it lied in sector III . If however the input voltage space vector is in sector I such that $-\frac{\pi}{6} \leq \theta_{i,sp} \leq 0$, the input current space vector will lie in sector II. The active vectors that should be applied during the input reactive current forming pulse half period, are then $\vec{i}_{rt}$ and $\vec{i}_{st}$. Since $\vec{v}_{i,sp}$ is still in sector I it is $\vec{i}_{rs}$ and $\vec{i}_{rt}$ that will be applied during the output voltage forming pulse half period. Hence there are only three different active vector that will be applied in total. Merging of the pulses is then possible without inversion of any of the VSI active vectors. However the DC link voltage e_{dc} will not be zero like in equation (3.140) in that case and the CSR modulation will infuence the output voltage formation. This is why an inversion is necessary anyway. The active vector that is not common for the output voltage and input reactive current forming pulse half period will be inversed, here $\vec{i}_{st}$. Consequently the active vector in the VSI modulation must be inversed as well. This case of the input voltage space vector lying in sector I such that $-\frac{\pi}{6} \leq \theta_{i,sp} \leq 0$ is illustrated in figure 3.28.

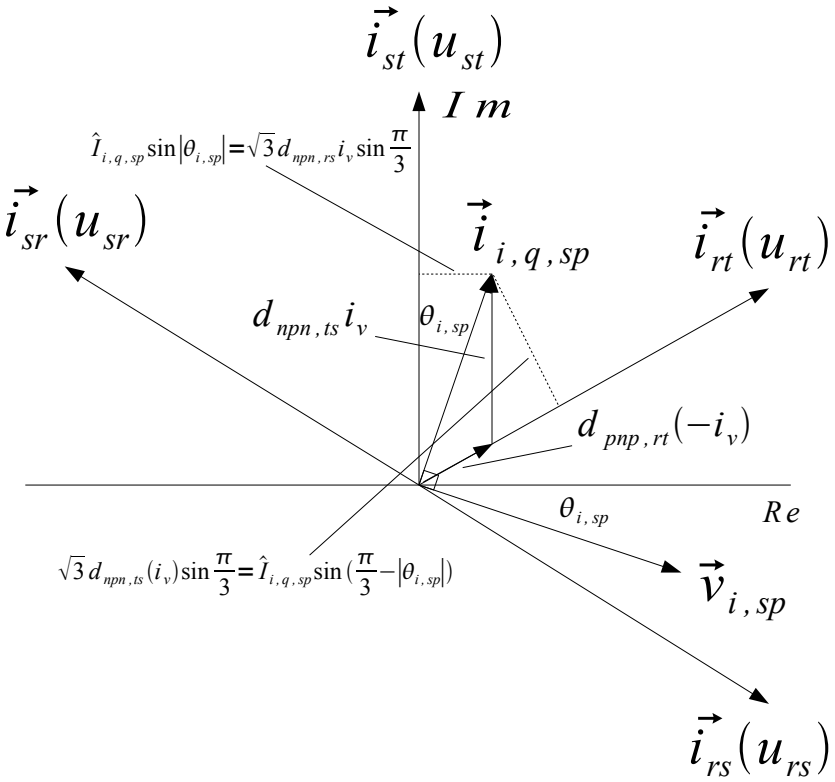

Figure 3.28: *The geometrical relations used to calculated the relative duty ratios $d_{npn,ts}$ and $d_{pnp,rt}$ in the second half of the pulse period dedicated to input reactive current formation, here for the input current space vector in sector II and $\theta_{i,sp} \leq 0$ and the output voltage space vector in sector I ($\vec{u}_{pnp}$ and $\vec{u}_{npn}$ used in VSI modulation).*

To calculate the relative duty ratios $d_{npn,ts}$ and $d_{pnp,rt}$ the same equations (3.137) and (3.140) are used with the absolute value of $\theta_{i,sp}$ to obtain positive duty ratios.

$$d_{pnp,rt} = \frac{\hat{I}_{i,q}\sin|\theta_{i,sp}|}{\hat{I}_o\cos(\theta_{o,sp}-\frac{\pi}{6})} \tag{3.142}$$

$$d_{npn,ts} = \frac{\hat{I}_{i,q}\cos(|\theta_{i,sp}|+\frac{\pi}{6})}{\hat{I}_o\cos(\theta_{o,sp}-\frac{\pi}{6})} \tag{3.143}$$

3.4.3 Merging of the voltage and reactive current formation pulses

In the two previous sections 3.4.1 and 3.4.2, the modified modulation was explained: the output voltage and the input voltage were created in two separate steps so that the CSR and VSI modulations would not undermine eachother like in the conventional modulation. However output voltage is only created in the first half of the switching period and thus the voltage transfer ratio will be lower than for the conventional modulation. Similarly the

reactive current is only created during the second half of the pulse period. The merging of the voltage forming and reactive current forming pulse half period will increase the voltage duty ratio as well as current transfer ratio. The merging technique will be explained with the help of the same generic example as before: input voltage space vector in sector I such that $\theta_{i,sp} \geq 0$, the input current space vector 90° ahead in sector III, the output voltage space vector in sector I and the output current space vector 90° behind. This generic example and the corresponding relative duty ratios calculated for the entire switching period are represented in figure 3.29. Figure 3.29 represents the switching pattern for one switching period of the three-vector-scheme modulation for the generic example if no pulse merging is implemented.

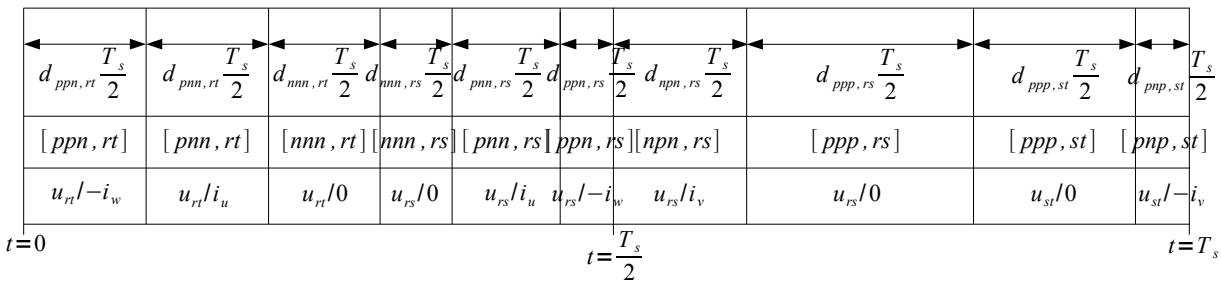

Figure 3.29: *The relative duty ratios (upper row) during the entire switching period, the corresponding switching combination (middle) and the input voltage and output current applied to the DC link (bottom row); for the generic case of the input voltage space vector in sector I such that $\theta_{i,sp} \geq 0$ and the input current space vector in sector III and the output voltage space vector in sector I.*

In figure 3.29 are represented the relative duty ratios $d_{nnn,rs}$ and $d_{nnn,rt}$ from the voltage forming period and $d_{ppp,rs}$ and $d_{ppp,st}$ from the reactive current forming period. No output voltage is formed when $[nnn, rs]$ and $[nnn, rt]$ are applied during the first half of the switching period because zero voltage vectors, $\vec{u}_{nnn}$ here, do not produce any output voltage. Similarly no reactive current is formed when $[ppp, rs]$ and $[ppp, st]$ are applied during the second half of the switching period because when a zero voltage vector, $\vec{u}_{ppp}$ here, is applied all the output phases are connected to one side of the DC link and thus there is a breach in the path of the DC link current which is then zero. If the DC link current is zero no input reactive current can be created. The switching combinations with zero voltage vectors are thus superficial. The time slots $d_{nnn,rs}$ and $d_{nnn,rt}$ of the output voltage forming pulse half period can be filled up with the reactive current forming pulses $[npn, rs]$ and $[pnp, st]$ according to the merging that will be presented next. Thus only the switching combinations $[ppp, rs]$ and $[ppp, st]$ remain in the reactive input current forming second half. These switching combinations can surely be dropped, they don't contribute to any reactive current formation, leaving an empty reactive current formation pulse half period. This means that the voltage formation pulse half period can now be expanded to the entire switching period. This will restore to some extent the modulation index to the value of the conventional modulation.

Now let's study closer the process of inserting the reactive current forming pulses $[npn, rs]$ and $[pnp, st]$ into the voltage forming pulse half period. The pulse $[pnp, st]$ is going to be inserted entirely in a zero voltage vector time slot. The other pulse, $[npn, rs]$, however is not. There would probably not be enough zero voltage vector time intervals anyway to fit both reactive current forming pulses $[npn, rs]$ and $[pnp, st]$. $[npn, rs]$ will be merged with a pulse that presents the same current active vector $\vec{i}_{rs}$, and as a consequence the same DC link voltage u_{rs}. Two candidate pulses present themselves: $[pnn, rs]$ and $[ppn, rs]$. The property $i_u + i_v + i_w = 0$ and thus $i_u + i_v = -i_w$ will be used because it states that it is equivalent to apply $i_u + i_v$ or $-i_w$ to the DC link. In practice this means that the pulse $[pnn, rs]$ with DC link current i_u and DC link voltage u_{rs} is a perfect match for merging with reactive forming pulse $[npn, rs]$ with DC link current i_v and DC link voltage u_{rs}. The merging of these two pulses will yield a pulse equivalent to $[ppn, rs]$ with DC link current $-i_w$ and DC link voltage u_{rs}. Thus the pulse $[ppn, rs]$, already present in voltage forming half period, see figure 3.29, can be extended with the time interval of the merging. The merging of the pulses $[npn, rs]$ and $[pnn, rs]$ can only last for the smallest duty ratios of the merged pulses, $min\,[d_{npn,rs}; d_{pnn,rs}]$. For the remaining time $|d_{npn,rs} - d_{pnn,rs}|$, the pulse with the longest duty ratio will be applied.

Now that all the output voltage forming pulses and the input reactive current forming pulses have been calculated and incorporated into the pulse pattern of the modified modulation, there might remain some time intervall in the switching period depending on whether the modulation indicis q and q_i are set to their maximum or not. The remaining time interval Δt is calculated as in equation (3.144):

$$\begin{aligned}\Delta t = T_s - \left|d^q_{npn,rs} - d_{pnn,rs}\right| - min\,[d_{npn,rs}; d_{pnn,rs}] \\ -d_{ppn,rs} - d_{ppn,rt} - d_{pnn,rt} - d^q_{pnp,rt}\end{aligned} \tag{3.144}$$

This remaining time interval Δt should be only be distributed among zero voltage vector so as not to destroy the modulation. However it doesn't matter how they are distributed [1]. They will hence be distributed equally as in equation (3.145).

$$d_{ppp,rs} = d_{ppp,rt} = d_{nnn,rt} = d_{nnn,st} = \frac{\Delta t}{4} \tag{3.145}$$

The choice between $\vec{u}_{ppp}$ or $\vec{u}_{nnn}$ is dictated by the desire of switching as little as possible. This same motivation leads to setting the current active vectors in the following order: $\vec{i}_{rs}$, $\vec{i}_{rt}$ and $\vec{i}_{st}$ such that only one commutation is needed from one vector to another. The final pattern of a switching period in the modified modulation is represented in figure 3.30.

$\lvert d_{pnn,rs} - d^q_{npn,rs} \rvert$		$d_{ppn,rs} + MIN(d_{pnn,rs}; d^q_{npn,rs})$	$d_{ppp,rs}$	$d_{ppp,rt}$	$d_{ppn,rt}$	$d_{pnn,rt}$	$d_{nnn,rt}$	$d_{nnn,st}$	$d^q_{pnp,st}$
$d^q_{npn,rs} > d_{pnn,rs}$ $[npn, rs]$	$d_{pnn,rs} > d^q_{npn,rs}$ $[pnn, rs]$	$[ppn, rs]$	$[ppp, rs]$	$[ppp, rt]$	$[ppn, rt]$	$[pnn, rt]$	$[nnn, rt]$	$[nnn, st]$	$[pnp, st]$
u_{rs}/i_v	u_{rs}/i_u	$u_{rs}/-i_w$	$u_{rs}/0$	$u_{rt}/0$	$u_{rt}/-i_w$	u_{rt}/i_u	$u_{rt}/0$	$u_{st}/0$	$u_{rs}/-i_v$
$\vec{u}_{inverse}/\vec{i}_{lower}$	$\vec{u}_{lower}/\vec{i}_{lower}$	$\vec{u}_{upper}/\vec{i}_{lower}$	$\vec{u}_{zero}/\vec{i}_{lower}$	$\vec{u}_{zero}/\vec{i}_{upper}$	$\vec{u}_{upper}/\vec{i}_{upper}$	$\vec{u}_{lower}/\vec{i}_{upper}$	$\vec{u}_{zero}/\vec{i}_{upper}$	$\vec{u}_{zero}/\vec{i}_{third}$	$\vec{u}_{max}/\vec{i}_{third}$

0 T_s

Figure 3.30: *The relative duty ratios (upper row) during the entire switching period after the merging, the corresponding switching combination (second row), the input voltage and output current applied to the DC link (third row) and generalized switching combination; for the generic case of the input voltage space vector in sector I such that $\theta_{i,sp} \geq 0$ and the input current space vector in sector III and the output voltage space vector in sector I.*

The last row of figure 3.30 is the generalized switching pattern for the case $\Phi_i = -90\,^\circ$ and $\Phi_o = 90\,^\circ$ when $\theta_{i,sp} \geq 0$. The subscripts "lower" and "upper" refer to respectively the lower and upper active vectors in the sector where the input and output voltage space vector lie. $\vec{u}_{zero}$ represents a zero vector: $\vec{u}_{nnn}$ or $\vec{u}_{ppp}$. The vectors $\vec{u}_{max}$ and $\vec{u}_{inverse}$ represent the voltage active vectors used in the reactive current forming pulse half period: $\vec{u}_{max}$ is the active vector that will yield maximum positive DC link current and $\vec{u}_{inverse}$ is the inverse vector. In the appendix are added the generalized switching pattern for the case of $\theta_{i,sp} \leq 0$ as well.

When the matrix converter is to draw reactive power, that is $\Phi_i = 90\,^\circ$, the modulation needs to be modified accordingly. The details will not be presented here as the same reasoning as was shown previously can be used. The generalized switching patterns are added in the appendix for $\Phi_i = 90\,^\circ$ and $\Phi_o = 90\,^\circ$ in the two cases $\theta_{i,sp} \geq 0$ and $\theta_{i,sp} \leq 0$.

3.4.4 Reactive power compensation range

The reactive power compensation range for the conventional indirect space vector modulation and the modified modulation, the Three-Vector-Scheme, are shown in figure 3.31. The latter is only shown for its area of application, which is the case of no active power transfer, that is for an output power factor equal to zero $\cos\Phi_o = 0$. From figure 3.31 we can see how the reactive power range is raised above $Q_i = 0$ with the three-vector-scheme modulation for $\cos\Phi_o = 0$.

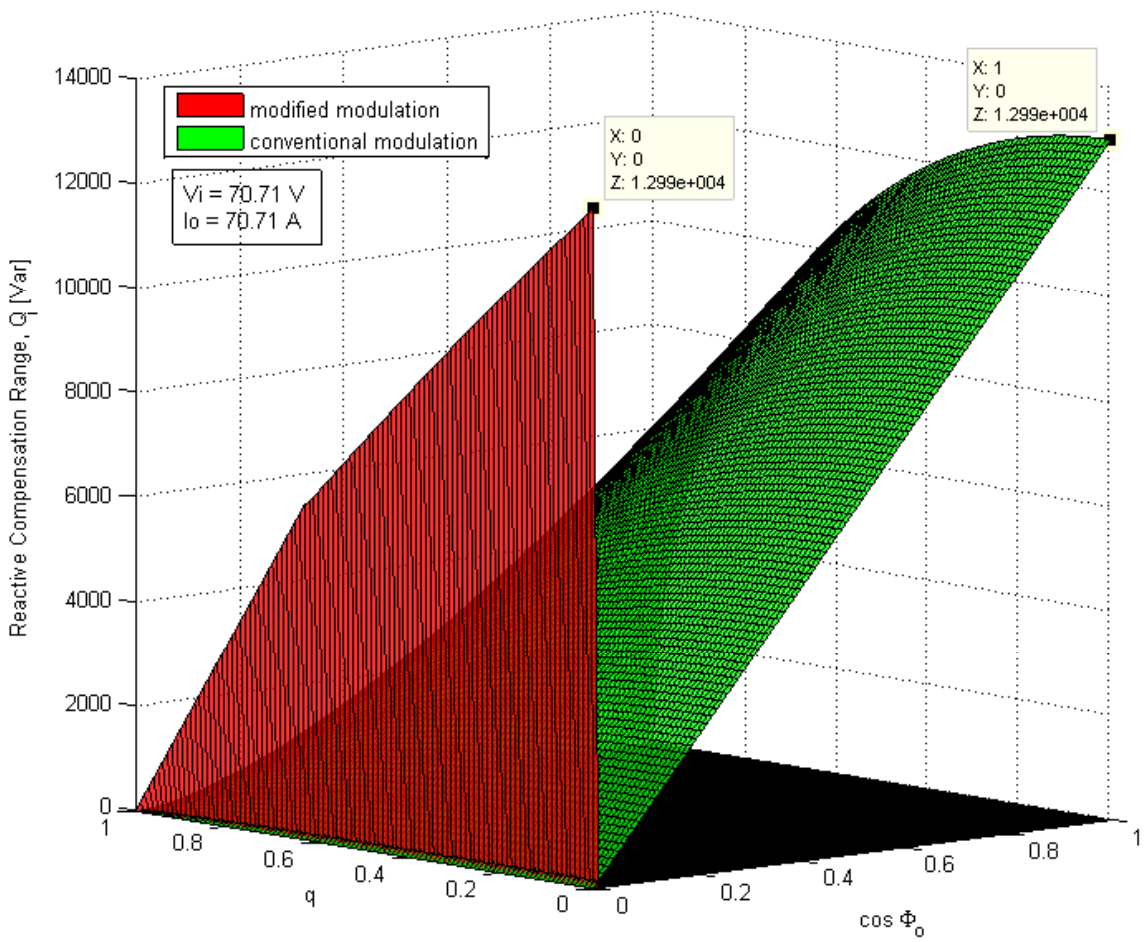

Figure 3.31: *The reactive power range (in [VAR]) at the input of the matrix converter as a function of the normalized modulation index* $q_n = \frac{q}{q_{max}} = \frac{2}{\sqrt{3}}\frac{\hat{V}_o}{\hat{V}_i}$, $q \in [0;1]$, *and the output power factor* $\cos\Phi_o$ *for the conventional indirect space vector modulation (in green) and for the Three-Vector-Scheme (in red) for constant output current magnitude* $\hat{I}_o = 100\,A$ *and constant input voltage* $\hat{V}_i = 100\,V$ *(The parameter values are indicated as RMS values in the graph).*

The reactive power range is calculated using equation (3.146).

$$Q_i = \frac{3}{2}\hat{I}_{i,q}\hat{V}_i = \frac{3}{2}q_{i,max}\hat{I}_o\hat{V}_i \tag{3.146}$$

The maximum current modulation index, q_i, was first computed in [21] and then corrected and slightly modified in [19]. For lower normalized voltage modulation indicis, $q_n = \frac{q}{\frac{\sqrt{3}}{2}} \leq \frac{28-6\sqrt{7}}{19} \approx 0.64$, the maximum normalized current modulation index is calculated as in (3.147).

$$q_{i,n} = \frac{1}{4}\left(\sqrt{16 - 3q_n^2} - 3q_n\right) \tag{3.147}$$

For higher voltage modulation indicis q the maximum normalized current modulation index

is calculated as in (3.148).

$$q_{i,n} = \frac{4}{3}\left(1 - q_n\right) \tag{3.148}$$

Simulation model and simulation results of the Matrix Converter-based Reactive Compensation System

This second part of the Master Thesis features the simulation results from three different simulation models, all built in Simulink Matlab. The first simulation model to be presented is that of a MCRC system with a matrix converter that is modulated with conventional indirect space vector modulation and a PM machine that is modelled by the simple three-phase equivalent circuit presented in chapter 2 of part I. the second simulation model is similar to the first one, except the matrix converter is modulated with the three-vector-scheme. In those two models the equivalent circuit of the PM synchronous machine is composed of a non-neglectable resistor to dampen quickly initial current oscillations, $R = 0.1\,\Omega$ (an explanation for the oscillation phenomena will be provided in chapter 5), a synchronous reactance, $X_s = 0.314\,\Omega$ ($L_s = 0.1\,H$) and an excitation voltage $\vec{E}_f$. The reactance value was chosen to be $X_s = 0.314\,\Omega$ as it is a standard value for the synchronous reactance [8]. In those two first models the input of the matrix converter is connected to a three-phase voltage source, $\vec{V}_i = \frac{100}{\sqrt{2}}\angle 0^\circ\,V$. The third simulation model represents the MCRC system with three-vector-scheme modulation connected to a grid. This last simulation model will be further described in section 5.

In all the three models, although the PM machine is represented by a simplified model, the matrix converter's model is detailed and no simplifications were made: The model contains all the switching information. In all simulations the switching frequency is set to $f_s = 10000\,Hz$. The choice of the switching frequency is a compromise between the benefits of high switching frequency (harmonics at higher frequencies and thus need for smaller input filter rating, smoother curves) and low computational speed at high switching frequency. As a rule of thumb the simulation step should be at least one tenth of the switching period for a acceptable resolution [16]. For $f_s = 10000\,Hz$, the switching period is $T_s = 1e^{-4}\,s$ and thus the simulation step should not exceed $T_{simulation} = 1e^{-6}\,s$. $T_{simulation} = 1e^{-6}\,s$ yields a reasonable computational speed in MATLAB Simulink and was thus set as the simulation step in the "Power GUI" along with a discrete solver. In the configuration parameters of the overall model, the solver Dorman-Price, "ode 45", was chosen in MATLAB. Also, the IGBTs and diodes in the bidirectional switches are modeled with on-state losses (on-state resistance $R_{on} = 0.001\,\Omega$) and snubbers. The IGBT model also contains switching losses with a finite current fall and tail time ($T_{fall} = 1e^{-6}\,s$ and $T_{tail} = 2e^{-6}\,s$).

In all the simulations the output voltage is modulated so as to be in phase with the input voltage and the frequency is $50\,Hz$ both at the input and the output of the matrix converter.

Chapter 4

Reactive compensation with conventional modulation

In this first chapter of part II of the Master's thesis, the studied simulation model of the MCRC system contains a matrix converter modulated with conventional space vector modulation. The simulation model built for these simulations is reported in appendix B, in the figures B.1, B.2, B.3, B.4, B.5 and B.6.

It is important to select carefully relevant data from the simulations to properly show the features of the reactive power compensation device. The very first feature of the MCRC system that should be presented are all the input and output voltage and current waveforms of the matrix converter.

The input displacement angle is kept to zero ($\Phi_{i,ref} = 0$), no reactive power at the input, the modulation index reference is set to $q_{ref} = 0.5$ and the excitation voltage is set to $\vec{E}_f = \frac{50}{\sqrt{2}}\angle -20\,^\circ$. The excitation voltage was chosen with a negative rotor angle so as to have the active power flow into the PM machine. The magnitude and phase angle were chosen so as to have a substantial power flow. The waveforms of only one phase are reported figure 4.1 for readability. The input current and output voltage contain harmonics as there is no input filter in these first simulations. While the output voltage and the input current contain a lot of harmonics, the output current is smoothened out by the inductance of the equivalent circuit of the PM machine. The fundamental component at $50\,Hz$ and phase angle of the previously shown waveforms are shown in figure 4.2 for the input voltage and current and in figure 4.3 for the output voltage and current. Also we can read from graph a) in figure 4.3 that $\hat{V}_o = 54\,V$ and from graph c) in figure 4.2 that $\Phi_i = 0.35\,^\circ$. The measured value correspond well to the reference. There is however a small discrepancy which could be due to the fact that the high harmonic content makes the measurements in MATLAB Simulink inaccurate. Another factor that should be taken into account when assessing the simulation results and their small errors compared with their references is that the solver in MATLAB does not give an exact solutions. For instance, using different

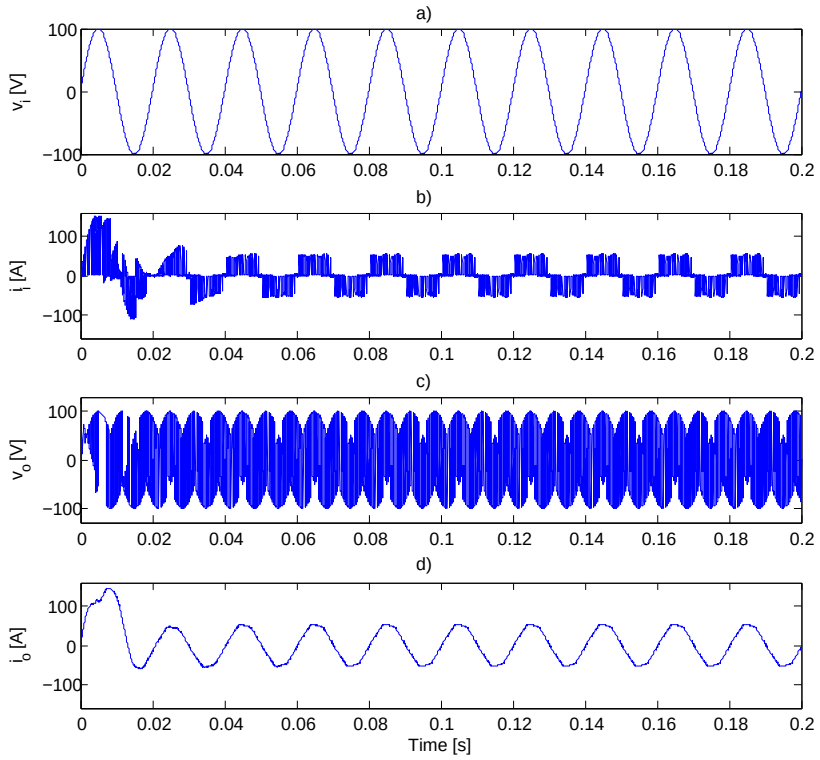

Figure 4.1: *One phase of the input voltage (a) and current (b) and output voltage (c) and current (d) waveforms for* $\Phi_{i,ref} = 0$ *and* $q_{ref} = 0.5$.

solvers or different time-step will yield slightly different results. Otherwise it could also be an error in the modulation, however it is then small because the matrix converter performs overall well and no errors could be found when inspecting the modulation closely several times.

The next feature presented is the modulation curve of the matrix converter. The input displacement angle reference, $\Phi_{i,ref}$, is still kept constant at zero (no input reactive power) and $\vec{E}_f = \frac{50}{\sqrt{2}}\angle -20\,^\circ$. Only the modulation index reference of the voltage q_{ref} is increased. The results of the simulations are reported in table 4.1. From looking at table 4.1 we see that the output voltage magnitude, $\hat{V}_{o,meas}$, increases along with the modulation index reference q. In figure 4.4 which shows the output voltage versus the modulation index, it is clear that the measured output voltage magnitude, $\hat{V}_{o,meas}$, represented by the red curve, follows approximately linearly the modulation index q_{ref}. As was explained in section 3.1 the modulation index q cannot exceed $q_{max} = \frac{\sqrt{3}}{2}$. When the modulation index is however increased above this limit, the output voltage will saturate at a value a little above the limit of $\hat{V}_{max} = q_{max}\hat{V}_i = 86\,V$. The red curve in figure 4.4 settles at about $91\,V$. The theoretical modulation curve, qV_i, is added in blue in figure 4.4 for comparison. The theoretical modulation curve was set to settle at $V_{max} = 86.6\,V$ because ideally to avoid increased harmonics in the output voltage and input current this limit should not

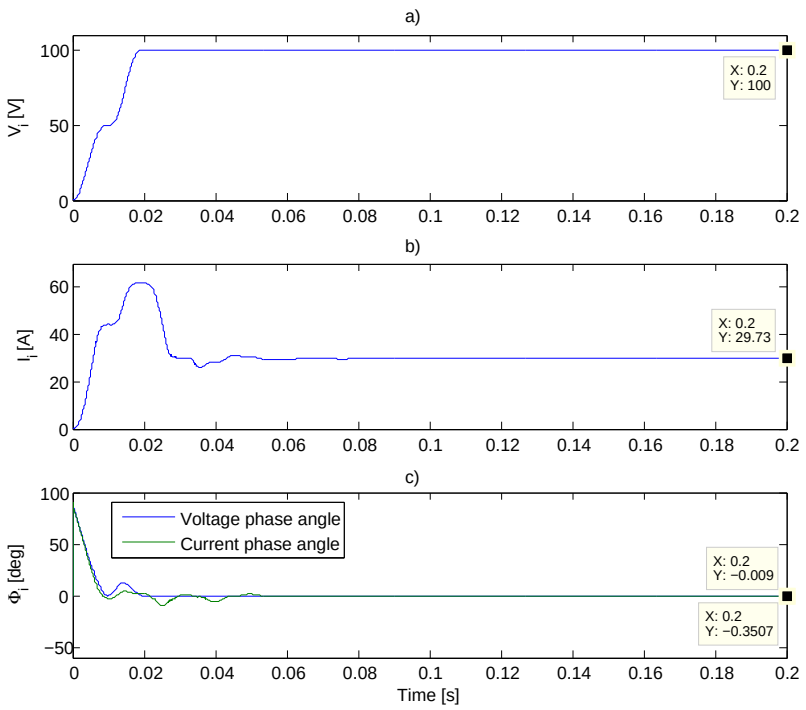

Figure 4.2: *The magnitude of the input voltage (a) and current (b) and input voltage and current phase angle (c) for* $\Phi_{i,ref} = 0$ *and* $q_{ref} = 0.5$.

be exceeded. When comparing the theoretical and experimental curves it is clear that the experimental curve is a little bit above the theoretical curve. This is probably due to the same reason as before; inaccurate Simulink measurement box or solver.

Let's now look at the other measured entities reported in table 4.1. $\Phi_{i,meas}$ is very close to zero, its reference, for the lower modulation indicis. For $q_{ref} \geq q_{max}$ the angle starts to deviate sligthly from the reference. This is due to matrix converter entering overmodulation. The losses ΔP in the matrix converter which is the difference between the input active power P_i and the output power P_o, are reported in the rightmost column. The power losses decrease for low modulation indicis. For q_{ref} above 0.5 the losses increase again. The losses in the converter follow the same trend as the output current $\hat{I}_{o,meas}$ which is normal as the losses are strongly dependent on the current.

Now the behaviour of the matrix converter will be investigated for an input displacement angle Φ_i different from zero. In the next battery of simulations the modulation index reference is kept constant at $q_{ref} = 0.5$ and the excitation voltage is kept at $\vec{E}_f = \frac{50}{\sqrt{2}}\angle{-20}\,^\circ$. The input displacement angle is increased from $\Phi_i = 0$ to $\Phi_i = -90\,^\circ$. The results are reported in table 4.2.

The measured input displacement angle follows quite nicely the reference Φ_{ref}. The input active and reactive powers were measured and reported in table 4.2. As excpected the active power decreases when the input displacement angle is increased while the reactive

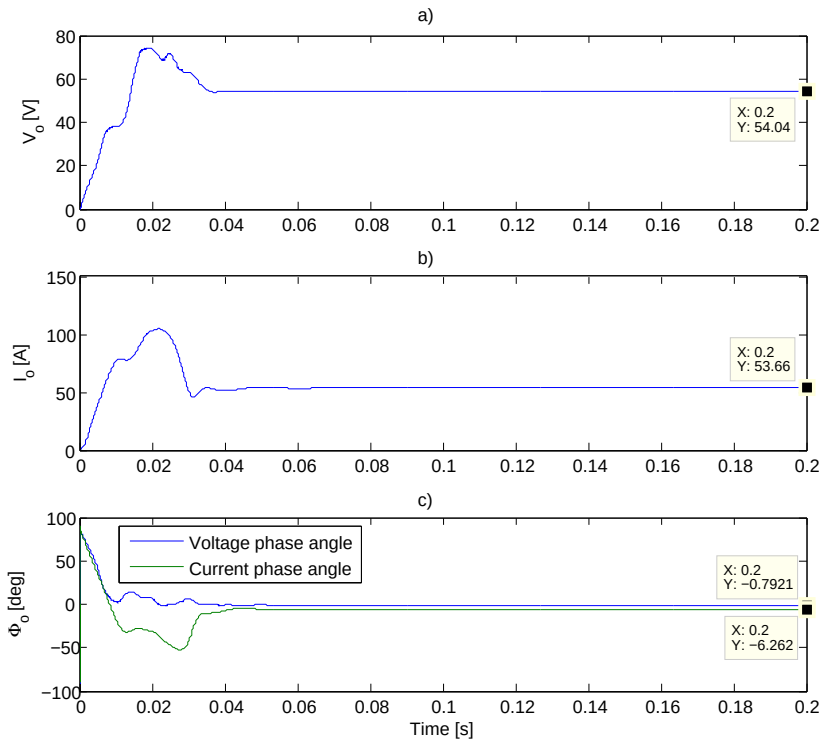

Figure 4.3: *The magnitude of the output voltage (a) and current (b) and output voltage and current phase angle (c) for* $\Phi_{i,ref} = 0$ *and* $q_{ref} = 0.5$.

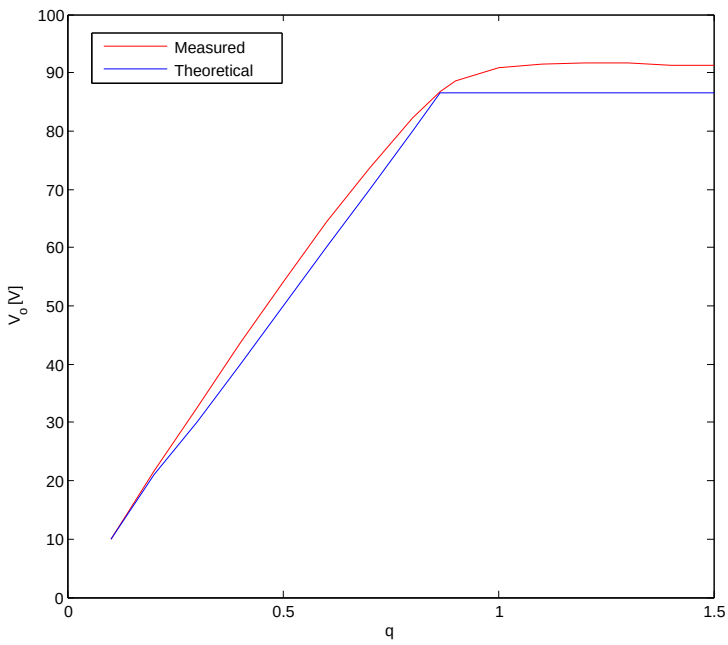

Figure 4.4: *Modulation curves of the output voltage* $\hat{V}_o$ *versus the modulation index* q_{ref} *build with experimental data from simulations (upper curve in red) and build with the theoretical values (lower curve in blue).*

Table 4.1: *Results of the simulations done with constant input displacement angle reference $\Phi_{i,ref} = 0$ and the modulation index reference q_{ref} increased from 0.1 to 1.5; From left to right: The reference modulation index q_{ref}, the measured output voltage $\hat{V}_{o,meas}$, the measured output current $\hat{I}_{o,meas}$, the measured output and input displacement angle $\Phi_{o,meas}$ and $\Phi_{i,meas}$, the measured input and output powers $P_{i,meas}$ and $P_{o,meas}$, the absolute matrix converter losses $\Delta P = P_i - P_o$.*

q_{ref}	$\hat{V}_{o,meas}$ $[V]$	$\hat{I}_{o,meas}$ $[A]$	$\Phi_{o,meas}$ $[°]$	$\Phi_{i,meas}$ $[°]$	$P_{i,meas}$ $[W]$	$P_{o,meas}$ $[W]$	ΔP $[W]$
0.1	9.9	123	-85	-0.8	360	143	217
0.2	21.7	91.5	-75	-1.4	910	740	170
0.3	32.6	66	-60	0.05	1779	1634	145
0.4	43.6	50.5	-30	0.3	2985	2845	140
0.5	54.1	53.5	5.2	0.4	4455	4350	105
0.6	64.3	72	29	0.7	6191	6064	127
0.7	73.6	94	41.2	1.5	8015	7870	145
0.8	82.2	116	48.2	3.2	9720	9560	160
0.866	86.8	128	51.2	4.3	10650	10490	160
0.9	88.7	133	53	4.6	11040	10890	150
1.0	90.9	139	53	4.5	11550	11405	145
1.1	91.5	141.5	53	4	11800	11644	156
1.2	91.6	143	52.5	4	12090	11928	162
1.3	91.6	145	52	4.1	12430	12274	156
1.4	91.3	146	51	4	12800	12650	150
1.5	91.2	147.8	50	4.2	13250	13085	165

Table 4.2: *Results of simulations done with constant modulation index reference $q_{ref} = 0.5$ and with the input displacement angle reference Φ_i decreased from 0 to $-90\,°$; From left to right: The reference input displacement angle $\Phi_{i,ref}$, the measured input displacement angle $\Phi_{i,meas}$, the measured output voltage $\hat{V}_o$, the measured output current $\hat{I}_o$, the measured output displacement angle Φ_o, the measured input current $\hat{I}_i$ A, the input active and reactive powers $P_{i,meas}$ and $Q_{i,meas}$.*

$\Phi_{i,ref}$ $[°]$	$\Phi_{i,meas}$ $[°]$	$\hat{V}_{o,meas}$ $[V]$	$\hat{I}_{o,meas}$ $[A]$	$\Phi_{o,meas}$ $[°]$	$I_{i,meas}$ $[A]$	$P_{i,meas}$ $[W]$	$Q_{i,meas}$ $[Var]$
0	0.35	54.1	53.7	5.0	29.7	4455	27.2
-10	-10.5	54.0	52.0	4.0	29	4280	793
-20	-20	54.0	48.1	4.7	28.1	3970	1445
-30	-27.8	54.5	42.5	7.5	26.5	3510	1480
-40	-37.3	54.9	42.7	7.9	29.4	3540	2696
-50	-48.5	52.8	41.1	2.0	33.5	3327	3760
-60	-60	47.0	34.2	-26.7	29	2205	3819
-70	-74	33.1	58.4	-72.1	23	940	3278
-80	-77.7	18	119	-44.6	74.7	2380	10915
-90	-84	1.6	147	-99.4	2.6	88.5	842

power increases for $\Phi_{ref} \geq -50\,°$. This is the excpected behaviour according to figure 3.18 in section 3.3. The $P_i - Q_i$ circle can be consulted for $\Phi_{ref} \geq -50\,°$ because the output voltage is approximately constant ($q_{ref} = 0.5$ for all simulations) and thus the output current and power factor are also approximately constant. The input apparent power is therefore a circle and the active and reactive power shares are determined by the displacement angle. For $\Phi_{ref} \leq -50\,°$, the active and reactive powers' values can no longer be explained with the $P_i - Q_i$ circle since $\hat{V}_{o,meas}$, $\hat{I}_{o,meas}$ and $\Phi_{o,meas}$ are not constant even though the modulation index is constant. In table 4.2 we see that the output voltage $\hat{V}_o$ collapses for the input displacement angle above $\Phi_i = -60\,°$ and can not be maintained to its reference value of $50\,V$. This is due to the fact that Φ_i and q limit eachother according to the equation $\cos\Phi_i = \frac{q}{\frac{\sqrt{3}}{2}}$ as was seen in section 3.3. Thus the maximum input displacement angle is $\Phi_{i,max} = \cos^{-1}\left(\frac{0.5}{\frac{\sqrt{3}}{2}}\right) = 54.7\,°$. The fact that the voltage cannot be maintained at its reference value is a serious drawback as the output voltage needs to be controlled in the MCRC system to control the PM machine. For an input displacement angle of $\Phi_i = -80\,°$ the system has a peak in the reactive power it provides to the grid. The input reactive power is $Q_i = 10915\,Var$. The peak is due to the input displacement angle being large and also to a peak in the ouput current $\hat{I}_o$. From a first glance at table 4.2 this could seem like a good operation set point to provide maximum reactive power. However, when looking closely at table 4.2, it is clear that this is not a viable compensation mode as the matrix converter modulation is really not functioning properly as was explained before. Also it is clear from table 4.2 that for $\Phi_i = -90\,°$ the modulation of the matrix converter collapses totally. The output voltage is down to $\hat{V}_{o,meas} = 1.6\,V$ and the input current is only $\hat{I}_{i,meas} = 2.6\,A$ although $\hat{I}_{o,meas} = 147\,A$.

We should now examine whether the active and reactive power ranges calculated with equation (3.89) and (3.90) in section 3.3 are obtainable with the built simulation model. The active and corresponding maximum reactive powers are calculated as a function of the modulation index q, $\hat{E}_f$ and δ and are reported in figure 4.5 in blue. To measure the active power and the corresponding maximum reactive power the maximum input displacement angle was tracked for each modulation index using the equation $\Phi_{i,max} = \cos^{-1}\left(\frac{q}{\frac{\sqrt{3}}{2}}\right)$. Since the reference and the measured input displacement angles are always a little off, the reference needed to be adjusted to obtain the rreal maximum input displacement angle. The results are reported in table 4.3. The measured input active and reactive powers are plotted in red in figure 4.5. A good agreement is obtained between the theoretical and measured values and we can see that while the active power flow in the MCRC system increases with the modulation index q, the input reactive power first increases and then falls down to zero for the maximum modulation index q_{max}. The maximum input reactive power occures for $q = 0.6$, which corresponds to a maximum input displacement angle of approximately $-45\,°$. From figure 3.18 in section 3.3 we know that for this angle the active and reactive powers are equal. This is also clear from figure 4.5 as the active and reactive power curves cross at $q = 0.6$. With an increasing modulation index q, the active

Table 4.3: *Results of simulations done with the modulation index reference increased from $q_{ref} = 0$ to $q_{ref} = 0.866$ and with the input displacement angle reference Φ_i set to its maximum possible value; From left to right: The reference modulation index q_{ref}, the theoretical maximum displacement angle $\Phi_{i,max}$ calculated according to $\Phi_{i,max} = \cos^{-1}\left(\frac{2q}{\sqrt{3}}\right)$, the measured input displacement angle $\Phi_{i,meas}$, the measured output voltage $\hat{V}_{o,meas}$, the measured output current $\hat{I}_{o,meas}$, the measured output displacement angle $\Phi_{o,meas}$, the measured input active and reactive powers $P_{i,meas}$ and $Q_{i,meas}$.*

q_{ref}	$\Phi_{i,max}$ [°]	$\Phi_{i,meas}$ [°]	$P_{i,meas}$ $[W]$	$Q_{i,meas}$ $[Var]$
0.05	-86.7	-86	170	2431
0.1	-83.4	-83.5	330	2922
0.2	-76.6	-76.6	815	3421
0.3	-69.7	-68.8	1675	4318
0.4	-62.5	-62	2872	5401
0.5	-54.9	-53.4	4180	5628
0.6	-46.2	-46.6	5570	5890
0.7	-35.5	-35.4	7300	5188
0.8	-22.5	-21	8950	3435
0.866	0	1	11400	-199

power share of the apparent power increases while the reactive power share decreases, see figure 3.18. For modulation indicis lower than $q = 0.6$, corresponding to maximum input displacement angles lower than $-45\,^\circ$, the reactive power share is larger than the active power share, see figure 3.18. So as P_i increases, Q_i also increases but with a slower slope as q increases. For $q = 0.6$ and correspondingly $\Phi_{i,max}$ the reactive power at the input is maximum. For modulation indicis above $q = 0.6$, the active power share becomes so large that the reactive power share can no longer increase and starts decreasing toward zero.

Now let's finally look at the waveforms for $\Phi_{i,ref} = -90\,^\circ$ and $q_{ref} = 0.5$ and see how the matrix converter behaves. In figure 4.6 are represented the input voltage and current magnitudes and the input displacement angle. In figure 4.7 are represented the output voltage, current and displacement angle. From both figures it is again clear that the modulation collapses for a displacement angle of $-90°$.

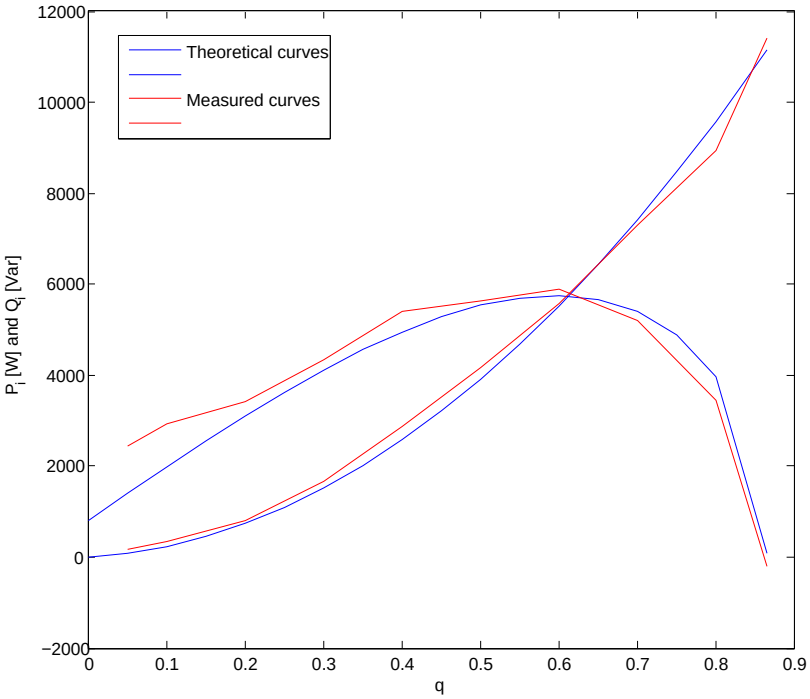

Figure 4.5: *The active and the reactive power ranges at the input of the MCRC device; the theoretical powers are in blue and the measured are in red; the active powers are the growing curves while the reactive powers are the first increasing and then decreasing curves.*

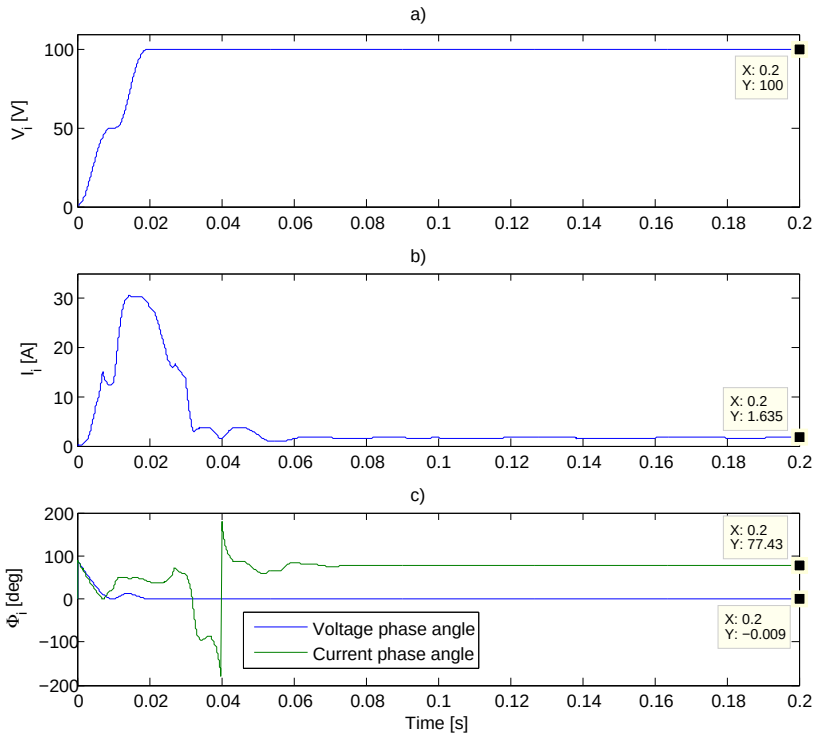

Figure 4.6: *The magnitude of the input voltage (a) and current (b) and input voltage and current phase angle (c) for* $\Phi_{i,ref} = -90\,^{\circ}$ *and* $q_{ref} = 0.5$.

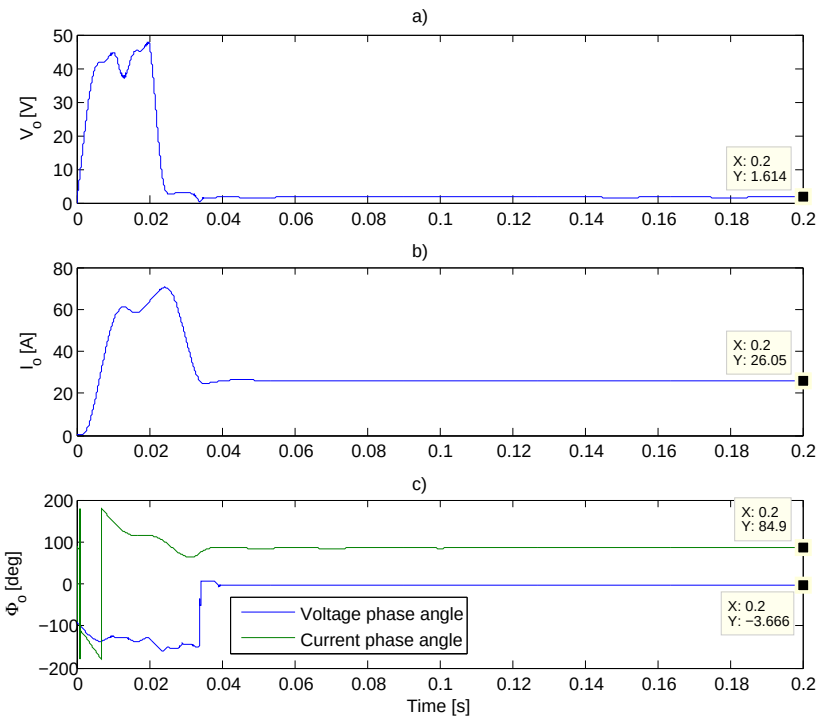

Figure 4.7: *The magnitude of the output voltage (a) and current (b) and output voltage and current phase angle (c) for* $\Phi_{i,ref} = -90\,^{\circ}$ *and* $q_{ref} = 0.5$.

Chapter 5

Improved reactive compensation with the three-vector-scheme modulation

The last simulation in the previous section showed how the conventional indirect space vector modulation collapses for an input phase displacement angle of $\Phi_i = -90\,^\circ$, as was predicted by the analysis in section 3.3. In section 3.4 is presented the three-vector-scheme that makes pure reactive power compensation possible. The modulation was implemented in MATLAB Simulink and the simulation model is to be found in appendix C in figure C.1, C.2, C.3, C.4, C.5 and C.6. The simulation model was built such that the input and output voltages are in phase ($\theta_{i,sp} = \theta_{o,sp}$) and $\Phi_i = -90\,^\circ$ and $\Phi_o = 90\,^\circ$ in order to keep the modulation simple. In figure A.2 in appendix A, the switching patterns for all 6 sectors, used for the modulation of the simulation model, are added. Since the modulation is implemented so that $\Phi_o = 90\,^\circ$, this condition needs to actually be fullfilled at the output of the matrix converter or terminal of the PM machine. To obtain approximately zero power factor the resistance needs to be lowered compared with the reactance. A high resistance was used for the previous simulations in order to dampen out initial oscillations faster. In the next simulations the resistance will be set to $R = 0.01\,\Omega$ while the reactance is kept at $X_s = 0.314\,\Omega$ as before. Thus the simulations need to run longer so as to see the oscillations disappear. Another parameter that needs to be modified with respect to the previous simulations is the excitation voltage. First of all the rotor angle should be set to zero since no active power should flow through the matrix converter for this case of pure reactive compensation. Secondly the amplitude of the excitation voltage should be set to a low value (below terminal voltage amplitude) in order to obtain $\Phi_o = 90\,^\circ$. From figure 2.2 in section 2.1 we see that when $V_o \geq E_f$ the current phasor lags the terminal voltage with $90\,^\circ$ which is what we want to obtain. On the other hand when $V_o \leq E_f$ the current phasor leads the terminal voltage phasor. The excitation voltage is set to $\vec{E}_f = \frac{10}{\sqrt{2}}\angle 0\,V$.

For the first simulation the input and output voltage and current waveforms are presented. The voltage ratio reference q_{ref} and the current ratio reference $q_{i,ref}$ can be set to different values as was explained in section 3.4. The ratios will be set at an operating point located

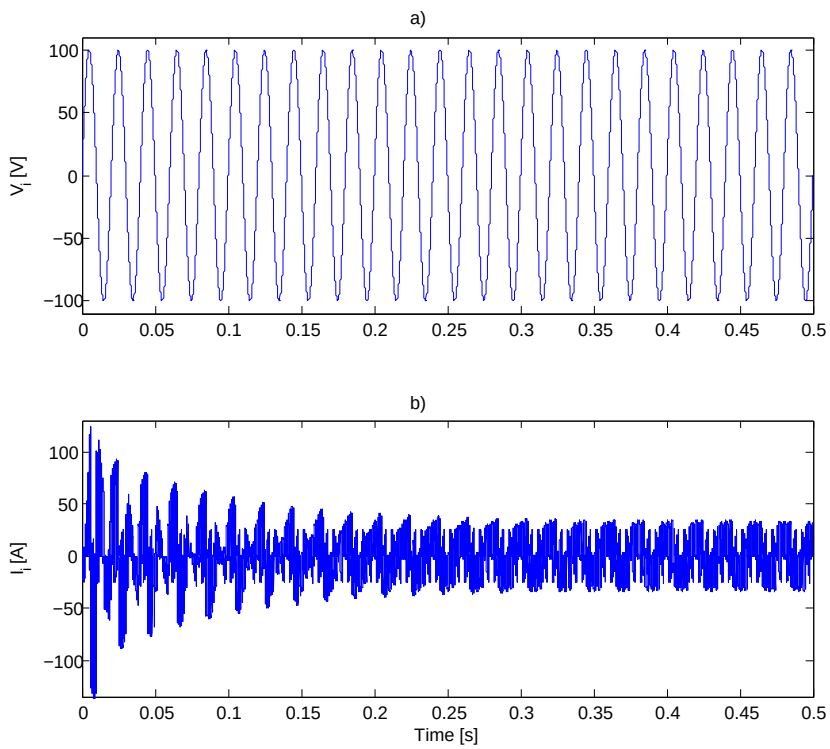

Figure 5.1: *The input voltage (a) and current (b) waveforms for $q = 0.2$ and $q = 0.7$.*

on the upper limit of the operation range of the three-vector-scheme modulated matrix converter. For $q = 0.2$ the maximum q_i can be calculated with equation (3.147) from section 3.4 to be appromimately $q_i = 0.7$. One phase of the input voltage and current are shown in figure 5.1 and one phase of the output voltage and all the phase of the output current are shown in figure 5.2. All the three phases of the output current are presented to show the initial oscillations that slowly damp out. The initial oscillations are also visible in the input current waveform in figure 5.1. Now that the oscillations are so large because of low resistance value, it is in order to give an explanation to this phenomenon. We call it oscillations but in figure 5.1 and 5.2 they rather manifest as DC-offsets. We call them oscillations anyway because the fundamental components become oscillatory because of the DC-offset in the waveforms, see the current magnitude in figure 5.3 and 5.4. We observe that the output current contains a DC-offset component that fades away with time, in addition to the forced AC response driven by the excitation voltage source. This is typical of short-circuit currents in a synchronous machine [13] p.128. The DC offset is the natural response of the synchronous machine (or R-L circuit here) to a short-circuit. The DC current are induced to keep the flux linkage constant in the reactance coil at the instant of short-circuit. The IGBTs are all initially OFF, that is open state, and when the simulation starts and the IGBTs start switching the R-L circuit sees it as a short-circuit. The oscillations also propagates to the input since the input current is build with output current fragments. The corresponding magnitude and angle displacement are shown in

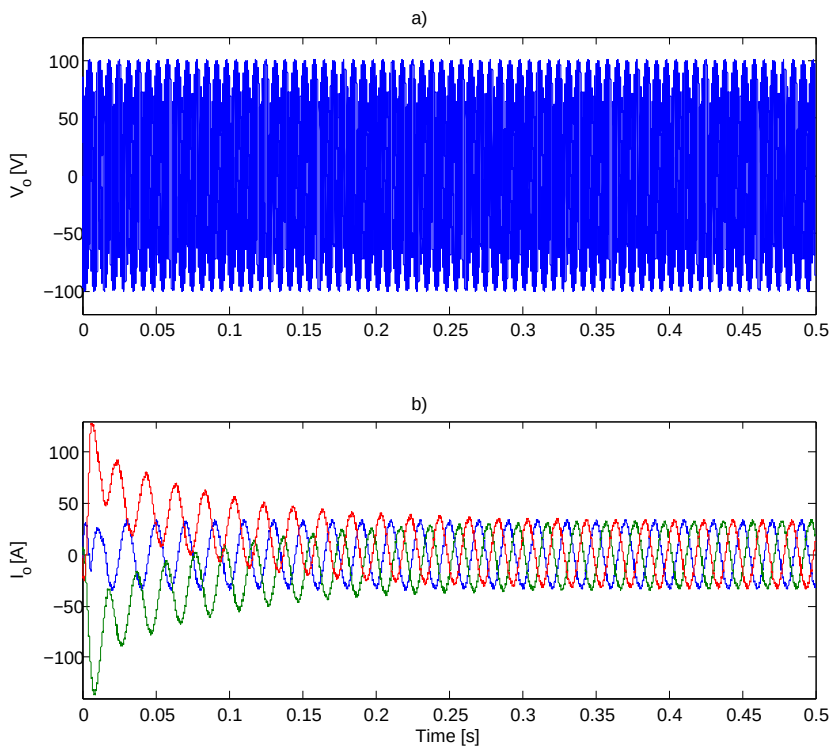

Figure 5.2: *The output voltage (a) and current (b) waveforms for $q = 0.2$ and $q = 0.7$.*

figure 5.3 and 5.4. The measured output voltage is $\hat{V}_o = 20.02\,V$ which is very close to its reference $q\hat{V}_i = 20\,V$. The output current is measured to be $\hat{I}_o = 31.98\,A$ and the input current is $\hat{I}_i = 22.28\,A$. This is also very close to the reference of $q_i\hat{I}_o = 0.7{*}31.98 = 22.39\,A$.

The last simulation result to be presented in this Master thesis will demonstrate how the MCRC device can be used for voltage support. The MCRC device is connected to a grid to which a three-phase symmetrical fault is connected after $t = 1\,s$ so as to reduce the grid voltage by 23.4%. The MCRC device is set to start reactive power compensation at $t = 1.5\,s$ to bring the voltage back to its nominal pre-fault value.

As we saw in the previous simulations the input current contains a lot of harmonics. These needs to filtered away before the current can be injected into the grid. A simple RLC filter is connected at the input of the matrix converter. The filter inductance L and capacitance C are chosen such that the cut-off frequency is $f_c = \frac{1}{2\pi\sqrt{LC}} \approx 178\,Hz$: $L = 2\,mH$, $C = 400\,\mu F$ and $R = 4\,\Omega$ [22]. Having a filter at the input of the matrix converter modifies the voltage at the input of the converter. This voltage change should be compensated for by a regulator that provides a new reference to the modulation of the matrix converter. Also changes in the gridside voltage due to a short-circuit fault on the grid should be compensated for by a regulator. This has not been done in this thesis as no control system has been implemented. Therefore the input voltage of the matrix converter will vary causing in turn the output

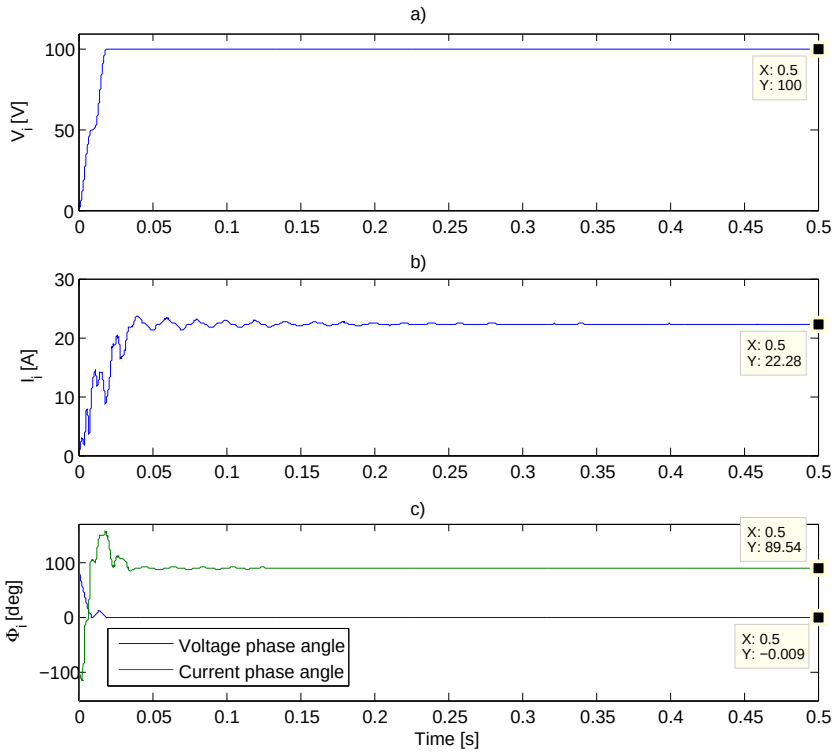

Figure 5.3: *The magnitude of the input voltage $\hat{V}_i$ (a), current $\hat{I}_i$ (b) and the input displacement angle Φ_i (c) for $q = 0.2$ and $q = 0.7$.*

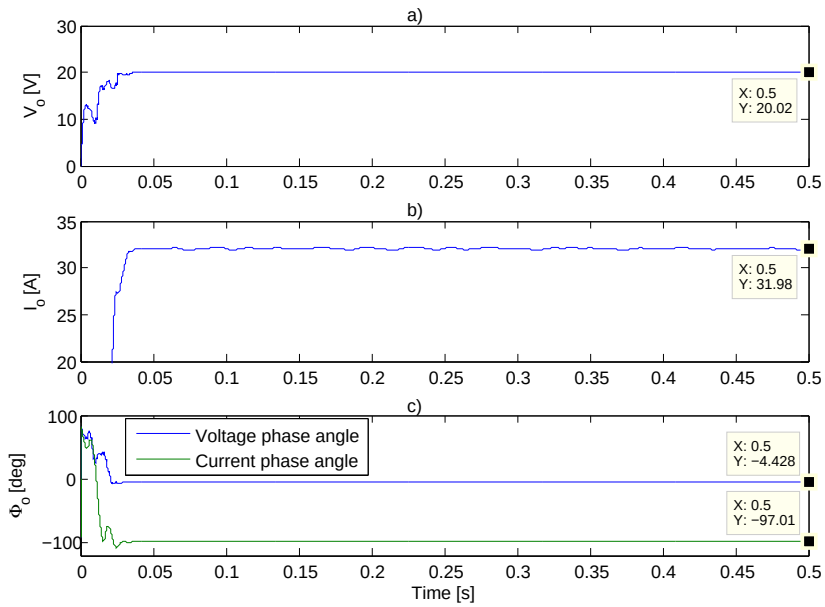

Figure 5.4: *The magnitude of the output voltage $\hat{V}_o$ (a), current $\hat{I}_o$ (b) and the output displacement angle Φ_o (c) for $q = 0.2$ and $q = 0.7$.*

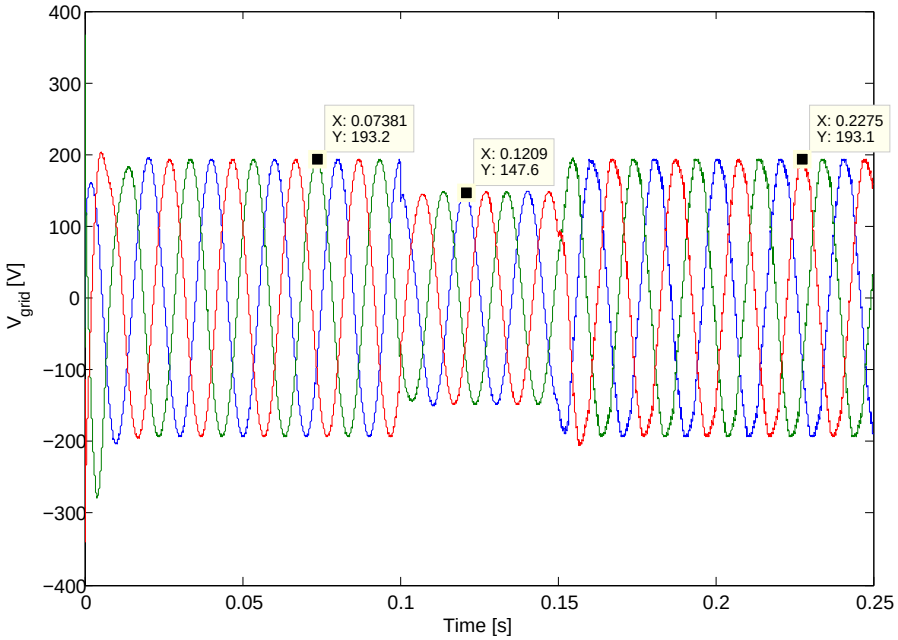

Figure 5.5: *The gridside voltage: a fault occures at $t = 0.1\,s$ such that the voltage has a 23% drop, the compensation device is set to start at $t = 0.15\,s$ to bring back the voltage to its pre-fault value.*

voltage to vary and as a consequence the output current also. It is therefore difficult to control the input current into the grid in these conditions, not to say impossible. To be able to show the reactive power compensation feature of the MCRC device anyway, the equivalent circuit of the PM machine is replaced by a constant current source such that $\vec{I}_o = 60\angle -90\,^\circ\,A$. The MATLAB Simulink simulation model is shown in figure D.1 in appendix D. The voltage on the gridside is shown in figure 5.5. We see that the voltage is brought back to its pre-fault value immediately after the MCRC is set to work.

Chapter 6

Conclusion and further work

6.1 Conclusion

A new application for the matrix converter was investigated in this Master's thesis: A matrix converter-based reactive power compensation device or MCRC device. In combination with a PM machine, the matrix converter can provide or extract reactive power to a grid it is shunt-connected to. When the PM machine is loaded, the MCRC device can act as an energy buffer in addition to compensating for reactive power. When the PM machine runs at no-load, the device provides pure reactive compensation.

The first part of the thesis was a theoretical analysis of the MCRC device. The two main components of the device were presented: The PM machine and the matrix converter. The aim of the PM machine analysis, in addtion to understanding the general functioning of the machine, was to identify the conditions it imposes at the output of the matrix converter for the two operation modes: loaded and at no-load. The equation for the output current and output power factor were developed for the loaded operation mode. In the no-load situation, the analysis showed that the output current is purely reactive and the output power factor is zero. No active power flows through the matrix converter and the input power factor is also zero.

The matrix converter was the next component to be analyzed. The modulation of the matrix converter influences strongly the reactive power transfer at the input of the matrix converter. The conventional indirect space vector modulation influences it such that the input reactive power is dependent on the active power flow through the matrix converter. The output power factor determines the amount of apparent power at the input of the matrix converter. The input displacement angle will then decide how the apparent power distributes in active and reactive power. The bigger the input displacement angle is, the larger the reactive power share. The modulation index on the other hand increases the active power share. However the input displacement angle and modulation index are inversely

proportional. If the modulation index is increased, the maximum input displacement angle is decreased and vice versa.

Despite this trade-off between the active and reactive power at the input of the matrix converter, the following feature was found to be a characteristic of the indirect space vector modulation: There cannot be any reactive power at the input of the matrix converter if no active power flows through it. As a conclusion, when the matrix converter is modulated with the conventional indirect space vector modulation, it cannot be used for pure reactive compensation. It can only be used in combination with active power transfer and with an energy buffer, load on the rotor shaft.

For pure reactive power compensation with the MCRC device another modulation must be used: The three-vector-scheme was suggested instead of the conventional modulation. This modulation is a modified version of the indirect space vector modulation and performs very well for zero active power transfer. Both the conventional indirect space vector modulation and the three-vector-scheme were described in details such that all the information needed to implement simulation models is provided.

The second part of the thesis was dedicated to experimental results. Simulation models for the MCRC device were implemented with a matrix converter modulated with the conventional indirect space vector modulation and the three-vector-scheme. The PM machine was modeled by a simple equivalent circuit. Simulations done with the conventionally modulated matrix converter included: Input and output current and voltage waveforms, a modulation curve of the output voltage versus the modulation index, the active and input reactive power for a constant modulation index but varying input displacement angle and the active power and the maximum input reactive power as functions of the modulation index. The measured values corresponded overall quite well to the references. Deviations from the reference were discussed to be due to inaccurate solver or inaccurate measuring toolboxes.

The modulation curve confirmed that the absolute upper limit of the modulation index is $q_{max} = \frac{\sqrt{3}}{2}$. When the active and reactive power were measured for a constant modulation index but varying input displacement angle it was clear that when the angle exceeded the limit $\Phi_{i,max} = \cos^{-1} \frac{q}{\frac{\sqrt{3}}{2}}$, the modulation collapsed and the voltage reference could not be followed anymore. However for angles below the limit $\Phi_{i,max}$, the simulation results showed clearly the inherent trade-off between the active and reactive power at the input of the matrix converter. The active power and the corresponding maximum input reactive power as functions of the modulation index corresponded well to the theoretically calculated powers and showed that the maximum reactive power compensation is obtainable for $q = 0.6$. $q = 0.6$ is the modulation index corresponding to $\Phi_{i,max} \approx -45\,^\circ$ for which the active power is equal to the reactive power. The last simulation with the conventional modulation were performed with no active power transfer. The modulation collapsed again and the voltage reference could not be followed at all.

Finally simulations were performed with the three-vector-scheme modulated matrix con-

verter. Input and output current and voltage waveforms were presented showing that the modulation functions very well. A simplified version of the MCRC device where the equivalent cicuit model of the PM machine was replaced with a current source and equipped with a RLC filter, was connected to a grid. A three-phase symmetrical fault was connected to the grid after some time. The device was able to compensate for reactive power and bring the voltage back to its pre-fault value, thus proving that the MCRC can perform reactive power compensation and voltage support.

6.2 Further work

As was made clear in this Master's thesis no control system was investigated for the MCRC system. This did not really impair the investigations but further work should be dedicated to building a control system that regulates the PM machine speed and that would compensate for the current when an input filter is added or compensate for the voltage when voltage variations occur on the gridside, due to a fault for instance. This would also mean that a more precise model of a PM machine than the equivalent circuit should be introduced.

Bibliography

[1] E-mail correspondance with F. Schafmeister, 2010.

[2] A. Alesina and M. Venturini. Intrinsic amplitude limits and optimum design of 9-switches direct pwm ac-ac converters. In *Power Electronics Specialists Conference, 1988. PESC '88 Record., 19th Annual IEEE*, pages 1284–1291 vol.2, April 1988.

[3] R. Cardenas, R. Pena, P. Wheeler, J. Clare, and G. Asher. Control of the reactive power supplied by a wecs based on an induction generator fed by a matrix converter. *Industrial Electronics, IEEE Transactions on*, 56(2):429–438, Feb. 2009.

[4] D. Casadei, G. Serra, A. Tani, and L. Zarri. Matrix converter modulation strategies: a new general approach based on space-vector representation of the switch state. *Industrial Electronics, IEEE Transactions on*, 49(2):370–381, Apr 2002.

[5] Nichicon Corporation. General description of aluminium electrolytic capacitor. *http://www.nichicon.co.jp/english/products/pdf/aluminum.pdf*.

[6] L. Gyugyi and B. R. Pelly. *Static Power Frequency Changers*. John Wiley & Sons, 1976.

[7] N. Holtsmark. Specialization project: Reactive power compensation using a matrix converter. Master's thesis, Norwegian University of Science and Technology, 2009.

[8] C. Hubert. *Electric Machines: Theory, Operation, Applications, Adjustment, and Control*. Prentice Hall, 2002.

[9] J. Irwin David. *The industrial Electronics Handbook*. CRC Press LLC, 1997.

[10] J. I. Itoh and S. Tamada. A novel engine generator system with active filter functions using a matrix converter, slides from presentation in trondheim, 2007.

[11] Jun-Ichi Itoh, I. Sato, A. Odaka, H. Ohguchi, H. Kodachi, and N. Eguchi. A novel approach to practical matrix converter motor drive system with reverse blocking igbt. *Power Electronics, IEEE Transactions on*, 20(6):1356–1363, Nov. 2005.

[12] J. W. Kolar and T. Friedli. The essence of matrix converters, swiss federal institute of technology (eth) zurich, power electronic systems laboratory, iecon'08, 2008.

[13] J. Machowski, J. W. Bialek, and J. R. Bumby. *Power system Dynamics, Stability and Control*. John Wiley & Sons, Ltd, second edition edition, 2008.

[14] N. Mohan. *Advanced Electric Drives, Analysis, Control and Modeling using Simulink*. MNPERE, 2001.

[15] N. Mohan. *Electric Drives, An Integrative Approach*. Mnpere, 2003.

[16] N. Mohan. *First Course on Power Electronics*. MNPERE, 2007.

[17] Robbins Mohan, Undeland. *Power Electronics, Converter, Applications, and Design*. John Wiley & Sons, Inc., third edition, 2003.

[18] V.H. Prasad. Analysis and comparison of space vector modulation schemes for three-leg and four-leg voltage source inverters. Master's thesis, Virginia Polytechnic Institute and State University, 1997.

[19] F. Schafmeister. *Indirekte Sparse-Matrix Konverter*. PhD thesis, Eidgenössischen Technischen Hochschule Zürich, 2008.

[20] F. Schafmeister and J.W. Kolar. Novel hybrid modulation schemes extending the reactive power control range of conventional and sparse matrix converters operating at maximum output voltage. *International Power Electronics and Motion Control Conference, 2004. EPE-PEMC 04. 2004 IEEE 11th Annual*, 2004.

[21] F. Schafmeister and J.W. Kolar. Novel modulation schemes for conventional and sparse matrix converters facilitating reactive power transfer independent of active power flow. *Power Electronics Specialists Conference, 2004. PESC 04. 2004 IEEE 35th Annual*, 4:2917 – 2923 Vol.4, 2004.

[22] Bingsen Wang and Jimmie J. Cathey. DSP-controlled, space-vector PWM, current source converter for STATCOM application. *Electric Power Systems Research*, 67(2):123 – 131, 2003.

[23] P. Wheeler and D. Grant. Optimised input filter design and low-loss switching techniques for a practical matrix converter. *Electric Power Applications, IEE Proceedings -*, 144(1):53–60, Jan 1997.

[24] Qingguang Yu, Pei Li, Wenhua Liu, and Xiaorong Xie. Overview of statcom technologies. In *Electric Utility Deregulation, Restructuring and Power Technologies, 2004. (DRPT 2004). Proceedings of the 2004 IEEE International Conference on*, volume 2, pages 647–652 Vol.2, April 2004.

Appendix A

Modulation sequence in three-vector-scheme modulation

$\Phi_i = -90^\circ$ $\Phi_o = 90^\circ$	$\theta_{i,sp} \geq 0$	$\vec{u}_{inverse}/\vec{i}_{lower}$	$\vec{u}_{lower}/\vec{i}_{lower}$	$\vec{u}_{upper}/\vec{i}_{lower}$	$\vec{u}_{zero}/\vec{i}_{lower}$	$\vec{u}_{zero}/\vec{i}_{upper}$	$\vec{u}_{upper}/\vec{i}_{upper}$	$\vec{u}_{lower}/\vec{i}_{upper}$	$\vec{u}_{zero}/\vec{i}_{upper}$	$\vec{u}_{zero}/\vec{i}_{third}$	$\vec{u}_{max}/\vec{i}_{third}$
	$\theta_{i,sp} \leq 0$	$\vec{u}_{max}/\vec{i}_{lower}$	$\vec{u}_{upper}/\vec{i}_{upper}$	$\vec{u}_{lower}/\vec{i}_{upper}$	$\vec{u}_{zero}/\vec{i}_{upper}$	$\vec{u}_{zero}/\vec{i}_{lower}$	$\vec{u}_{lower}/\vec{i}_{lower}$	$\vec{u}_{upper}/\vec{i}_{lower}$	$\vec{u}_{zero}/\vec{i}_{lower}$	$\vec{u}_{zero}/\vec{i}_{third}$	$\vec{u}_{inverse}/\vec{i}_{third}$
$\Phi_i = 90^\circ$ $\Phi_o = 90^\circ$	$\theta_{i,sp} \geq 0$	$\vec{u}_{max}/\vec{i}_{lower}$	$\vec{u}_{upper}/\vec{i}_{lower}$	$\vec{u}_{lower}/\vec{i}_{lower}$	$\vec{u}_{zero}/\vec{i}_{lower}$	$\vec{u}_{zero}/\vec{i}_{upper}$	$\vec{u}_{lower}/\vec{i}_{upper}$	$\vec{u}_{upper}/\vec{i}_{upper}$	$\vec{u}_{zero}/\vec{i}_{upper}$	$\vec{u}_{zero}/\vec{i}_{third}$	$\vec{u}_{inverse}/\vec{i}_{third}$
	$\theta_{i,sp} \leq 0$	$\vec{u}_{inverse}/\vec{i}_{upper}$	$\vec{u}_{lower}/\vec{i}_{upper}$	$\vec{u}_{upper}/\vec{i}_{upper}$	$\vec{u}_{zero}/\vec{i}_{upper}$	$\vec{u}_{zero}/\vec{i}_{lower}$	$\vec{u}_{upper}/\vec{i}_{lower}$	$\vec{u}_{lower}/\vec{i}_{lower}$	$\vec{u}_{zero}/\vec{i}_{lower}$	$\vec{u}_{zero}/\vec{i}_{third}$	$\vec{u}_{max}/\vec{i}_{third}$

Figure A.1: *Generalized switching patterns used for the modulation of the matrix converter with the three-vector-scheme; for $\Phi_i = -90^\circ$ and $\Phi_o = 90^\circ$ (two upper rows), $\theta_{i,sp} \geq 0$ (first row) and $\theta_{i,sp} \leq 0$ (second row); for $\Phi_i = 90^\circ$ and $\Phi_o = 90^\circ$ (two bottom rows), $\theta_{i,sp} \geq 0$ (third row) and $\theta_{i,sp} \leq 0$ (fourth row).*

	$\theta_{i,sp}\geq 0$										$\theta_{i,sp}\leq 0$									
SECTOR I	$\lvert d_{pnn,rs}-d^q_{npn,rs}\rvert$		$d_{ppn,rs}+MIN(d_{pnn,rs};d^q_{npn,rs})$	$d_{ppp,rs}$	$d_{ppp,rt}$	$d_{ppn,rt}$	$d_{pnn,rt}$	$d_{nnn,rt}$	$d_{nnn,st}$	$d^q_{pnp,st}$	$\lvert d_{pnn,rt}-d^q_{nnp,rt}\rvert$		$d_{pnp,rt}+MIN(d_{pnn,rt};d^q_{nnp,rt})$	$d_{nnn,rt}$	$d_{nnn,rs}$	$d_{pnn,rs}$	$d_{pnp,rs}$	$d_{ppp,rs}$	$d_{ppp,ts}$	$d^q_{ppn,ts}$
	$d^q_{npn,rs}>d_{pnn,rs}$ $[npn,rs]$	$d_{pnn,rs}>d^q_{npn,rs}$ $[pnn,rs]$	$[ppn,rs]$	$[ppp,rs]$	$[ppp,rt]$	$[ppn,rt]$	$[pnn,rt]$	$[nnn,rt]$	$[nnn,st]$	$[pnp,st]$	$d^q_{nnp,rt}>d_{pnn,rt}$ $[nnp,rt]$	$d_{pnn,rt}>d^q_{nnp,rt}$ $[pnn,rt]$	$[pnp,rt]$	$[nnn,rs]$	$[nnn,rs]$	$[pnn,rs]$	$[pnp,rs]$	$[ppp,rs]$	$[ppp,ts]$	$[ppn,ts]$
	u_{rs}/i_v	u_{rs}/i_u	$u_{rs}/-i_w$	$u_{rs}/0$	$u_{rt}/0$	$u_{rt}/-i_w$	u_{rt}/i_u	$u_{rt}/0$	$u_{st}/0$	$u_{rs}/-i_v$	u_{rt}/i_w	u_{rt}/i_u	$u_{rt}/-i_v$	$u_{rt}/0$	$u_{rs}/0$	u_{rs}/i_u	$u_{rs}/-i_v$	$u_{rs}/0$	$u_{ts}/0$	$u_{ts}/-i_w$
SECTOR II	$\lvert d_{ppn,rt}-d^q_{npp,rt}\rvert$		$d_{npn,rt}+MIN(d_{ppn,rt};d^q_{npp,rt})$	$d_{nnn,rt}$	$d_{nnn,st}$	$d_{npn,st}$	$d_{ppn,st}$	$d_{ppp,st}$	$d_{ppp,sr}$	$d^q_{pnn,sr}$	$\lvert d_{ppn,st}-d^q_{pnp,st}\rvert$		$d_{pnn,st}+MIN(d_{ppn,st};d^q_{pnp,st})$	$d_{ppp,st}$	$d_{ppp,rt}$	$d_{ppn,rt}$	$d_{pnn,rt}$	$d_{nnn,rt}$	$d_{nnn,rs}$	$d^q_{npn,rs}$
	$d^q_{npp,rt}>d_{ppn,rt}$ $[npp,rt]$	$d_{ppn,rt}>d^q_{npp,rt}$ $[ppn,rt]$	$[npn,rt]$	$[nnn,rt]$	$[nnn,st]$	$[npn,st]$	$[ppn,st]$	$[ppp,st]$	$[ppp,sr]$	$[pnn,sr]$	$d^q_{pnp,st}>d_{ppn,st}$ $[pnp,st]$	$d_{ppn,st}>d^q_{pnp,st}$ $[ppn,st]$	$[pnn,st]$	$[ppp,st]$	$[ppp,rt]$	$[ppn,rt]$	$[pnn,rt]$	$[nnn,rt]$	$[nnn,rs]$	$[npn,rs]$
	$u_{rt}/-i_u$	$u_{rt}/-i_w$	u_{rt}/i_v	$u_{rt}/0$	$u_{st}/0$	u_{st}/i_v	$u_{st}/-i_w$	$u_{st}/0$	$u_{sr}/0$	u_{sr}/i_u	$u_{st}/-i_v$	$u_{st}/-i_w$	u_{st}/i_u	$u_{st}/0$	$u_{rt}/0$	$u_{rt}/-i_w$	u_{rt}/i_u	$u_{rt}/0$	$u_{rs}/0$	u_{rs}/i_v
SECTOR III	$\lvert d_{npn,st}-d^q_{nnp,st}\rvert$		$d_{npp,st}+MIN(d_{npn,st};d^q_{nnp,st})$	$d_{ppp,st}$	$d_{ppp,sr}$	$d_{npp,sr}$	$d_{npn,sr}$	$d_{nnn,sr}$	$d_{nnn,tr}$	$d^q_{ppn,tr}$	$\lvert d_{npn,sr}-d^q_{pnn,sr}\rvert$		$d_{ppn,sr}+MIN(d_{npn,sr};d^q_{pnn,sr})$	$d_{nnn,sr}$	$d_{nnn,st}$	$d_{npn,st}$	$d_{ppn,st}$	$d_{ppp,st}$	$d_{ppp,rt}$	$d^q_{npp,rt}$
	$d^q_{nnp,st}>d_{npn,st}$ $[nnp,st]$	$d_{npn,st}>d^q_{nnp,st}$ $[npn,st]$	$[npp,st]$	$[ppp,st]$	$[ppp,sr]$	$[npp,sr]$	$[npn,sr]$	$[nnn,sr]$	$[nnn,tr]$	$[ppn,tr]$	$d^q_{pnn,sr}>d_{npn,sr}$ $[pnn,sr]$	$d_{npn,sr}>d^q_{pnn,sr}$ $[npn,sr]$	$[ppn,sr]$	$[nnn,sr]$	$[nnn,st]$	$[npn,st]$	$[ppn,st]$	$[ppp,st]$	$[ppp,rt]$	$[npp,rt]$
	u_{st}/i_w	u_{st}/i_v	$u_{st}/-i_u$	$u_{st}/0$	$u_{sr}/0$	$u_{sr}/-i_u$	u_{sr}/i_v	$u_{sr}/0$	$u_{tr}/0$	$u_{tr}/-i_w$	u_{sr}/i_u	u_{sr}/i_v	$u_{sr}/-i_w$	$u_{sr}/0$	$u_{st}/0$	u_{st}/i_v	$u_{st}/-i_w$	$u_{st}/0$	$u_{rt}/0$	$u_{rt}/-i_u$
SECTOR IV	$\lvert d_{npp,sr}-d^q_{pnp,sr}\rvert$		$d_{nnp,sr}+MIN(d_{npp,sr};d^q_{pnp,sr})$	$d_{nnn,sr}$	$d_{nnn,tr}$	$d_{nnp,tr}$	$d_{npp,tr}$	$d_{ppp,tr}$	$d_{ppp,ts}$	$d^q_{npn,ts}$	$\lvert d_{npp,tr}-d^q_{ppn,tr}\rvert$		$d_{npn,tr}+MIN(d_{npp,tr};d^q_{ppn,tr})$	$d_{ppp,tr}$	$d_{ppp,sr}$	$d_{npp,sr}$	$d_{npn,sr}$	$d_{nnn,sr}$	$d_{nnn,st}$	$d^q_{nnp,st}$
	$d^q_{pnp,sr}>d_{npp,sr}$ $[pnp,sr]$	$d_{npp,sr}>d^q_{pnp,sr}$ $[npp,sr]$	$[nnp,sr]$	$[nnn,sr]$	$[nnn,tr]$	$[nnp,tr]$	$[npp,tr]$	$[ppp,tr]$	$[ppp,ts]$	$[npn,ts]$	$d^q_{ppn,tr}>d_{npp,tr}$ $[ppn,tr]$	$d_{npp,tr}>d^q_{ppn,tr}$ $[npp,tr]$	$[npn,tr]$	$[ppp,tr]$	$[ppp,sr]$	$[npp,sr]$	$[npn,sr]$	$[nnn,sr]$	$[nnn,st]$	$[nnp,st]$
	$u_{sr}/-i_v$	$u_{sr}/-i_u$	u_{sr}/i_w	$u_{sr}/0$	$u_{tr}/0$	u_{tr}/i_w	$u_{tr}/-i_u$	$u_{tr}/0$	$u_{ts}/0$	u_{ts}/i_v	$u_{tr}/-i_w$	$u_{tr}/-i_u$	u_{tr}/i_v	$u_{tr}/0$	$u_{sr}/0$	$u_{sr}/-i_u$	u_{sr}/i_u	$u_{sr}/0$	$u_{st}/0$	u_{st}/i_w
SECTOR V	$\lvert d_{nnp,tr}-d^q_{pnn,tr}\rvert$		$d_{pnp,tr}+MIN(d_{nnp,tr};d^q_{pnn,tr})$	$d_{ppp,tr}$	$d_{ppp,ts}$	$d_{pnp,ts}$	$d_{nnp,ts}$	$d_{nnn,ts}$	$d_{nnn,rs}$	$d^q_{npp,rs}$	$\lvert d_{nnp,ts}-d^q_{npn,ts}\rvert$		$d_{npp,ts}+MIN(d_{nnp,ts};d^q_{npn,ts})$	$d_{nnn,ts}$	$d_{nnn,tr}$	$d_{nnp,tr}$	$d_{npp,tr}$	$d_{ppp,tr}$	$d_{ppp,sr}$	$d^q_{pnp,sr}$
	$d^q_{pnn,tr}>d_{nnp,tr}$ $[pnn,tr]$	$d_{nnp,tr}>d^q_{pnn,tr}$ $[nnp,tr]$	$[pnp,tr]$	$[ppp,tr]$	$[ppp,ts]$	$[pnp,ts]$	$[nnp,ts]$	$[nnn,ts]$	$[nnn,rs]$	$[npp,rs]$	$d^q_{npn,ts}>d_{nnp,ts}$ $[npn,ts]$	$d_{nnp,ts}>d^q_{npn,ts}$ $[nnp,ts]$	$[npp,ts]$	$[nnn,ts]$	$[nnn,tr]$	$[nnp,tr]$	$[npp,tr]$	$[ppp,tr]$	$[ppp,sr]$	$[pnp,sr]$
	u_{tr}/i_u	u_{tr}/i_w	$u_{tr}/-i_v$	$u_{tr}/0$	$u_{ts}/0$	$u_{ts}/-i_v$	u_{ts}/i_w	$u_{ts}/0$	$u_{rs}/0$	$u_{rs}/-i_u$	u_{ts}/i_v	u_{ts}/i_w	$u_{ts}/-i_u$	$u_{ts}/0$	$u_{tr}/0$	u_{tr}/i_w	$u_{tr}/-i_u$	$u_{tr}/0$	$u_{sr}/0$	$u_{sr}/-i_v$
SECTOR VI	$\lvert d_{pnp,ts}-d^q_{ppn,ts}\rvert$		$d_{pnn,ts}+MIN(d_{pnp,ts};d^q_{ppn,ts})$	$d_{nnn,ts}$	$d_{nnn,rs}$	$d_{pnn,rs}$	$d_{pnp,rs}$	$d_{ppp,rs}$	$d_{ppp,rt}$	$d^q_{nnp,rt}$	$\lvert d_{pnp,rs}-d^q_{npp,rs}\rvert$		$d_{nnp,rs}+MIN(d_{pnp,rs};d^q_{npp,rs})$	$d_{ppp,rs}$	$d_{ppp,ts}$	$d_{pnp,ts}$	$d_{nnp,ts}$	$d_{nnn,ts}$	$d_{nnn,tr}$	$d^q_{pnn,tr}$
	$d^q_{ppn,ts}>d_{pnp,ts}$ $[ppn,ts]$	$d_{pnp,ts}>d^q_{ppn,ts}$ $[pnp,ts]$	$[pnn,ts]$	$[nnn,ts]$	$[nnn,rs]$	$[pnn,rs]$	$[pnp,rs]$	$[ppp,rs]$	$[ppp,rt]$	$[nnp,rt]$	$d^q_{npp,rs}>d_{pnp,rs}$ $[npp,rs]$	$d_{pnp,rs}>d^q_{npp,rs}$ $[pnp,rs]$	$[nnp,rs]$	$[ppp,rs]$	$[ppp,ts]$	$[pnp,ts]$	$[nnp,ts]$	$[nnn,ts]$	$[nnn,tr]$	$[pnn,tr]$
	$u_{ts}/-i_w$	$u_{ts}/-i_v$	u_{ts}/i_u	$u_{ts}/0$	$u_{rs}/0$	u_{rs}/i_u	$u_{rs}/-i_v$	$u_{rs}/0$	$u_{rt}/0$	u_{rt}/i_w	$u_{rs}/-i_u$	$u_{rs}/-i_v$	u_{rs}/i_w	$u_{rs}/0$	$u_{ts}/0$	$u_{ts}/-i_v$	u_{ts}/i_w	$u_{ts}/0$	$u_{tr}/0$	u_{tr}/i_u

Figure A.2: *Switching patterns used for the modulation of the matrix converter with the three-vector-scheme; with input space vector in phase with the output space vector and $\Phi_i = -90^\circ$ and $\Phi_o = 90^\circ$.*

Appendix B

Simulation model of matrix converter with conventional space vector modulation

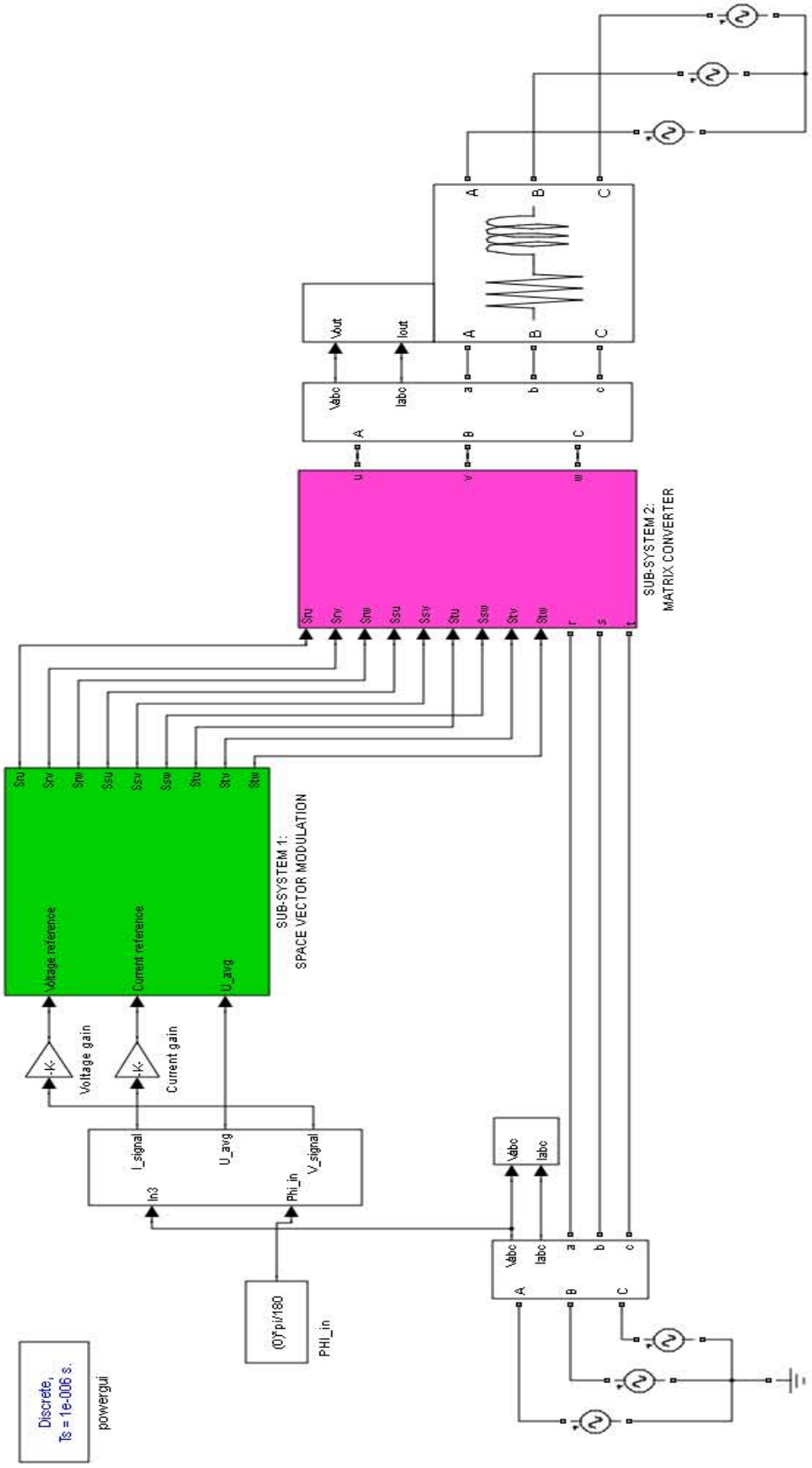

Figure B.1: *The matrix converter, in the pink subsystem 2, is connected to a voltage source on the input side and the equivalent circuit of a PM synchronous machine at the output; the modulation of the converter is located in the green subystem 1.*

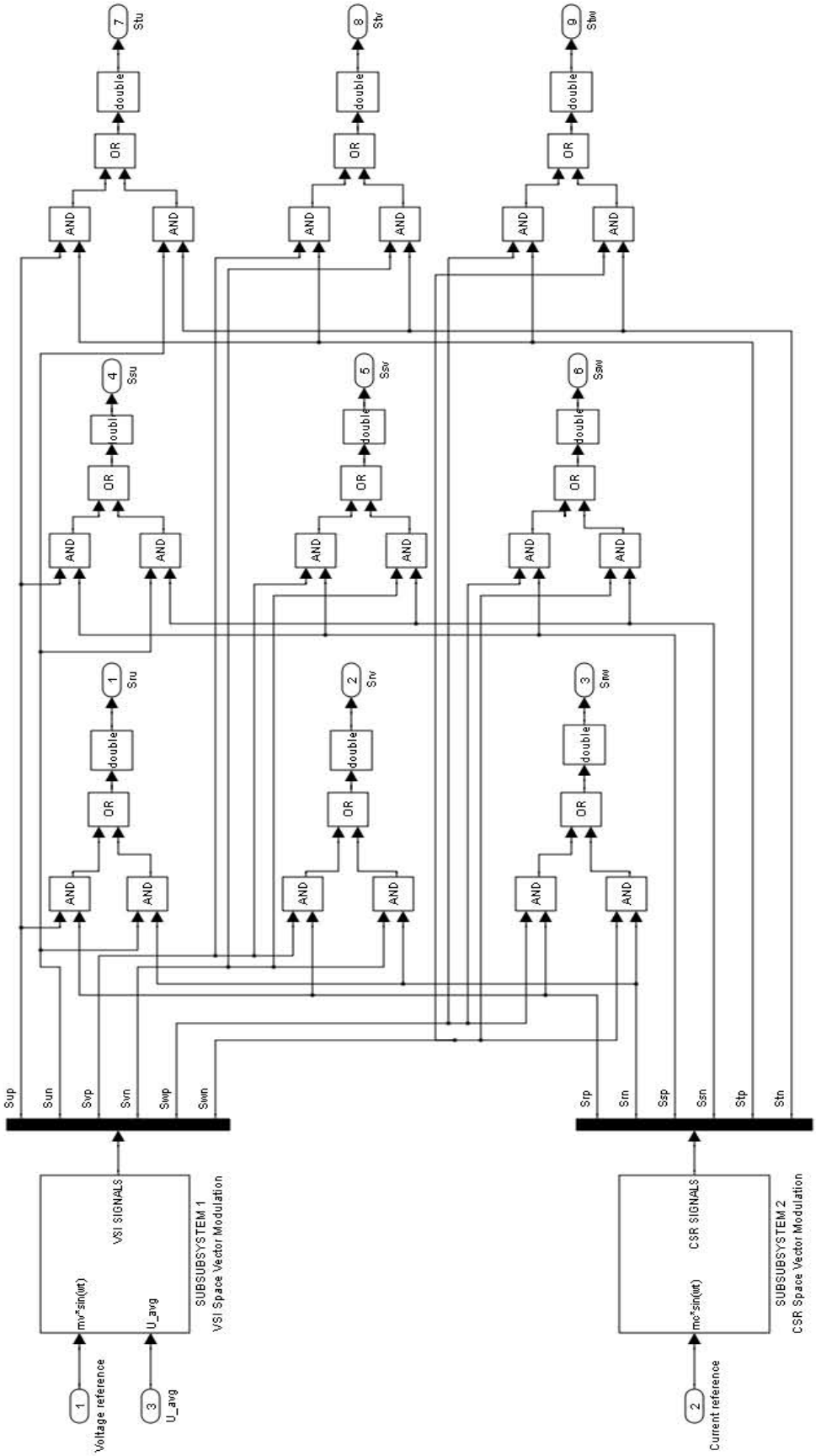

Figure B.2: *Subsystem 1: The indirect space vector modulation of the matrix converter is separated into the VSI modulation, susubsystem 1 and the CSR modulation, subsubsystem 2; the logic circuit combines the 6 signals from the VSI and the 6 signals from the CSR into 9 signals to provide for the matrix converter.*

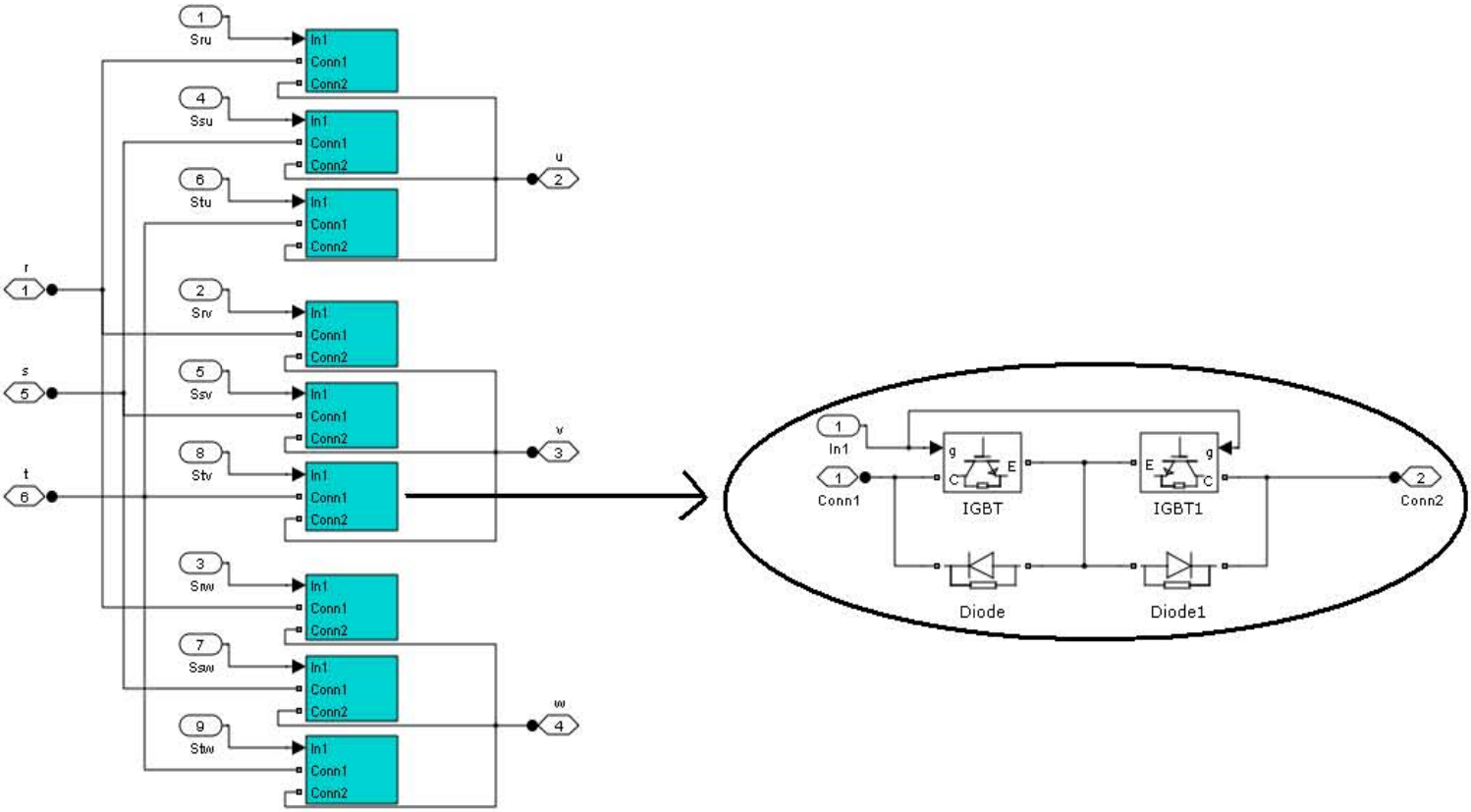

Figure B.3: *Subsystem 2: The matrix converter and the bidirectional switch.*

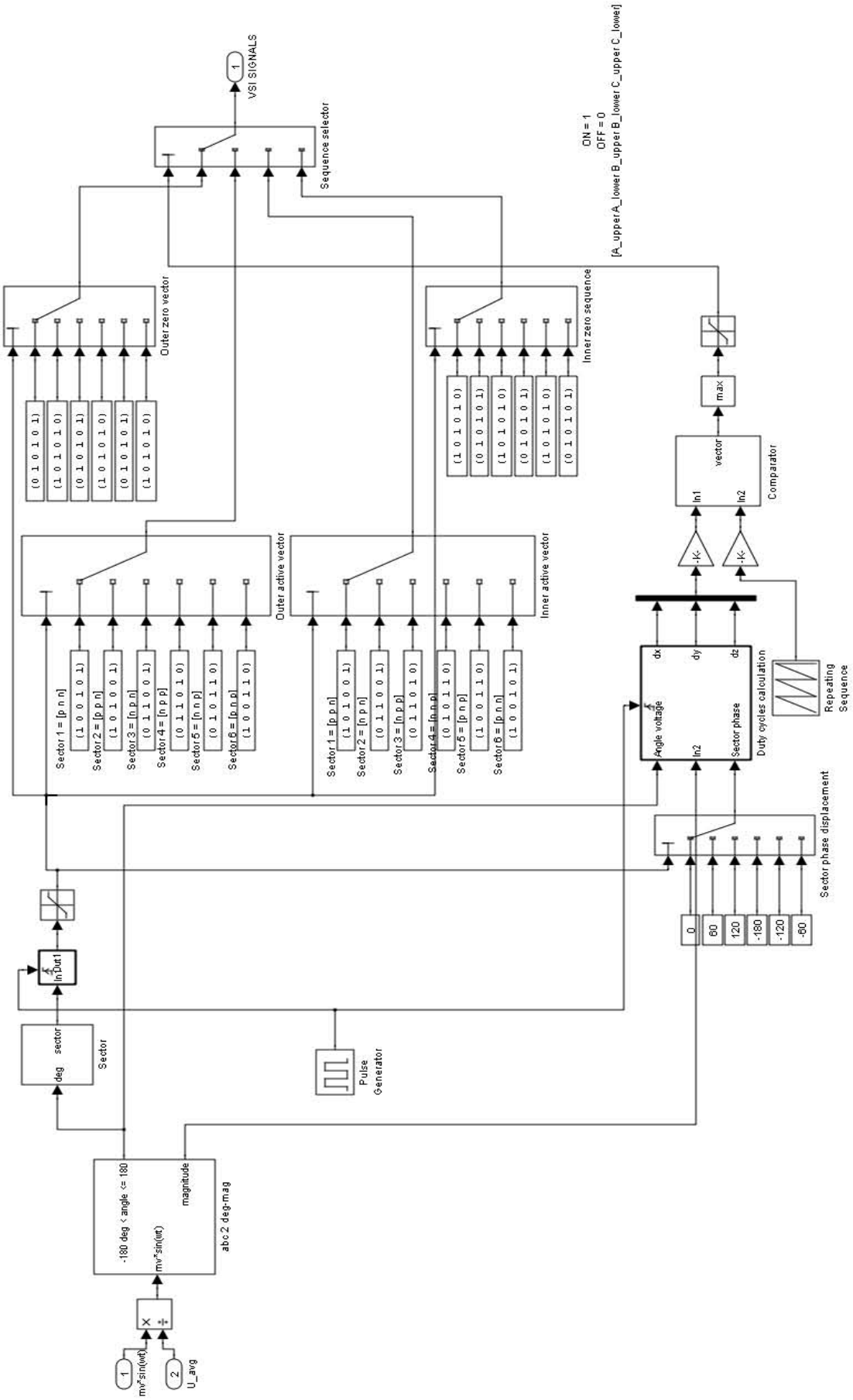

Figure B.4: *Subsubsystem 1: The VSI modulation.*

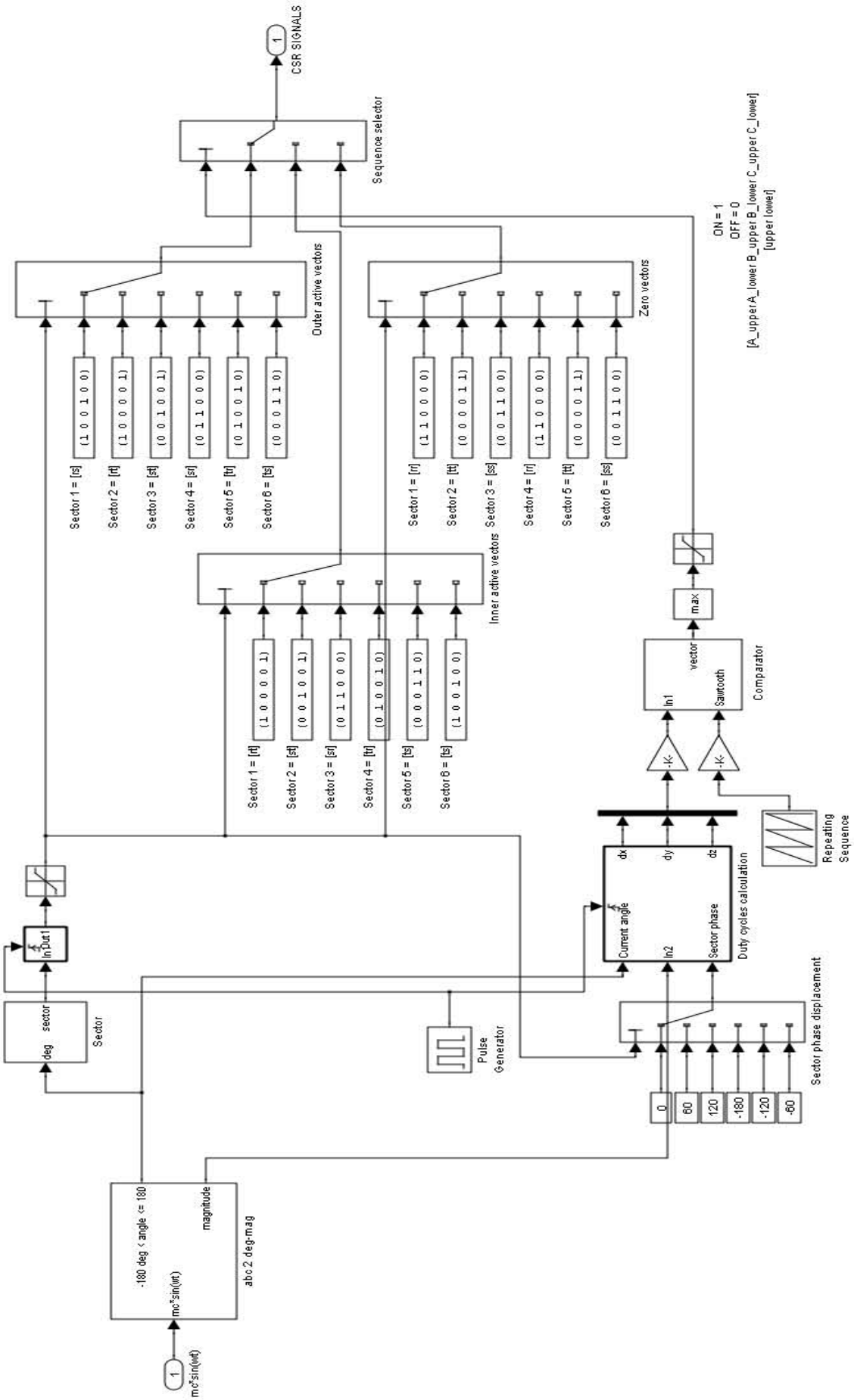

Figure B.5: *Subsubsystem 2: The CSR modulation.*

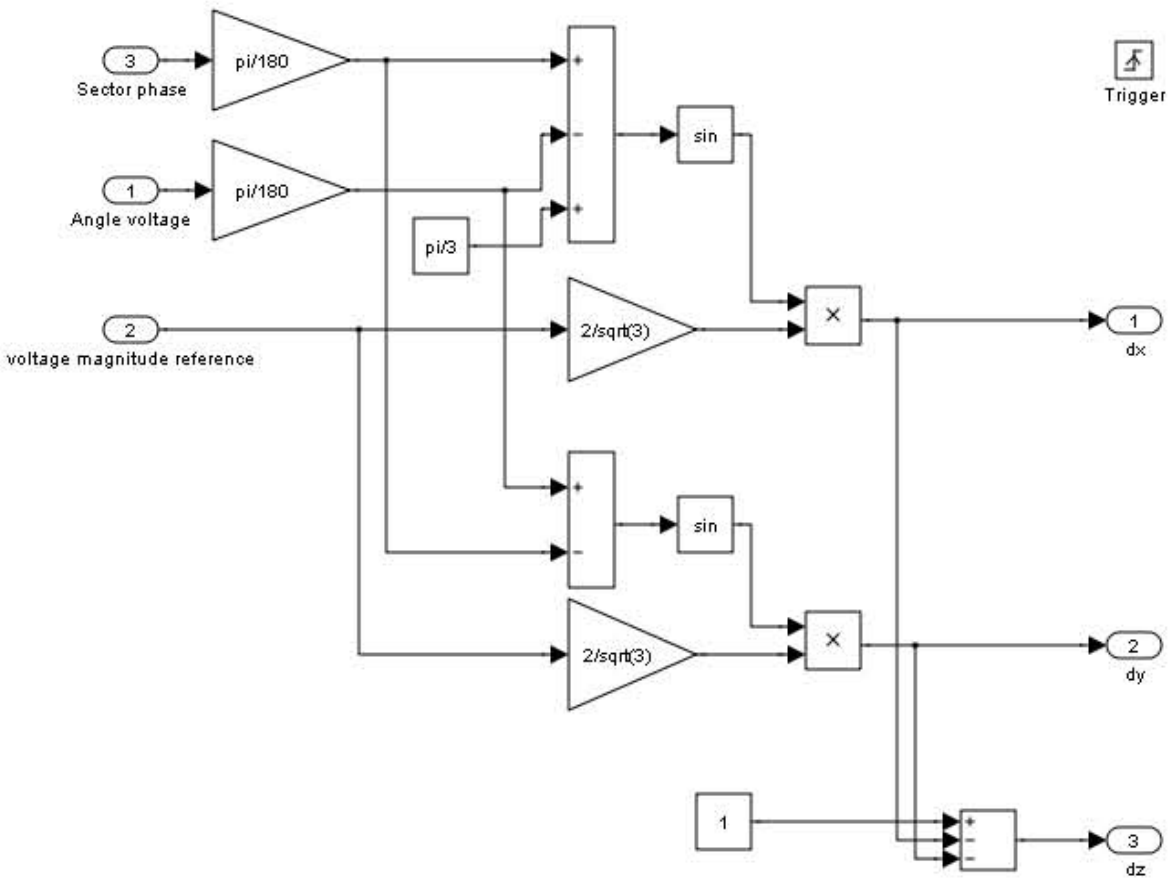

Figure B.6: *The duty cycle calculation subsystem within the VSI modulation; the duty cycle calculation subsystem in the CSR modulation is identical to the VSI subsystem except for a* 30° *phase shift.*

Appendix C

Simulation model of matrix converter with the three-vector-scheme modulation

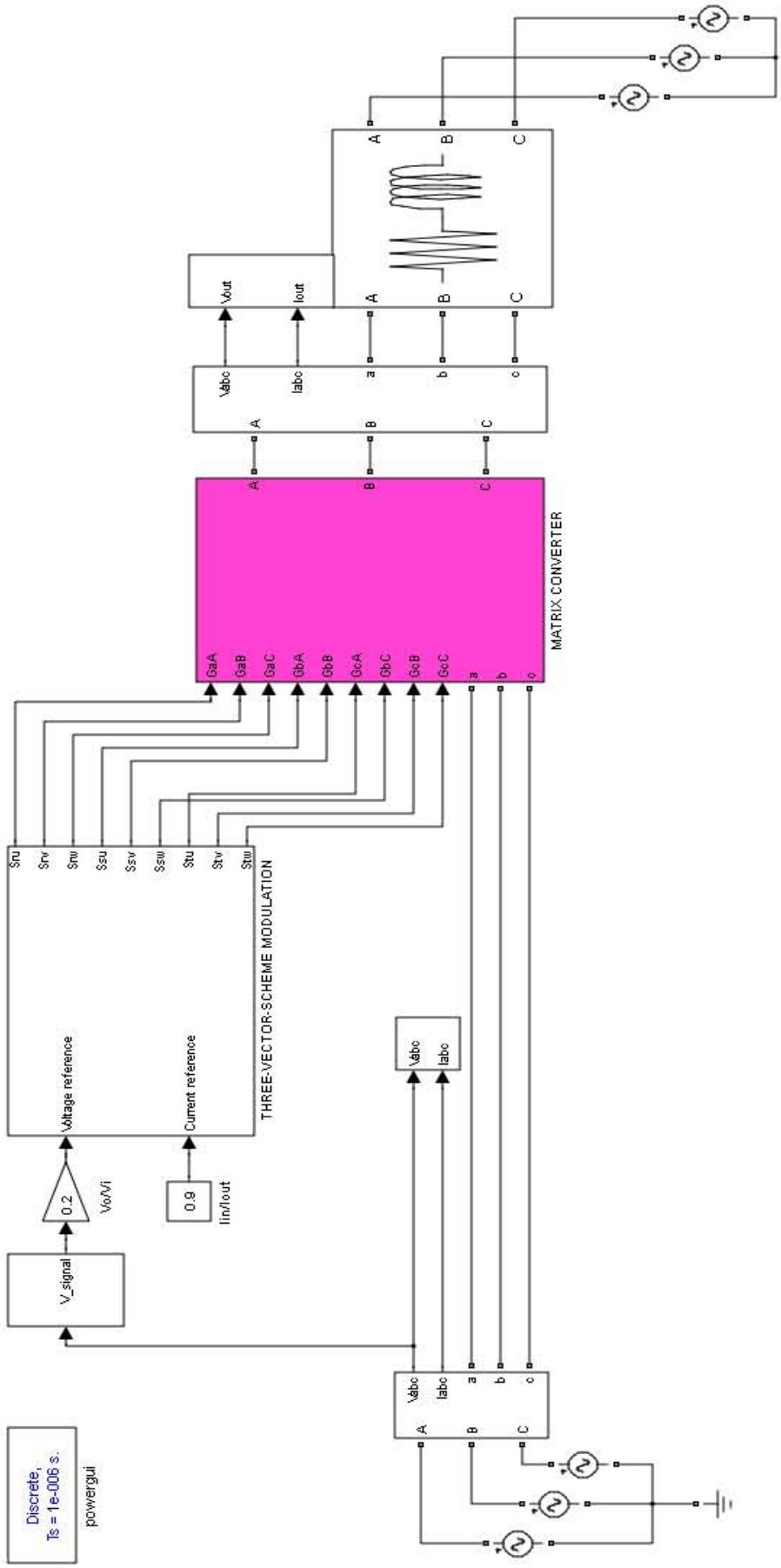

Figure C.1: *The simulation model of the three-vector-scheme modulated matrix converter connected to an equivalent circuit of the PM machine at the output and to a voltage source at the input.*

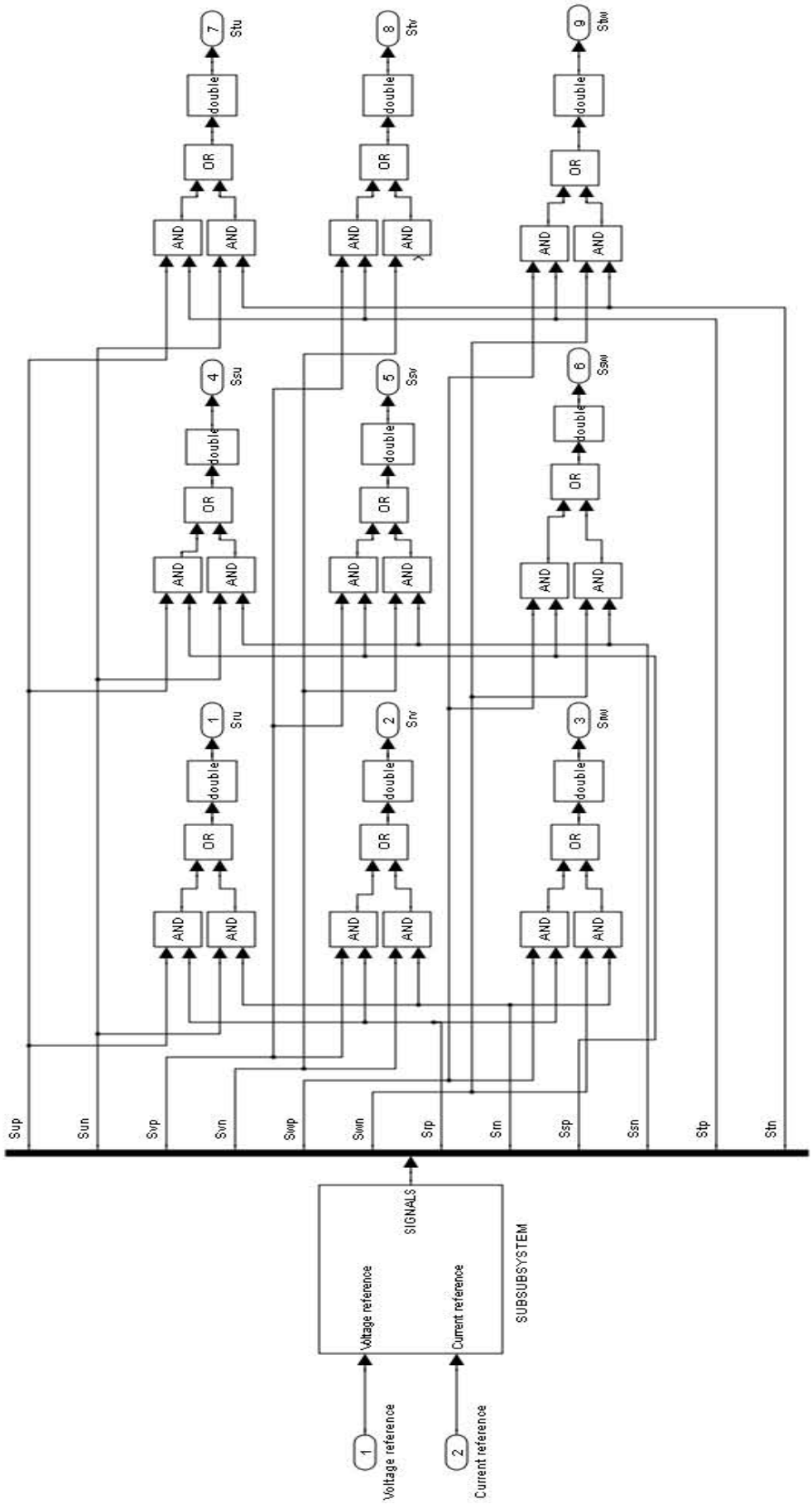

Figure C.2: *The three-vector-scheme modulation subsystem and the logic circuit.*

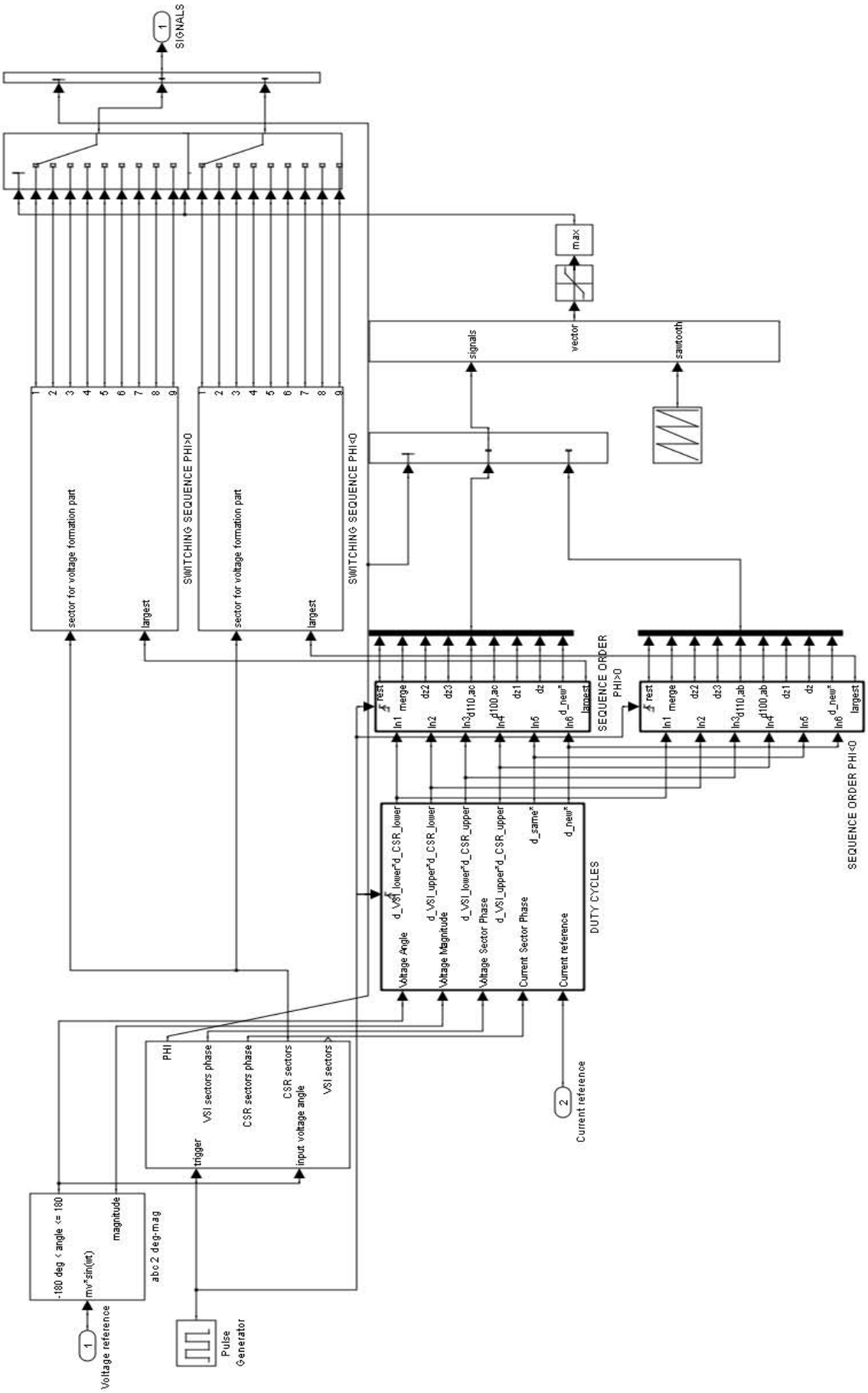

Figure C.3: *The subsubsystem: the three-vector-scheme modulation implemented only for $\theta_{i,sp} = \theta_{o,so}$ and $\Phi_i = -90\,^\circ$ and $\Phi_o = 90\,^\circ$ in order to keep the modulation simple.*

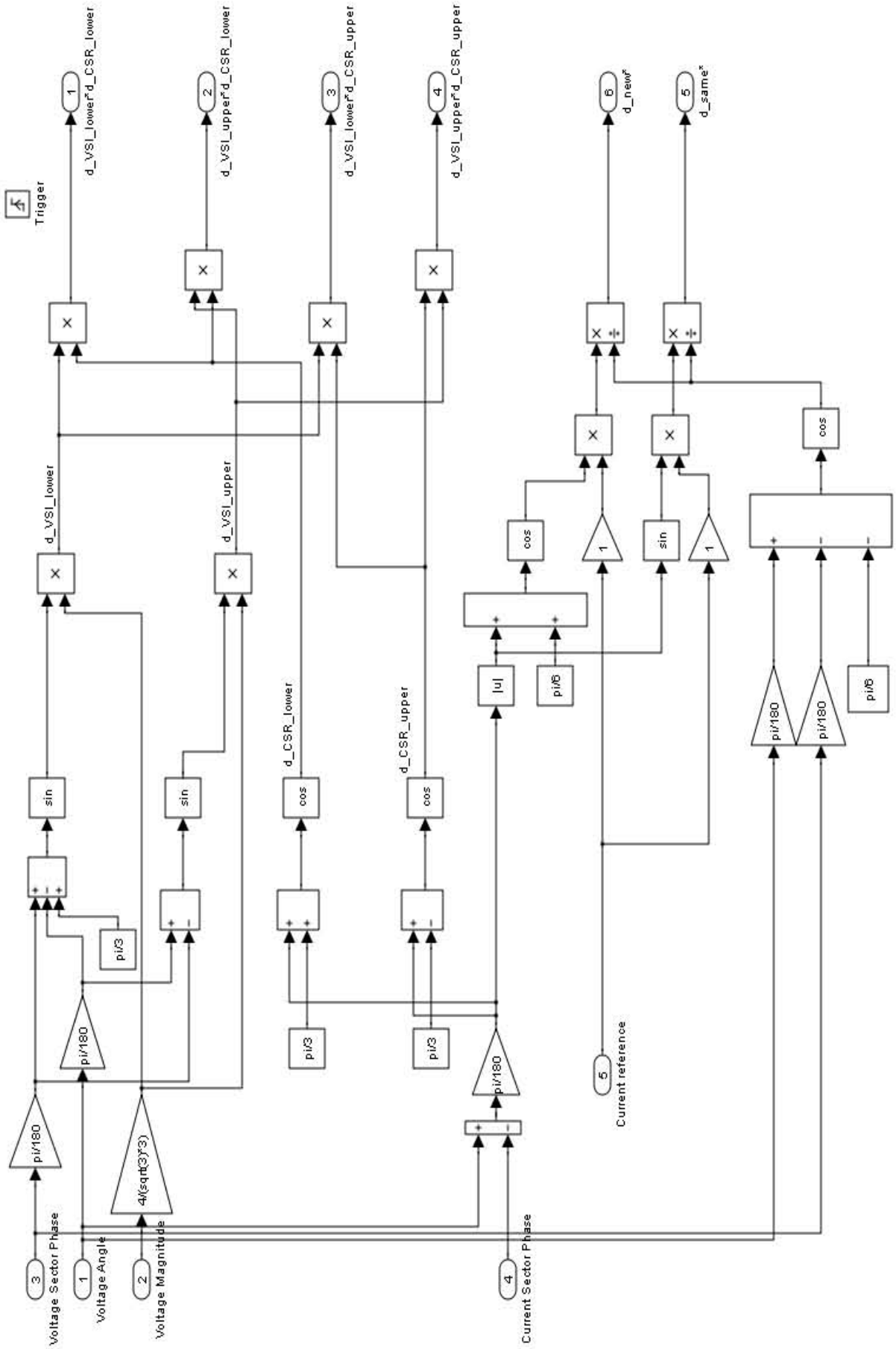

Figure C.4: *The relative duty cycle calculation subsystem.*

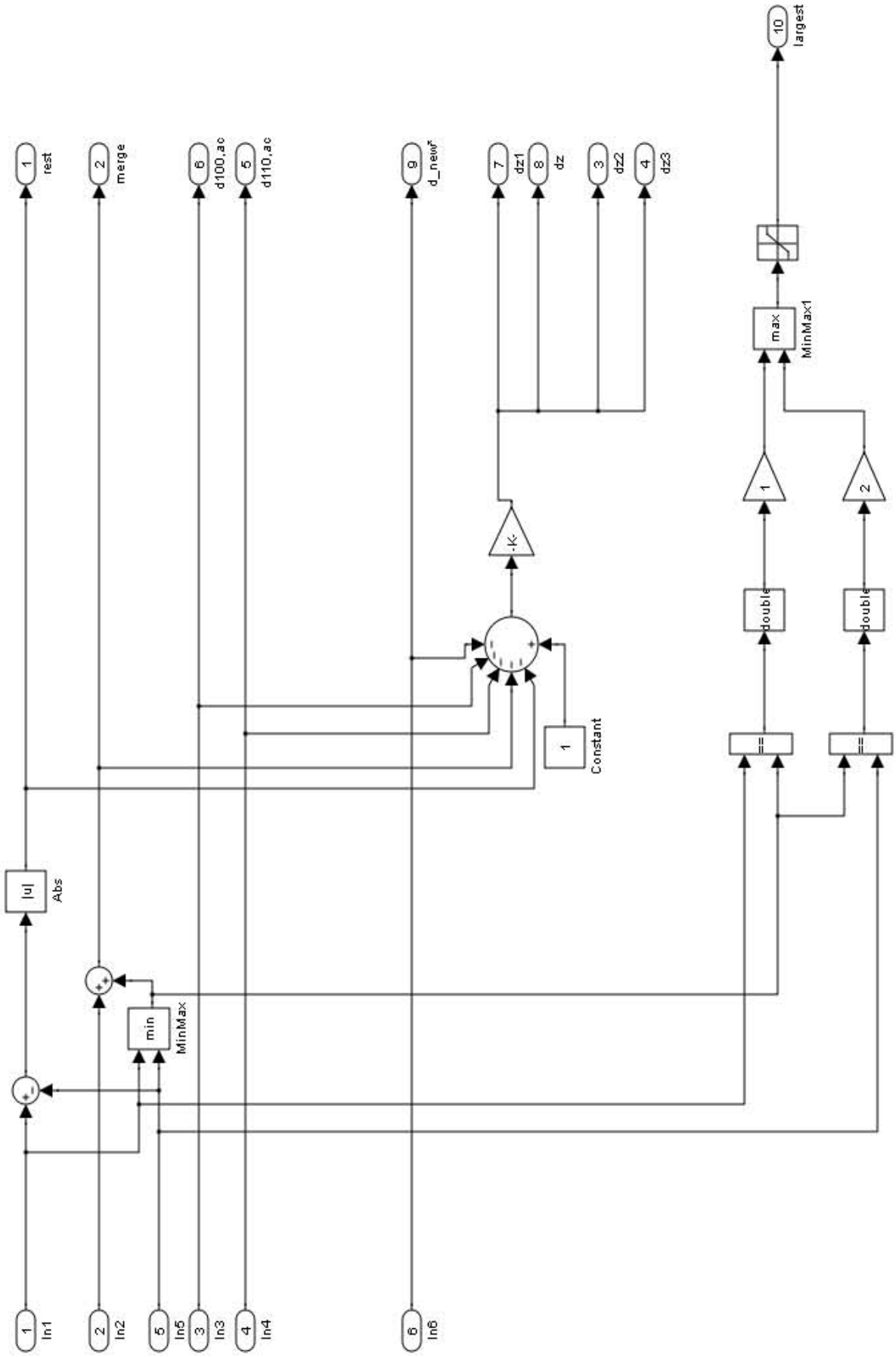

Figure C.5: *The sequence ordering subsystem depends on whether $\theta_{i,sp} \geq 0$ or $\theta_{i,sp} \leq 0$; here depicted for $\theta_{i,sp} \geq 0$.*

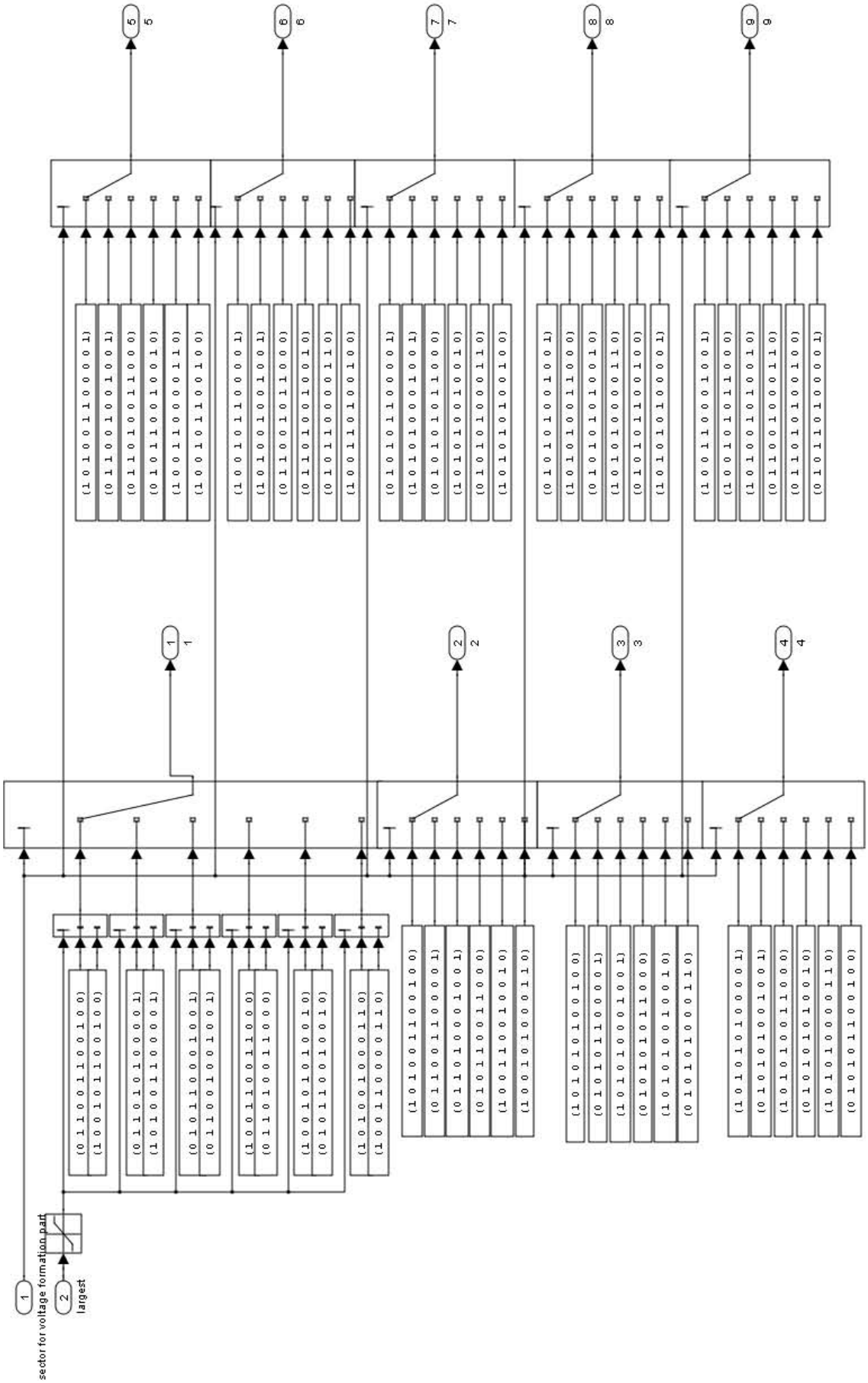

Figure C.6: *The switching combinations for the 6 sectors for $\theta_{i,sp} \geq 0$ as shown in figure 3.30 in section 3.4; the first switching combination depends on which of the two merged pulses is the largest, this is determined in the sequence ordering subsystem in figure C.5.*

Appendix D

Simulation model of the MCRC system connected to a grid for voltage support

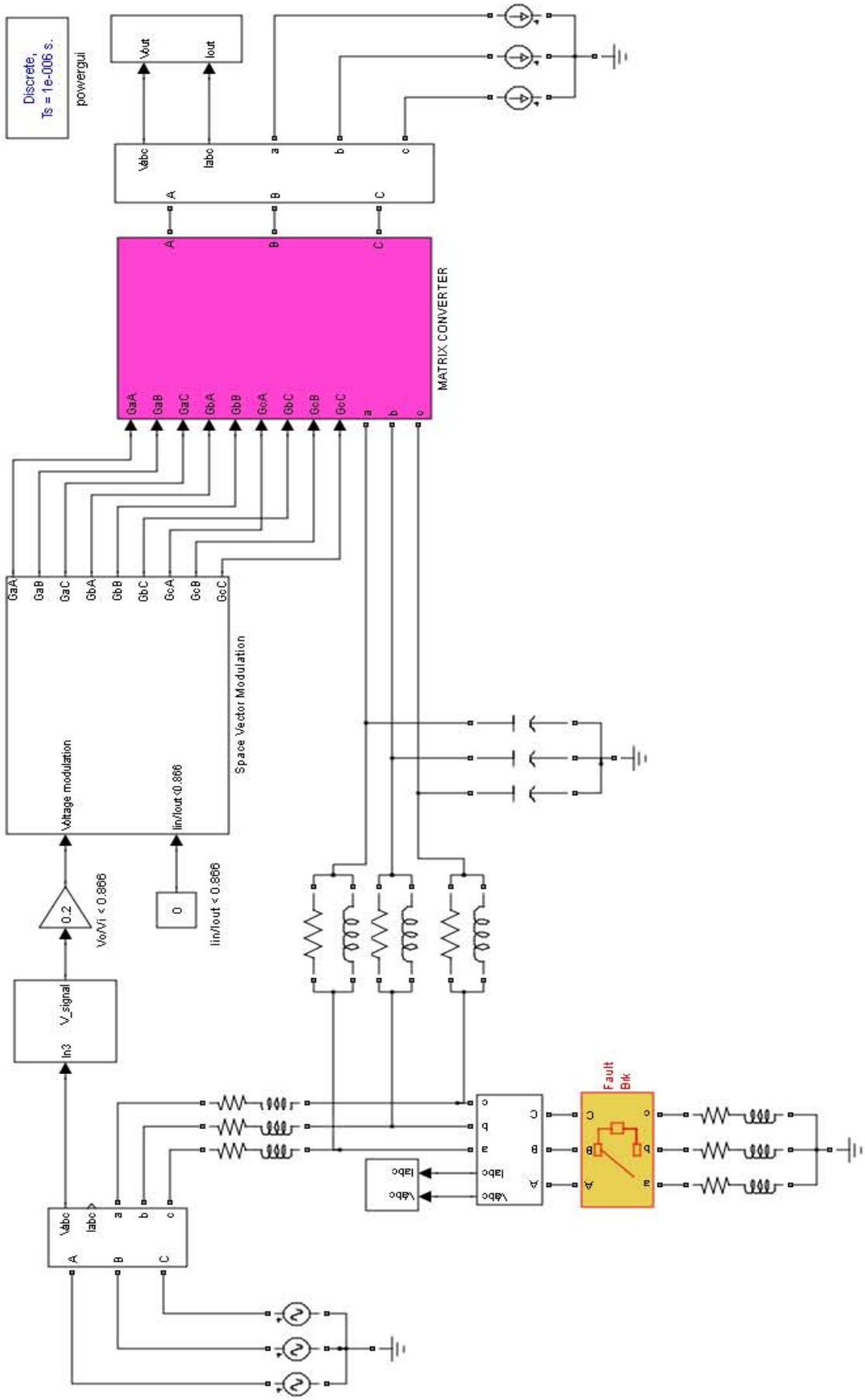

Figure D.1: *The MCRC system is connected to the grid for voltage support during a three-phase symmetrical fault.*

Appendix E

Conference paper

I wrote a paper for the IEEE-ISIE 2010 Symposium on Industrial Electronics which has been accepted. I will attend the conference in july and is attached in this appendix.

Reactive Power Compensation using an indirectly Space Vector-modulated Matrix Converter

Nathalie Holtsmark, Marta Molinas
Department of Electrical Engineering
NTNU
Trondheim, Norway
Email: holtsmar@stud.ntnu.no

***Abstract*—This paper investigates the implementation of a matrix converter for shunt reactive power compensation. The input of the matrix converter can be connected to the power grid and the output to a Permanent Magnet Synchronous Machine (PMSM). By controlling the input displacement angle Φ_i, the reactive power flowing into the grid can be controlled.**

To prove the concept of reactive power compensation using the matrix converter, a simulation model of the matrix converter-based reactive power compensation system is build in MATLAB Simulink. The matrix converter model is implemented with the direct topology, although the control strategy considers the matrix converter as if it has an indirect topology and hence is separated into a Voltage Source Inverter (VSI) part and a Current Source Rectifier (CSR) part. As a result the input current and output voltage can be controlled separately. The PMSM is modelled by a simple equivalent circuit.

The range and limitation of reactive power compensation of the system are analyzed theoretically and investigated by simulations. The results show that reactive power is indeed respectively provided to or drawn from the grid according to the investigations made.

I. Introduction

Reactive power compensation enables more active power to be transmitted in a power line and allows the voltage along the power line to be controlled [1]. FACTs controllers can be used to perform fast reactive compensation. There are many different types of FACTS, mainly divided into variable impedance type FACTS, like SVCs (Static VAR Compensators), and VSC based type FACTS like STATCOMs (Static synchronous Compensators). VSC based controllers seem to be superior to variable impedance type controllers in several ways. If we compare the SVC with the newer STATCOM we find that the latter is utilizing less volume for the same ratings. This is due to the fact that less passive components are needed. In a STATCOM the capacitor is on the DC side and can therefore be polarized. It would be enough with an electrolytic capacitor for instance. In a SVC the capacitor needs to handle AC voltage and will be larger and more expensive [2].

Following this trend of replacing passive elements like capacitors with semiconductor devices, the matrix converter might be next in line to further reduce the size, weight and increase the lifetime of FACTS devices. As a FACTS controller, the matrix converter would be connected in shunt to the grid through its input side. The feature of the converter that will be used for reactive compensation is that the reactive power at its input can be directly controlled by the input power factor angle. The output is connected to a PMSM for energy buffering. The PMSM is, as the matrix converter, small in volume, yielding a potentially very compact reactive power compensation device. This paper shows the features of a matrix converter based static reactive power compensator device. Simulation results show how effectively reactive power compensation is achieved.

II. Modulation of the matrix converter

The Matrix Converter is a direct AC-AC converter made up of only semiconductor-based bidirectional switches. It contains no energy storage components such as capacitors or reactors, although a small input filter is needed. There are two main topologies for the matrix converter: direct matrix converter, figure 1a) and indirect matrix converter, figure 1b).

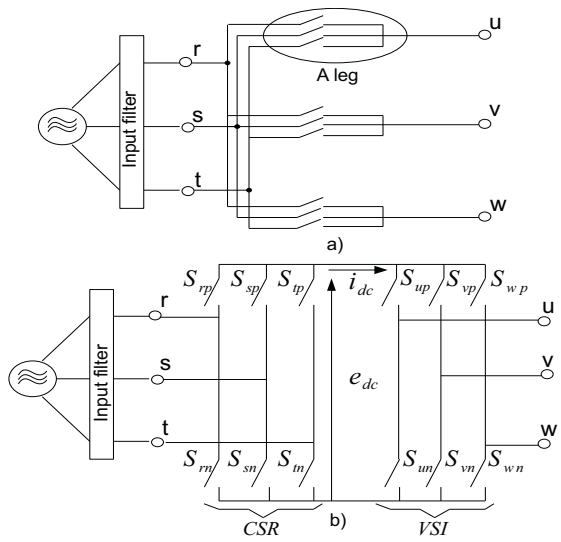

Fig. 1. a) The direct matrix converter b) The indirect matrix converter.

The matrix converter considered in this paper is built in MATLAB following the configuration of the direct topology. The space vector modulation technique however corresponds to that of an indirect matrix converter. This is a well-known modulation technique, called virtual indirect modulation as the space vector modulation outputs 12 gating signals as if it was providing the twelve switches of an indirect matrix

converter; six signals to the switches of the VSI part and six signals to the switches of the CSR part, see figure 1. With a logic circuit the 12 signals will be combined into 9 signals to provide for the real matrix converter switches. The modulation technique of the matrix converter will decide along with the load displacement factor, the magnitude and polarity of the input reactive power [3]. It is therefore important to study the modulation technique carefully to understand what limitation it will impose on the input reactive power formation.

A. The Space Vector Modulation of the Virtual VSI

The output phase voltages, $v_u^*(t) = \hat{V}_o^* \sin(\omega t - \xi_o^*)$, $v_v^*(t)$ and $v_w^*(t)$ (all entities marked with an asterisk are desired entities and all angles are measured with reference to the input voltage) are the parameters we want to control in the VSI. We want the output and input voltage to be in phase and hence $\xi_o^* = 0$. A space vector, $\vec{v}_{sp}^*(t)$ will be given as the reference to the modulation unit.

$$\vec{v}_{sp}^*(t) = \frac{3}{2}\hat{V}_o^* e^{j\omega t} = \frac{3}{2} q^* \hat{V}_i e^{j\theta_{sp}^*(t)} \tag{1}$$

As we see from equation (1) the reference space vector is a vector of constant length $\frac{3}{2}\hat{V}_o^*$ rotating at a constant angular speed ω. Here we need to define the modulation index $q = \frac{\hat{V}_o}{\hat{V}_i}$ introduced in equation (1). When the input displacement angle, Φ_i, is zero, the maximum possible modulation index that is achievable is $q_{max} = \frac{\sqrt{3}}{2}$ [4].

A VSI has $2^3 = 8$ switching states as the upper and lower switches of a phase are complementary in order not to short-circuit the input and not to diconnect the output load, especially harmful if the load is of inductive nature. Each of the eight switching states corresponds to a fixed vector when translated into space vectors. Six of these vectors are called active vectors and are distributed like shown in figure 2. In figure 2, the angle θ_{sp}, introduced first in equation (1), which is the angle between the real axis and the space vector, is also depicted. The two remaining switching states, which occur when all the three lower switches are ON together or all the upper switches are ON together, are called zero vectors. The output voltages are then short-circuited. The active vectors define 6 so-called sectors also indicated in figure 2. Let's take the active vector $\vec{u}_1$ and see how it is built. S_{up}, S_{nv} and S_{wn} are ON. $v_{v,out}(t)$ and $v_w(t)$ are short-circuited, while the virtual dc link voltage, e_{dc}, is across $v_u(t)$. Hence the space vector corresponding to this switching state is:

$$\vec{u}_1 = e_{dc} + 0e^{j\frac{2\pi}{3}} + 0e^{j\frac{-2\pi}{3}} = e_{dc} \tag{2}$$

The other active vectors are calculated in a similar manner and all have length e_{dc}.

The reference vector which sweeps along the sectors in figure 2 at an angular speed ω is build by the two adjacent active vectors, $\vec{u}_x$ and $\vec{u}_y$, of the sector where it lies, and a specifically chosen zero vector $\vec{u}_z$. The time intervals T_x, T_y and T_z for applying respectively $\vec{u}_x$, $\vec{u}_y$ and $\vec{u}_z$ must be

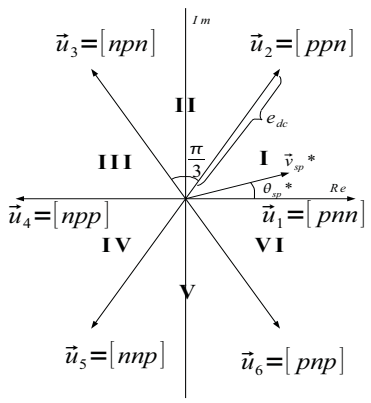

Fig. 2. The voltage space vectors in the complex plane.

computed using the following equations for sector I [5]:

$$T_1 = T_s \frac{3}{2} \frac{\hat{V}_o^* \sin(\frac{\pi}{3} - \theta_{sp}^*)}{e_{dc} \sin\frac{\pi}{3}} = T_s \frac{3}{2} \frac{q\hat{V}_i \sin(\frac{\pi}{3} - \theta_{sp}^*)}{e_{dc} \sin\frac{\pi}{3}} \tag{3}$$

$$T_2 = T_s \frac{3}{2} \frac{\hat{V}_o^* \sin\theta_{sp}^*}{e_{dc} \sin\frac{\pi}{3}} = T_s \frac{3}{2} \frac{q\hat{V}_i \sin\theta_{sp}^*}{e_{dc} \sin\frac{\pi}{3}} \tag{4}$$

$$T_z = T_s - T_1 - T_2 \tag{5}$$

The virtual DC link, e_{dc}, must be computed and is found by equating the input and virtual DC link power:

$$P_i = P_{dc} \tag{6}$$

$$\frac{3}{2}\hat{V}_i \hat{I}_i^* \cos\Phi_i^* = e_{dc} i_{dc} \tag{7}$$

$$e_{dc} = \frac{3}{2} \frac{\hat{V}_i \hat{I}_i^* \cos\Phi_i^*}{i_{dc}} = \frac{3}{2}\hat{V}_i \cos\Phi_i^* \tag{8}$$

We fix the ratio $\frac{\hat{I}_i^*}{i_{dc}} = 1$; with $\hat{I}_i$ the magnitude of the input phase current and i_{dc} the dc link current. By doing that we lock the value of the input current magnitude. However the input current angle can still be controlled as we please, see section II-B. The same gate-timing formulas can be used for the other five sectors by simply phase-shifting back to sector I. An interesting observation worth mentioning at this point is that equation (8) also implies that if the input displacement angle is $90\,^\circ$, which is the optimal for reactive compensation, where only reactive power is drawn or fed into the grid, the virtual DC link voltage will be zero. Hence the active vectors $\vec{u}_x$ and $\vec{u}_y$, which have length e_{dc}, will also be zero and it will only be possible to build an output voltage of value zero [5].

B. Space vector modulation of the Virtual CSR

The space vector modulation of the virtual CSR part is similar to the modulation of the VSI part. The main difference is that the input phase currents, $i_r^*(t) = \hat{I}_i^* sin(\omega t - \Phi_i^*)$, $i_s^*(t)$

and $i_t^*(t)$ are the parameters we want to control. The current space vector, $\vec{i}_{sp}^*(t)$ is:

$$\vec{i}_{sp}^*(t) = \frac{3}{2}\hat{I}_i^* e^{j\underbrace{(\omega t - \Phi_i^*)}_{\theta_{sp}^*(t)}} \tag{9}$$

The CSR has $3^2 = 9$ switching states as only one of the upper switches $(S_{rp}, S_{sp} or S_{tp})$ and only one of the lower switches should be ON at any time $(S_{rn}, S_{sn} or S_{tn})$: At least one because the current always must have a path to flow in and no more than one to avoid short-circuiting the input voltages. The active vectors are distributed like in figure 3. The three remaining states, that occur when the two switches connected to the same input phase are ON together, are the zero vectors. With a $+\frac{\pi}{6}$ phase shift of all the vectors, the vector "star" in

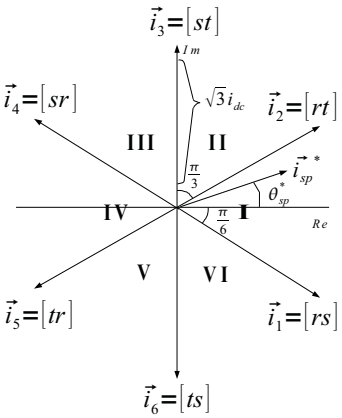

Fig. 3. The current space vectors in the complex plane.

figure 3 will correspond to the voltage vector "star" of figure 2. We can then use the gate-timing formulas (3),(4) and (5) we derived for the voltage space vector modulation:

$$T_x = T_s \frac{3}{2} \frac{\hat{I}_i^* \sin(\frac{\pi}{3} - (\theta_{sp} + \frac{\pi}{6})}{\sqrt{3} i_{dc} \sin\frac{\pi}{3}} \tag{10}$$

$$T_y = T_s \frac{3}{2} \frac{\hat{I}_i^* \sin(\theta_{sp} + \frac{\pi}{6})}{\sqrt{3} i_{dc} \sin\frac{\pi}{3}} \tag{11}$$

As previously mentioned the ratio $\frac{\hat{I}_i^*}{i_{dc}} = 1$ is fixed. Only the angle θ_{sp} is controlled. Following the same procedure as in the previous section, we want to look at the effect of the VSI modulation on the virtual DC link current. The average power balance of the VSI part of the matrix converter is:

$$P_o = P_{dc} \tag{12}$$

$$i_{dc} = \frac{3}{2} \frac{\hat{V}_o^* \hat{I}_o \cos\Phi_o^*}{e_{dc}} \tag{13}$$

We clearly see from equation (13) that if the output displacement angle is $90\,^\circ$, the DC link current is zero. Hence the active vectors in figure 3 are zero and no input current can be build [5].

III. Reactive power compensation with the matrix converter

In [6] it is suggested to connect the input of the matrix converter to the power grid and its output to an PMSM which will serve the purpose of an energy buffer. The layout is shown in figure 4. In this section the range of reactive power

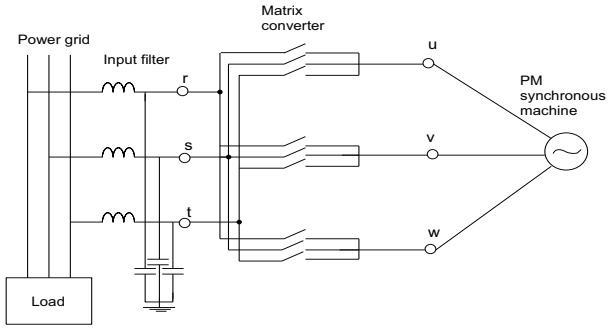

Fig. 4. The matrix converter connected to the grid for reactive compensation.

compensation capacity of the device is examined. However in order to conduct this analysis, a simple model of the system will first be derived.

A. Model of the matrix converter based reactive power compensating system

The PM synchronous machine can be modelled by an equivalent circuit consiting of the excitation voltage which is created in the armature winding as the permanent magnets and the rotating flux they generate, sweep across the stator conductors. The excitation voltage depends only on the permanent magnet properties and will therefore be represented by a voltage source $\vec{E}_f$ in our model in figure 5.

$$\vec{E}_f = E_f \angle \delta \tag{14}$$

The angle δ is called the rotor angle and is the phase angle of the excitation voltage with respect to the voltage at the terminal of the synchronous machine $\vec{V}_o$ which is also in phase with the grid voltage $\vec{V}_i$. The other component of the equivalent circuit is the synchronous reactance which is again composed of the synchronous and leakage reactance. The three-phase currents flowing in the stator also generates a rotating field flux called armature-reaction flux. This will induce a voltage in the stator windings. The armature-reaction flux and induced voltage depend on the armature current's magnitude and phase angle. The armature-reaction voltage is therefore represented in our model in figure 5 by a fictitious armature-reaction reactance X_{ar}. In addition the model includes an armature leakage reactance X_l which accounts for the flux leakage in the armature windings [7]. This equivalent circuit of the PMSM is used in the MATLAB simulation model. The matrix converter is represented in figure 5 as a black box which transforms the voltage and current levels. The active power drawn or provided to a synchronous machine can be calculated

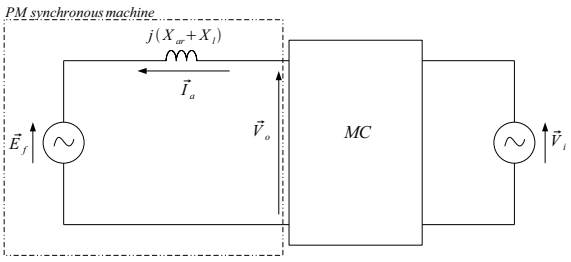

Fig. 5. The per-phase simplified representation of the MCRC system.

as in (15) [7].

$$P_o = 3\frac{V_o E_f}{X_l + X_{ar}} \sin\delta = 3\frac{qV_i E_f}{X_l + X_{ar}} \sin\delta \tag{15}$$

B. Reactive power compensation capacity

The reactive power at the input of the matrix converter is governed by the following formula, considering the converter to be lossless:

$$Q_i = P_i tan\Phi_i^* = P_o \tan\Phi_i^* = 3\frac{q^* V_i E_f}{X_l + X_{ar}} \sin\delta \tan\Phi_i^* \tag{16}$$

All the parameters are fixed except for q and Φ_i. Equation (16) shows that the reactive power transfer is directly linked to the transfer of active power [8]. This was also shown in section II, where the special case of $90\,^\circ$ input displacement angle was examined. $90\,^\circ$ input displacement angle corresponds to zero input active power and hence $90\,^\circ$ output displacement angle to satisfy the active power balance. As seen from equation (13) this will yield the DC link current to be zero. No current can then be formed at the input, and no reactive power neither. In conclusion, when using indirect space vector modulation as such, there must be som active power transfer in order to have reactive power creation at the input of the matrix converter. Furthermore, because of these characteristics of the modulation, there is a trade-off between the modulation index q and the input displacement angle Φ_i. When the input displacement angle is different from zero, the maximum achievable modulation index is reduced [9].

$$q_{max,\Phi} = q_{max}\cos\Phi_i = \frac{\sqrt{3}}{2}\cos\Phi_i \tag{17}$$

Similarly Φ_i is limited by q such that:

$$\Phi_{i,max} = \cos^{-1}\frac{q}{q_{max}} \tag{18}$$

This trade-off is not necessarily a serious drawback for the reactive power compensating system as the active power transfer should be kept as low as possible, by keeping q low and thus $\Phi_{i,max}$ larger. This is illustrated in figure 14 in section IV where the theoretical values of Q_i and P_i are plotted for different values of q. P_i is calculated using equation (15) and Q_i using equation (16) with the maximum possible input displacement angle calculated with equation (18). The system parameters used in the calculations are the same as were used in the simulations and are all given in section IV.

IV. Simulation results

In all simulations, the input voltage has amplitude $\hat{V}_i = 100V$, the input and output frequency is $f = 50Hz$ and the switching frequency is $f = 5000Hz$. The excitation voltage of the PMSM has amplitude $\hat{E}_f = 50V$. The rotor angle is set at $\delta = -10\,^\circ$ for operation in motor mode, a low value that will yield low active power transfer, and zero for the special case of no active power transfer. The values of $\hat{E}_f$ was chosen as a compromise between the size of the PMSM and the compensation range of the device. The synchronous reactance was set at a typical values for synchronous machines of $X_s = 1.3\Omega$ [7]. The set up used for the simulations is as shown in figure 6.

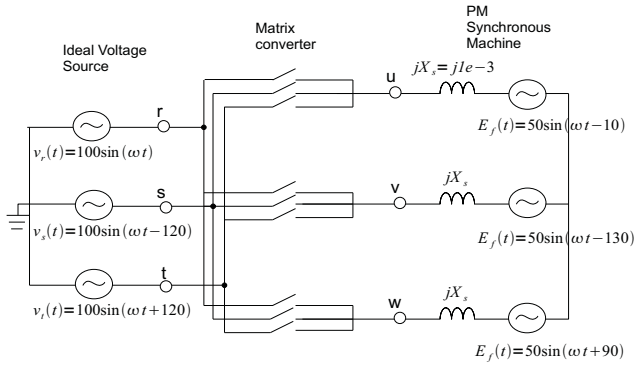

Fig. 6. The simulation set-up.

A. No reactive compensation, $\Phi_{in} = 0$

The simulations are first done with a reference input power factor angle equal to zero and a reference output voltage equal to the half the input voltage, $q = 0.5$. Figure 7 and figure 8

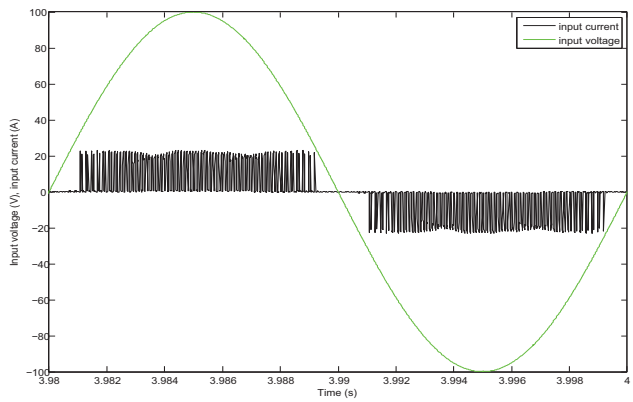

Fig. 7. The input voltage and current during one time period of 20 ms.

show respectively the input and output voltage and current over a time period of $T = 20ms$. There is no input filter, so as we can see in figure 7 the input current is highly distorted. On the other hand the output current is smoothened by the inductance of the PMSM.

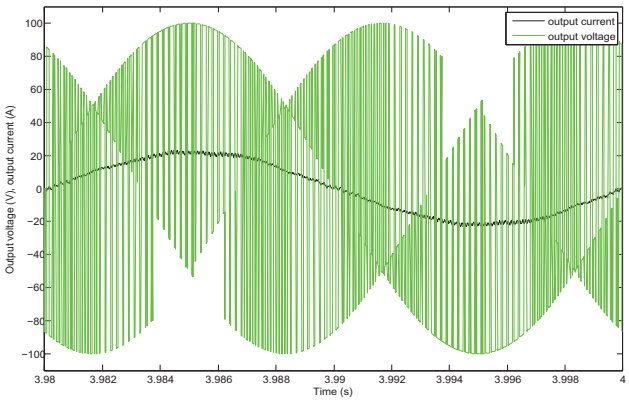

Fig. 8. The output voltage and current during one time period of 20 ms.

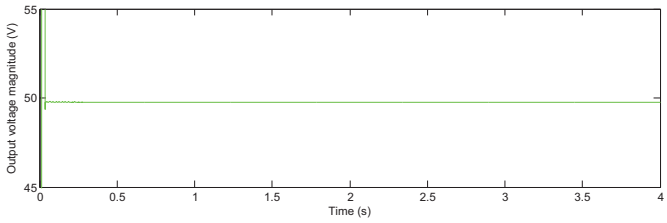

Fig. 9. The magnitude of the fundamental of the output voltage.

In figure 9 and 10 are shown respectively the magnitude of the output voltage and angle of the input voltage and current. As we see from figure 9 the output phase voltage is close to 50 V and figure 10 shows that the output voltage and current are in phase as we wanted. The input displacement angle, shown in figure 9b), is $\Phi_i = 2\,^\circ$ which is close to the desired unity power factor.

In order to compare the input and the output power, the input and output voltages and currents can be measured and injected into equation (19).

$$P = \frac{1}{T}\int_0^T v(t)i(t)dt = 50\int_0^{\frac{1}{50Hz}} v(t)i(t)dt \qquad (19)$$

For the previous case of the modulation index set to $q = 0.5$ and the input displacement angle set to $\Phi_{in} = 0$ the input active power is $P_i = 1703W$ and the ouput active power is $P_o = 1630W$. The difference comes from losses in the matrix converter which is not ideal in the simulation model. Let's compare this with the power calculated with equation (15). The rotor angle is measured to be $\delta = 7.8\,^\circ$, which is lower than the reference. The power fed to the machine is calculated to be $P_o = 1620W$ which corresponds to the previous value.

By changing the value of the modulation index q, the output voltage is accordingly changed. The curve in figure 11 shows that for values of q between 0 and $\frac{\sqrt{3}}{2}$ the variation of the output voltage scaled with the input voltage is proportional to the variation of the modulation index. For higher values of q however saturation is reached. The reaching of saturation at $q_{max} = \frac{\sqrt{3}}{2}$ is related to this value being a physical limit of the matrix converter voltage ratio [4], which if exceeded will

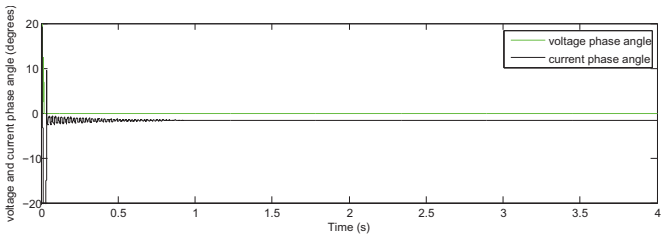

Fig. 10. The input displacement angle.

lead to low-frequency distortion in the output voltage [9] as was discussed in section II-A.

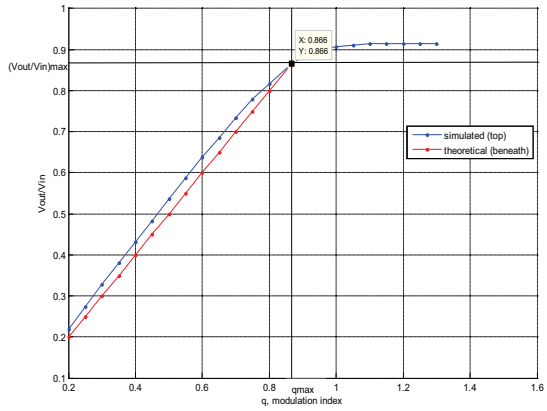

Fig. 11. The output voltage scaled with the input voltage.

B. *The case of no active power transfer,* $\Phi_i = 90\,^\circ$ *and* $\Phi_o = 90\,^\circ$

In section II, it was shown that when no active power is transferred no voltage can be build at the output of the matrix converter and no current can be build at the input of the matrix converter. To simulate this case the rotor angle δ was set to zero and the input displacement angle Φ_i was set to $90\,^\circ$. The modulation index is set to its maximum value which is zero as equation (17) indicates. The input and output powers are calculated with the voltage and current measurements using equation (19) and are obtained to be $P_i = 29.1W$ and $P_o = -71W$. Not only are the values close to zero but the opposite signs are a proof that there is no active power transfer from input to output. In figure 12 we see that the output voltage magnitude is indeed very low at a value of $0.5V$. In figure 13 is depicted the input displacement angle and it is clear that it is far from the reference angle. This indicates that the matrix converter does not function properly in this operation mode.

C. *Reactive power compensation capabilities*

We now want to observe the reactive power compensation capabibities of the matrix converter-based device. In figure 14 the active power and maximum possible reactive power measured with the MATLAB Simulink model are plotted versus the modulation index. For measuring the reactive power

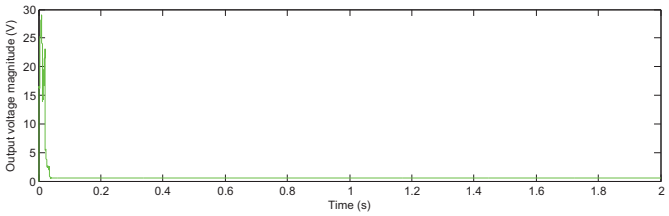

Fig. 12. The magnitude of the fundamental of the output voltage.

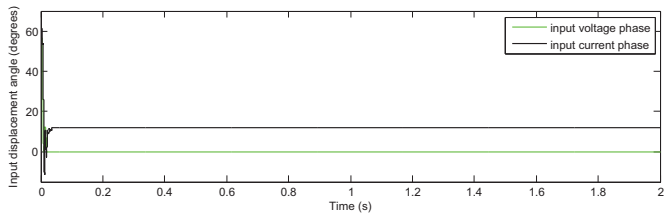

Fig. 13. The input displacement angle.

the input displacement angle was set at the maximum possible value at the given modulation index. The theoretical active and reactive powers calculated with equation (15) and (16) are also plotted in figure 14. We see that although the active and reactive power measurements have the same trend as the theoretically calculated power values, they are much lower in value. This is due to the fact that the rotor angle sets at values lower than the reference and thus the active power fed to the machine is lower. As a consequence the reactive power is lower than the predicted theoretical value. This is not a desirable behaviour, however it has the merit to illustrate how the reactive power and the active power are directly related through equation (16); if the active power transfer is lowered, the input reactive power will follow as well. Also figure 14 illustrates the saturation of the modulation index for values of q above $\frac{\sqrt{3}}{2}$, as we can see that the measured active power does not continue to increase above $\frac{\sqrt{3}}{2}$. The reactive power transfer to the grid is maximum for low modulation indexes and decreases as q increases. This is due to the trade-off between q and $\cos\Phi_i$ described in equation (18) and (17).

V. Conclusion

Simulations done with the matrix converter-based reactive power compensation system show that the device can indeed deliver reactive power to a grid, especially effective for low modulation indexes. However when using the indirectly space vector modulated matrix converter, the input reactive power is directly linked to the active power transfer and there must always be some active power transfer for reactive power to be delivered. This is not optimal for the purpose of such reactive power compensation system. Thus further work will be to look at possible modification of the modulation that would enable input reactive power creation without any active power transfer [10].

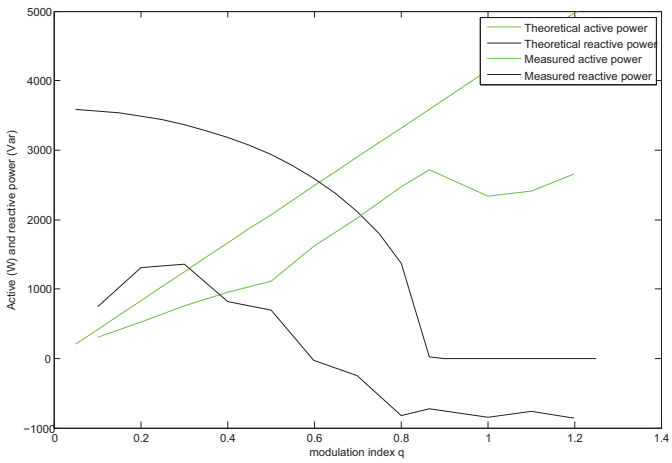

Fig. 14. The input theoretical and measured active and reactive powers.

References

[1] K. R. Padiyar, *FACTS Controllers in Power Transmission and Distribution, New Age International Publishers, 2007.*

[2] H. Ghasemi, C. A. Caizares, *Validation of a STATCOM Transient Stability Model through Small-Disturbance Stability Studies, IEEE International Conference on System of Systems Engineering, 2007. SoSE '07., 2007.*

[3] L. Gyugyi, B. R. Pelly, *Static Power Frequency Changers, John Wiley & Sons, 1976.*

[4] D. Casadei, G. Serra, A. Tani, L. Zarri, *Matrix Converter Modulation Strategies: A new General Approach Based on Space-Vector Representation of the Switch State, IEEE Transactions on Industrial Electronics, 2002.*

[5] J. W. Kolar, T. Friedli, *The Essence of Matrix Converters, Swiss Federal Institute of Technology (ETH) Zurich, Power Electronic Systems Laboratory, IECON'08.*

[6] J. I. Itoh, S. Tamada, *A novel Engine Generator System with Active Filter Functions using a Matrix Converter, Power Lab., Nagaoka University of technology, presentation in Trondheim in 2007.*

[7] C. I. Hubert, *Electric Machines, Theory, Operation, Applications, Adjustment, and Control, Prentice Hall, 2002.*

[8] J. W. Kolar, F. Schafmeister, S. D. Round, H. Ertl, *Novel Three-Phase AC-AC Sparse Matrix Converter, IEEE Transactions on Power Electronics, vol. 22, no. 5, 2007.*

[9] R. Cárdenas, R. Peña, P. Wheeler, J. Clare, G. Asher *Control of the Reactive Power Supplied by a WESC Based on Induction Generator Fed by a Matrix Converter, IEEE Transactions on Industrial Electronics, 2009.*

[10] F. Schafmeister, J. W. Kolar, *Novel Modulation Schemes for Conventional Sparse Matrix Converter facilitating Reactive Power Transfer independent of Active Power Flow, in Proc. PESC, 2004, pp.2917-2923.*